National Library of Canada

Bibliothèque nationale du Canada

Acquisitions and Bibliographic Services Branch

Direction des acquisitions et des services bibliographiques

395 Wellington Street
Ottawa, Ontario
K1A 0N4

395, rue Wellington
Ottawa (Ontario)
K1A 0N4

Your file Votre référence

Our file Notre référence

NOTICE

The quality of this microform is heavily dependent upon the quality of the original thesis submitted for microfilming. Every effort has been made to ensure the highest quality of reproduction possible.

If pages are missing, contact the university which granted the degree.

Some pages may have indistinct print especially if the original pages were typed with a poor typewriter ribbon or if the university sent us an inferior photocopy.

Reproduction in full or in part of this microform is governed by the Canadian Copyright Act, R.S.C. 1970, c. C-30, and subsequent amendments.

AVIS

La qualité de cette microforme dépend grandement de la qualité de la thèse soumise au microfilmage. Nous avons tout fait pour assurer une qualité supérieure de reproduction.

S'il manque des pages, veuillez communiquer avec l'université qui a conféré le grade.

La qualité d'impression de certaines pages peut laisser à désirer, surtout si les pages originales ont été dactylographiées à l'aide d'un ruban usé ou si l'université nous a fait parvenir une photocopie de qualité inférieure.

La reproduction, même partielle, de cette microforme est soumise à la Loi canadienne sur le droit d'auteur, SRC 1970, c. C-30, et ses amendements subséquents.

Canada

PHOTOELECTRONIC STUDY OF GaAs EPILAYERS AND $In_xGa_{1-x}As/GaAs$ QUANTUM WELLS

by

YE WANG

Submitted to the School of Graduate Studies of the University of Ottawa in partial fulfillment of the requirements for the degree of Master of Science

Department of Physics

Faculty of Science

University of Ottawa

Ottawa, Canada

© Ye Wang, Ottawa, Canada, 1992

National Library of Canada

Acquisitions and Bibliographic Services Branch

395 Wellington Street
Ottawa, Ontario
K1A 0N4

Bibliothèque nationale du Canada

Direction des acquisitions et des services bibliographiques

395, rue Wellington
Ottawa (Ontario)
K1A 0N4

Your file Votre référence

Our file Notre référence

The author has granted an irrevocable non-exclusive licence allowing the National Library of Canada to reproduce, loan, distribute or sell copies of his/her thesis by any means and in any form or format, making this thesis available to interested persons.

L'auteur a accordé une licence irrévocable et non exclusive permettant à la Bibliothèque nationale du Canada de reproduire, prêter, distribuer ou vendre des copies de sa thèse de quelque manière et sous quelque forme que ce soit pour mettre des exemplaires de cette thèse à la disposition des personnes intéressées.

The author retains ownership of the copyright in his/her thesis. Neither the thesis nor substantial extracts from it may be printed or otherwise reproduced without his/her permission.

L'auteur conserve la propriété du droit d'auteur qui protège sa thèse. Ni la thèse ni des extraits substantiels de celle-ci ne doivent être imprimés ou autrement reproduits sans son autorisation.

ISBN 0-315-85756-0

Canada

UNIVERSITÉ D'OTTAWA
UNIVERSITY OF OTTAWA

To my parants and my family

ABSTRACT

The photoelectromagnetic (PEM) effect was used to perform experiments on photocarriers' transport properties in GaAs substrates and epitaxial layers. For the undoped semi-insulating substrate, the carriers' mobility μ at T=77K was measured by PEM effect method, giving a value of μ=40,000 $cm^2\ V^{-1}\ s^{-1}$. It was found that the carriers' diffusion length is L_D=0.27 μm at T=300K and L_D=0.44 μm at T=77K. For the 3.4μm thick epitaxial layer grown by metal-organic chemical vapour deposition (MOCVD), the carriers' diffusion length was measured to be L_D=2.6 μm at T=300K, L_D=3.1 μm at T=77K and $L_D \approx$3.5 μm at T=5K.

A photocurrent (PC) spectroscopy study of $In_xGa_{1-x}As$/GaAs quantum wells on Cr-doped and undoped substrates has been performed. Several well-resolved structures related to inter-subband transitions are observed in the photoconductivity spectra for both T=300K and T=77K, and they are in good agreement with calculation taking into account the strain-induced splitting of the bands. Both Cr-doped and undoped substrates have been found to influence the results, as shown by optical quenching techniques.

SOMMAIRE

On a utilisé l'effect photoélectromagnétique pour réaliser des mesures de transport électronique dans des substrats et des couches épitaxiales de GaAs. Pour le substrat non-dôpé semi-isolant, on a mesuré des valeurs de 40,000 $cm^2/V \cdot s$ pour la mobilité μ à 77K, 0.27 μm pour la longueur de diffusion L_D des porteurs à 300K et 0.44 μm à 77K. Pour la couche épitaxiale de 3.4 μm d'épaisseur déposée par épitaxie en phase vapeur métallo-organique, des longueurs de diffusion L_D= 2.6 μm à 300K, 3.1 μm à 77K et 3.5 μm à 5K furent déterminées. Plusieurs puits quantiques au $In_xGa_{1-x}As/GaAs$ ont été étudiés par spectroscopie du photocourant. De nombreuses particularités spectrales reliées aux transitions inter-sousbandes sont clairement observées dans les spectres à 300 et 77K à des positions prévues par les calculs. Par des méthodes de quenching optique multi-source, on a pu aussi observer l'influence des divers substrats sur les caractéristiques des spectres des puits quantiques.

ACKNOWLEDGMENTS

I wish to thank Dr. E. Fortin for his suggesting the project, for his supervision and encouragment, and for his financial support throughout the period of this research.

Thanks are due to Dr. A. Roth at NRC for the samples provided for this research, also to Mr. S. Fafard for helpful suggestions and discussions. And to Dr. R. Hodgson, Dr. B. Joos, and Dr. P. Piercy for lectures given during my master's degree.

I acknowledge the staff at the department, and in particular the people from the workshop for their capable and prompt attention.

I would like to express my great thanks to my parents who sacrificed a lot to take care of my son, and to my husband, Binjun Zhao, for his continuous encouragement and patience during the course of this work.

TABLE OF CONTENT

Abstract i

Acknowledgments iii

Table of Content iv

Figure List vi

Table List xi

Chapter One:

Introduction 1

References of chapter 1 5

Chapter Two:

Photoelectromagnetic Effect 7

2.1 Theory 7

2.2 Experimental 16

2.2.1 Samples 16

2.2.2 Apparatus 20

2.2.3 Experimental procedure 26

2.3 Results and discussions 30

2.3.1 GaAs substrate 31

2.3.2 GaAs epitaxial layer 43

2.3.3 $In_xGa_{1-x}As/GaAs$ quantum well 58

2.3.4 Estimation of the diffusion length of the carriers for substrate and epilayer 60

2.4 Summary 64

2.5 Appendix 66

2.5.1 Estimation of the intensity of the laser output 66

2.5.2 Design and performance of a superconducting coil for PEM measurements at low temperatures 68

References of chapter 2 83

Chapter Three:

Photocurrent and Photovoltaic spectroscopy study in $In_xGa_{1-x}As/GaAs$ quantum wells 85

3.1 Theory 85

3.1.1 Quantum well Energy levels 85

3.1.2 Photoconductivity and photovoltage 91

3.2 Experimental 92

3.2.1 Samples 92

3.2.2 Apparatus 94

3.2.3 Experimental method 96

3.3 Results and discussions 100

3.3.1 PC spectroscopy 101

3.3.2 PV spectroscopy 129

3.4 Summary 136

References of chapter 3 143

Chapter Four:

Conclusion 144

FIGURE LIST

Figure		Page
2.1	PEM Principle	9
2.2	Configuration of the contacts on the samples	18
2.3	The set-up diagram for PEM measurement	21
2.4	The cross-section of the cryostat for PEM experiment	22
2.5	Field-current characteristics of the magnetic-field generator with KEPCO power supply	24
2.6	Field-current characteristics of the magnetic-field with Solid State Model TR36-12M power supply	25
2.7	Schematic of the sample in a three dimensional coordinate system	27
2.8	Diagram of PEM measurement	27
2.9	PEM spectrum for undoped GaAs substrate at T=300K	32
2.10	PEM spectra for undoped GaAs substrate at T=77K	33
2.11	V_{PEM} vs B at T=300K with $\lambda = 871$ nm for undoped GaAs substrate	34
2.12	V_{PEM} vs B at T=300K with λ=632.8 nm for undoped GaAs substrate	35
2.13	V_{PEM} vs B at T=77K with λ=822.5 nm for undoped GaAs substrate	37

Figure		Page
2.14	V_{PEM} vs B at T=77K with λ=632.8 nm for undoped GaAs substrate	38
2.15	V_{PEM} vs I/I_0 (I_0=2450 W/m^2) at T=300K with λ=632.8 nm and B=0.4 T for undoped GaAs substrate	40
2.16	V_{PEM} vs I/I_0 at T=77K with λ=822.3 nm and B=0.4 T for undoped GaAs substrate	41
2.17	V_{PEM} vs I/I_0 (I_0 = 2450 W/m^2) at T=77K with λ = 632.8 nm and B=0.4 T for undoped GaAs Substrate	42
2.18	PEM spectra for GaAs epilayer at T=300K	44
2.19	PEM spectra for GaAs epilayer at T=77K	45
2.20	PEM spectra for GaAs epilayer at T=5K	47
2.21	PEM spectra for GaAs epilayer at T=5K with wavelength from 600 to 850 nm	48
2.22	V_{PEM} vs B at T=300K with λ=871 nm for undoped GaAs epitaxial layer	49
2.23	V_{PEM} vs B at T=300K with λ=514 nm for GaAs epilayer	50
2.24	V_{PEM} vs B at T=77K with λ=822.3 nm for undoped GaAs epitaxial layer	51
2.25	V_{PEM} vs B at T=77K with λ=514 nm for GaAs epilayer	52
2.26	V_{PEM} vs B at T=5K with λ=632.8 nm for GaAs epilayer	53

Figure		Page
2.27	V_{PEM} vs intensity of the light with λ=514 nm at T=300K for epilayer	55
2.28	V_{PEM} vs I/I_0 at T=77K with λ=822.3 nm and B=0.4 T for undoped GaAs epitaxial layer	56
2.29	V_{PEM} vs Intensity of the light with λ =514 nm at T=77K for epilayer	57
2.30	V_{PEM} vs I/I_0 (I/I_0=2450W/m^2) at T=5K with λ=632.8 nm for GaAs epilayer	59
2.31	Light intensity distribution for laser beam	67
2.32	A three dimensional schetch of the superconducting coils' frame	70
2.33	The configuration of the superconducting wire	70
2.34	Definition of angles α, β for the finite coil	73
2.35	Four points (O, A, B, C) in three different types of finite coils	73
2.36	Schematic of the fields at four points (O, A, B, C)	81
3.1a	Possible energy-band configuration in a strained-layer $In_xGa_{1-x}As/GaAs$ quantum well	90
3.1b	Energy-band configuration of a strained $In_xGa_{1-x}As/GaAs$ QW and possible transitions between valence and conduction bands	90
3.2	Configuration of the QW samples' cross-section	93

Figure		Page
3.3	Circuit diagram for PC measurement	95
3.4	Cross-section of the cryostat for PC measurement	97
3.5	A sketch of PV measurement set-up	98
3.6	The circuit for PC measurements	96
3.7	PC spectrum for sample MO96 at T=77K in a dark environment	103
3.8	PC spectra for sample MO96 at T=77K with different voltages applied (V=18--2 volts) in a dark environment	104
3.9	PC spectrum for sample MO96 at T=77K with V=9 volts and with a white DC light on	105
3.10	PC spectrum for sample MO96 at T=300K	106
3.11	PC spectrum for Cr-doped GaAs substrate at T=77K	107
3.12	PC spectra for sample MO97 at T=77K in a dark environment.	111
3.13	PC spectra for sample MO97 at T=77K with DC white light on	112
3.14	PC spectrum for sample MO97 at T=300K	113
3.15	PC spectrum for sample MO98 at T=77K in a dark	117
3.16	PC spectra for sample MO98 at T=77K with different voltages applied (V=9--2 volts) in a dark environment	118
3.17	PC spectrum for sample MO98 at T=77K with DC white light on	119
3.18	PC spectrum for sample MO98 at T=300K in a dark environment	120

Figure		Page
3.19	PC spectrum for sample MO98 at T=300K with DC white light on	121
3.20	PL spectrum for sample MO98 at T=80K	124
3.21	PC spectra for sample MO33 at T=77K	126
3.22	PC spectrum for undoped GaAs substrate at T=77K	127
3.23	PC oscillatory spectra for sample MO33 at T=77K	130
3.24	PC oscillatory spectra for samle MO33 at T=77K	131
3.25	PC oscillatory spectra for sample MO33 at T=77K	132
3.26	PC spectrum for undoped GaAs substrate at T=77K	133
3.27	Blank spectrum from flat Si-detector	134
3.28	PC spectrum for GaAs epilayed at T=77K	135
3.29	PV spectrum for sample MO96 at T=77K in a dark environment	138
3.30	PV spectrum for sample MO96 at T=77K with DC white light on	139
3.31	PV spectrum for sample MO96 at T=77K in a dark environment	140
3.32	PV spectrum for sample MO98 at T=77K	141
3.33	PV spectrum for sample MO33 at T=77K	142

NB: In all graphs where the PEM was measured by AC techniques, values of V_{PEM} should be multiplied by a factor of two.

TABLE LIST

Table		Page
2.1	Growth parameters of quantum well samples	17
2.2	Intrinsic data of the GaAs epilayer	19
2.3	Resistance and conductivity of the GaAs substrate samples under different conditions	60
2.4	Value of μ and D of substrate at T=300K and T=77K	61
2.5	Resistance and conductivity of the GaAs epilayer samples under different conditions	62
2.6	Values of μ and D in the GaAs epilayer at T=300K, T=77K and T=5K	63
2.7	Summary of the results of the carriers' diffusion length from experiment	65
A.1	The practical and theoretical parameters of the superconductor	82
3.1	Samples' parameters for quantum wells	100
3.2	Band parameters from theoretical calculations for sample MO96	101
3.3	Identification of the PC spectral structure for MO96 at T=77K and T=300K	108
3.4	Calculated band structure parameters of sample MO97	110

Table		Page

3.5	Identification of the PC spectral structures for sample MO95 at T=77K and T=300K	115
3.6	Energy band structure parameters from theoretical calculation for sample MO98	116
3.7	Identification of PC spectral structures of sample MO98	122
3.8	Calculated band structure parameters for sample MO33	125
3.9	Identification of PC spectral structures for sample MO33	128

CHAPTER 1
INTRODUCTION

The study of carriers' transport in semiconducting materials is motivated by more than scientific interest and much attention has been paid to that subject. The carriers' diffusion length is an important parameter of studying those transport properties, which determine the character of the semiconducting material.[1.1] The diffusive behaviour of the photocarriers in GaAs substrates and epitaxial layers have been investigated by several methods[1.2] and each of them has its merits and limitations. Using the photoelectromagnetic (PEM) effect to determine the diffusion length of carrier is another way to study the carriers' transport properties. In this work, we performed the PEM effect study in undoped semi-insulating GaAs substrates and epilayers and used this effect to measure the carriers' diffusion length.

The PEM effect was first reported in 1934 by K. Kikion and M. Noskov[1.3] in Cu_2O and explained by J. Frenkel'.[1.4] Later on, B. R. Holenan and C. Hilsum studied the PEM effect in undoped semi-insulating GaAs single crystals.[1.5] In the 1970' s, A. J. BarBarie and E. Fortin carried out an extensive magneto-optical study for Ge and III--V compounds using this PEM effect.[1.6] S. S. Li and C. I. Huang also used the PEM effect to investigate the carriers' photoelectric properties in Cr-doped semi-insulating GaAs.[1.7] More recently, M. J. Pastamation and G. J. Papaioannou studied carriers' recombination processes in semi-insulating

Cr-doped GaAs employing the method of the PEM effect.[1.8]

When a semiconductor crystal is placed in a magnetic field in a Voigt configuration and a beam of light ($h\nu > \varepsilon_g$) is shone on it, an electric potential develops at its boundaries. This effect, called the PEM effect, arises as a result of the Hall effect associated with the diffusion of optically injected carriers. The PEM effect is thus expected to reflect the spectral distribution of the absorption coefficient in a semiconductor and can be used as a spectroscopic technique.

The PEM effect not only can be used to measure some semiconductor parameters, but also has some practical applications in the area of detectors.[1.9] The main advantage of a PEM detector is that it does not require any voltage bias (PC) or any barriers (PV).

In the last two decades, semiconductor material science has experienced a significant revolution. After Esaki and Tsu first reported their proposal of semiconductor superlattices,[1.10] the world has witnessed a marvellous progress in research of semiconductor superlattices and quantum wells. In 1974, Esaki and Dingle carried out the two basic experiments on the electron property of semiconductor heterostructures.[1.11] [1.12] Since then, more and more great efforts have been made toward the realization of artificial semiconductor heterostructures, starting from one-dimension quantum well to the quantum wires (two-dimension quantum well) and quantum dots (three-dimension well) where the carriers' motion is artificially confined in either one, two or three dimensions. Wonderful successes have been achieved in both theoretical and experimental researches. These great progresses

showed the world wide interest in both fundamental research and practical applications. In experimental research, a lot of techniques, such as transport and optics, have brought and keep bringing a wealth of detailed information on the near band edge electronic states of heterostructures.

Since Dingle's optical measurement directly showed the quantization of energy levels in quantum wells, which is the well-known elementary example of quantization in quantum mechanics, many semiconductor heterojunction materials were made and investigated in such field. $Al_xGa_{1-x}As/GaAs$ is one kind of well understood material, while the lattice-mismatched materials such as $In_xGa_{1-x}As/GaAs$ have been studied less extensively than $Al_xGa_{1-x}As$. Recently, more and more attention has been paid to the strain-layer $In_xGa_{1-x}As/GaAs$ system. These strained-layer heterostructures allow the use of lattice-mismatched materials without the generation of misfit dislocations, while showing the great potential for high speed and optoelectronic device applications. Some work has been done in the study of the band structure and quantum levels in strained-layer $In_xGa_{1-x}As/GaAs$ structures and transitions between the levels. Experimentally, various measurements using optical techniques have been conducted such as photovoltaic spectroscopy,[1.13] photocurrent spectroscopy,[1.14] or photoconductivity,[1.15] photoluminescence,[1.16] photoreflectance [1.17] [1.18] and absorption,[1.19] Raman scattering[1.20] etc. Among these methods, photocurrent (PC) measurement is a well known but not the most popular technique. We use this technique to study the PC spectra in $In_xGa_{1-x}As/GaAs$ quantum wells. Also, some PV measurements

have been conducted in the same quantum wells.

In this research project, studies have been focused on the investigation of the PEM effect in GaAs bulk and epilayers as well as $In_xGa_{1-x}As$ quantum wells, and photoconductivity (PC) effect in $In_xGA_{1-x}As/GaAs$ quantum wells. This thesis is composed of four parts. Chapter 1 is the introduction. Chapter 2 describes the study of the PEM effect on GaAs substrates and epitaxial layers and the attempt to investigate the PEM effect on $In_xGa_{1-x}As/GaAs$ quantum wells at room temperature, liquid Nitrogen temperature, and liquid Helium temperature (only for epilayer). This chapter includes a theoretical development explaining how the diffusion length can be obtained from the PEM effect, the experimental details and results as well as discussions. The magnetic-field generator associated with the small optical cryostat is not suitable for the Janis' cryostat. For measrement at 5K, superconducting split magneto-coils with optical access and associated sample holder were designed which can be put into a Janis optical cryostat. The design of the superconductor magneto-coils is described in an appendix of this chapter. Chapter 3 deals with the study of the PC effect in quantum wells at T=300K and T=77K including theoretical treatment, experimental details as well as discussions. A few photovoltaic spectra were plotted for some of these quantum well samples. Finally, a restatement of the major accomplishment of these works and concluding remarks are carried out in chapter 4. The theory and experimental technique parts were individually described in each relevant chapter.

REFERENCES

1. 1 G. W. 't Hooft, C. Van Opdrop, H. Veennvliet, A. T. Vink: J. Cryst. Growth 55, 173-82 (1981).

1. 2 D. K. Wight, P. E. Oliver, T. Printice, V. W. Steward: ibid 55, 183-91 (1981).

1. 3 I. K. Kikoin, M. M. Noskov, Physik Z. Sowajetunion, 5, 585 (1934)

1. 4 J. Frenkel', ibid 5, 597 (1934); 8, 185 (1938).

1. 5 B. R. Holeman and C. Hilsum, J. Phys. Chem. Solids 22, 19 (1961).

1. 6 A. J. Barbarie, E. Fortin, Can. J. Phys. Vol. 50 (14), 1593 (1972).

1. 7 S. S. Li and C. I. Huang, J. Appl. Phys. Vol.43 (4), 1757 (1972).

1. 8 M. J. Papastamation and G. J. Papaioannou, ibid, 68 (3), 1094 (1990).

1. 9 T. S. Moss, G. J. Burrell and B. Ellis, 1973. Semiconductor Opto-Electronics, John Willey and Sons, New York.

1. 10 L. Esaki and R. Tsu, IBM Res. Note, RC-2418 Mar. 1969.

1. 11 L. Esaki and L. L. Chang, Phys. Rev. Lett. 33, 495 (1974).

1. 12 R. Dingle, W, Wigman and C. H. Henry, ibid, 33, 827 (1974).

1. 13 B. Y. Hua, E. Fortin and A. P. Roth, R. A. Masut, Appl. Phys. Lett. 53 (12), (1988).

1. 14 X. M. Fang, X. C. shen, H. Q. Hou, W.Feng, J.M. Zhou and K. Koch, Surface Science 228, 351 (1990).

1. 15 I. J. Fritz, B. L. Doyle, T. J. Drummond, R. M. Biefeld and G. C. Osbourn, Appl. Phys. Lett. 48, 1606 (1986).

1. 16 A. P. Roth, R. A. Masut, M. Sacilotti, P. J. D'Arcy, G. I. Sproule, D.

F. Mitchell and Y. Lepage, Can. J. Phys. 65, 909 (1987).

1.17 S. H. Pan, H. Shen, F. H. Pollak, W. Zhuang, Q. Xu, A. P. Roth, R. Masut, and C. Lacelle, Phys. Rev. B 38, 3375 (1988).

1.18 D. Ji, D. Huang, U. K. Reddy, T. S. Henderson, R. Houdré and H. Morkoc, J. Appl. Phys. 62, 3366 (1987).

1.19 J. Y. Marzin, M. N. Charasse and Sermage, Phys. Rev. B 31 8298 (1985).

1.20 J. Menendez, A. Pinczuk, D. J. Werder, S. K. Sputz, R. C. Miller, D. L. Sivco and A. Y. Cho, ibid, B 36, 8165 (1987).

CHAPTER 2

PHOTOELECTROMAGNETIC EFFECT

This chapter is dealing especially with the PEM effect. We begin by reviewing some of the fundamental theoretical developments concerning the carriers' diffusion length in semiconductors and the relationship between the PEM effect and the applied magnetic field, the intensity of radiation as well as the wavelength of incident light. Follows the description of the equipment, experimental methods, and sample preparation. Finally, the results and discussions of the experiment are given.

2.1 Theory

When the wavelength of a beam of light is in a certain range, it can be absorbed sufficiently strongly by a certain kind of semiconductor. If a beam of this kind of light is incident on the surface of a semiconductor, it will create carriers near the surface of the crystal. This causes a carrier density gradient along the direction of propagation of the light and it will be accompanied by the diffusion of nonequilibrium carriers from the illuminated surface of the sample into the interior. Because of the difference between electron and hole mobilities, there will usually be a potential difference developed in the direction of the diffusion. This is the Dember effect.

If at the same time, a magnetic field is applied across the semiconductor and it is perpendicular to the direction of propagation of the radiation, a Lorentz force which acts on the diffusing carriers will deflect them in the third direction which is at right angle to the directions of both the field and the radiation. Then electrons are accumulated at one side of the semiconductor (a) and holes are accumulated at another side of the semiconductor (b). Consequently, an electric field and a potential difference take place between a and b. This is the Photomagnetoelectric (PEM) effect. The potential difference between a and b is the PEM emf..

As shown in Fig. 2.1, if the diffusion currents are in the direction of the x axis, the magnetic field is along the z axis, the Lorentz forces are developed along the y axis. The components of the current densities in the direction of y are given by:[2.1]

$$i_{ny}=e\mu_n nE_y+\tan\vartheta_n i_{nx} \tag{2.1}$$

$$i_{py}=e\mu_p pE_y-\tan\vartheta_p i_{px} \tag{2.2}$$

$$i_{nx}+i_{px}=0 \tag{2.3}$$

where indices "$_n$" and "$_p$" represent electron and hole. i_{nx}, i_{px}, i_{ny}, i_{py} are the components of the current density along the x and y axes. n and p are the electron and hole concentrations inside the crystal. E_y is the PEM field.

ϑ_n, ϑ_p are the Hall angles:

$$\tan\vartheta_n=\mu_n B \tag{2.4}$$

$$\tan\vartheta_p=\mu_p B \tag{2.5}$$

We assume that the magnetic field B is so weak that it does not cause other

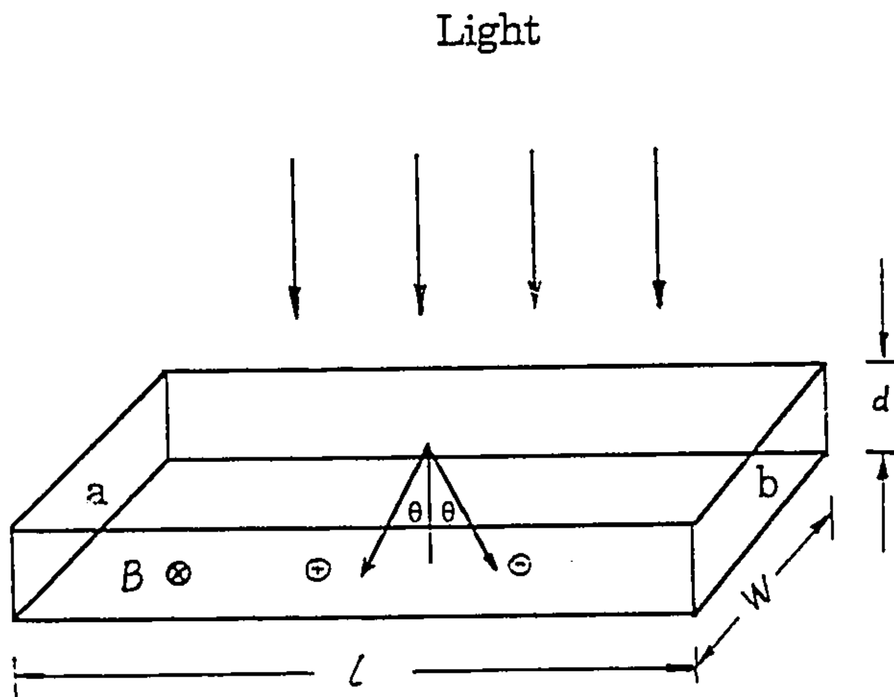

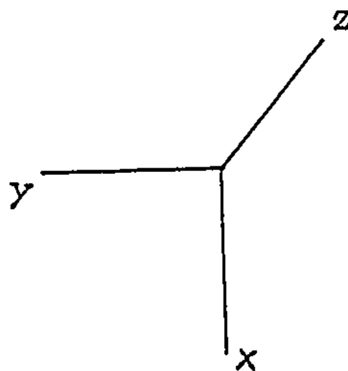

Fig. 2.1 PEM principle

magnetic effects such as Landau splitting of the band etc..

In the short circuit conditions (E_y=0), the total current along the y direction is:

$$I_{SC}=W\int_0^d (i_{ny}+i_{py})dx$$

$$=W(\tan\theta_n+\tan\theta_p)\int_0^d i_{px}dx$$

$$=WB(\mu_n+\mu_p)\int_0^d i_{px}dx \qquad (2.6)$$

Here d and W are the thickness and width of the sample respectively, and i_{px} can be solved as:[2.2]

$$i_{px}=-eD\frac{d\Delta p}{dx} \qquad (2.7)$$

where D is the diffusion coefficient and Δp is the change in hole concentration.

For the open circuit case (i_{ny}=0, i_{py}=0), the PEM voltage can be derived from the following:

From equations (2.1), (2.2). (2.3), we get:

$$e(\mu_n n+\mu_p p)E_y=(\tan\theta_n+\tan\theta_p)i_{px} \qquad (2.8)$$

considering of (2.4) and (2.5), the following equation can be derived:

$$e(\mu_n n+\mu_p p)E_y=B(\mu_n+\mu_p)i_{px}$$

or:

$$e[\mu_n(n_0+\Delta n)+\mu_p(p_0+\Delta p)]E_y=B(\mu_n+\mu_p)i_{px} \qquad (2.9)$$

where Δn is the change in electron concentration.

Rearranging both side of the above equation, we have:

$$[\sigma_0+e(\mu_n\Delta n+\mu_p\Delta p)]E_y=B(\mu_n+\mu_p)i_{px} \tag{2.10}$$

where $\sigma_0=e(\mu_n n_0+\mu_p p_0)$ is the dark conductivity; n_0 and p_0 are the concentrations of carriers in the absence of illumination.

Integrating both sides of this equation over x with E_y constant:

$$\int_0^d [\sigma_0+e(\mu_n\Delta n+\mu_p\Delta p)]E_y dx=\int_0^d B(\mu_n+\mu_p)i_{px}dx$$

or:

$$[\sigma_0 d+e\int_0^d (\mu_n\Delta n+\mu_p\Delta p)dx]E_y=B(\mu_n+\mu_p)\int_0^d i_{px}dx \tag{2.11}$$

E_y can thus be expressed as follows:

$$E_y=\frac{B(\mu_n+\mu_p)\int_0^d i_{px}dx}{\sigma_0 d+e\int_0^d (\mu_n\Delta n+\mu_p\Delta p)dx} \tag{2.12}$$

Therefore:

$$V_{PEM}=E_y l=\frac{lB(\mu_n+\mu_p)\int_0^d i_{px}dx}{\sigma_0 d+e\int_0^d (\mu_n\Delta n+\mu_p\Delta p)dx} \tag{2.13}$$

Where l is the sample's length.

Under condition of approximate neutrality: $\Delta p = \Delta n$, (2.13) becomes:

$$V_{PEM} = \frac{lB(\mu_n + \mu_p)\int_0^d i_{px}dx}{\sigma_0 d + e(\mu_n + \mu_p)\int_0^d \Delta p dx} \qquad (2.14)$$

Substituting equation (2.7) into the above equation, we get:

$$V_{PEM} = \frac{lB(\mu_n + \mu_p)\{-eD\int_{\Delta p(0)}^{\Delta p(d)} d\Delta p\}}{\sigma_0 d + e(\mu_n + \mu_p)\int_0^d \Delta p dx}$$

or:

$$V_{PEM} = \frac{lBeD(\mu_n + \mu_p)[\Delta p(0) - \Delta p(d)]}{\sigma_0 d + e(\mu_n + \mu_p)\int_0^d \Delta p dx} \qquad (2.15)$$

Now let's consider two very different situations:

(1) At low excitation level ($\Delta p \ll p_0$, $\Delta n \ll n_0$):

The second term in the denominator of equation (2.14) or (2.15) can be neglected. Together with equation (2.6), there is a relationship between V_{PEM} and I_{sc}:

$$V_{PEM} = \frac{l}{Wd}\frac{I_{sc}}{\sigma_0} \qquad (2.16)$$

In the presence of a magnetic field B, the carriers diffuse into the crystal in two opposite directions through the Hall angle (Fig. 2.1). The displacement of carriers along the x direction is: $L_D\cos\theta = L_D\cos\mu B \approx L_D$ with $\mu B \ll 1$, which will give a charge contribution Δq to the component of current density i_{px} along x direction:

$$\Delta q = \frac{eL_D}{d} \tag{2.17}$$

Since $i_{px} \propto \Delta q$ and $i_{px} \propto I$ (I is the intensity of illumination), we have:

$$i_{px} = -i_{nx} = \beta I \Delta q = \beta I \frac{eL_D}{d} \tag{2.18}$$

where β is the quantum yield.

Substituting above expression of i_{px} into equation (2.6) and integrating it over x, I_{sc} can be expressed as follows:

$$I_{SC} = W\beta IBe(\mu_n+\mu_p)L_D \tag{2.19}$$

Therefore equation (2.16) becomes:

$$V_{PEM} = \frac{l}{d} \cdot \frac{\beta IBe(\mu_n+\mu_p)L_D}{\sigma_0} \tag{2.20}$$

i.e. the PEM voltage is proportional to I and B. From the slope of V(I) or

V(B), the diffusion length L_D can be calculated.

(2) At high excitation level ($\Delta p \gg p_0$, $\Delta n \gg n_0$):

The first term in the denominator of equation (2.14) or (2.15) can be neglected:

$$V_{PEM}=\frac{IDB[\Delta p(0)-\Delta p(d)]}{\int_0^d \Delta p dx} \tag{2.21}$$

Since the density of non-equilibrium carriers decreases along the x axis in accordance with:

$$\Delta p(x)=\Delta p(0)e^{-x/L_D} \tag{2.22}$$

at the unilluminated surface (back surface) x=d, we have:

$$\Delta p(d)=\Delta p(0)e^{-d/L_D} \tag{2.23}$$

We integrate both side of equation (2.22):

$$\int_0^d \Delta p(x)dx=\Delta p(0)L_D(1-e^{-d/L_D}) \tag{2.24}$$

Bringing equation (2.23), (2.24) into equation (2.21), yields:

$$V_{PEM}=\frac{IDB}{L_D} \tag{2.25}$$

which demonstrates that V_{PEM} is independent of I.

Considering both equations (2.20) and (2.25), we have a general expression for V_{PEM}:

$$V_{PEM}=\frac{AI}{K+I} \tag{2.26}$$

where A, K are the constants as far as I is concerned.[2.2]

Also, the relationship between V_{PEM} and B under two different conditions can be written as:[2.3] [2.4] [2.5]

(1) In the case of high surface recombination, i.e. the velocity of carriers' recombination at the surface is high:

$$V_{PEM}=C\frac{B}{1+(\mu B)^2} \tag{2.27}$$

(2) In the case of low surface recombination, i.e. the velocity of the carriers' recombination at the surface is low:

$$V_{PEM}=C'\frac{B}{[1+(\mu B)^2]^{1/2}} \tag{2.28}$$

Both C and C' are the constants; μ is the effective combined mobility; its value is not much different from the value of $(\mu_n+\mu_p)$.[2.3]

In equation (2.27), when $(\mu B)^2 \ll 1$, V_{PEM} is proportional to B, while for $(\mu B)^2 \gg 1$, V_{PEM} is proportional to 1/B. Differentiating equation (2.27) with

respect to B, one can find that when $B=\pm1/\mu$, V_{PEM} reaches a maximum. Therefore, from the relationship between V_{PEM} and B, once the special B which corresponds to the maximum V_{PEM} is found, the carriers' mobility μ can be determined since $\mu=|1/B|$.

In equation (2.28), when $(\mu B)^2 \ll 1$, then $V_{PEM} \propto B$, and when $(\mu B)^2 \gg 1$, V_{PEM} is independent of B, which means that at high B, V_{PEM} reaches saturation.

2.2 Experimental

2.2.1 Samples

In this section, several samples have been studied. One is an undoped semi-insulating GaAs substrate (100) about 0.5 mm thick; another one is a pure GaAs epitaxial layer (100) with thickness of 3.4 μm grown by metal-organic chemical vapour deposition (MOCVD) on the same substrate as above. The quantum well samples which have been tried are $In_xGa_{1-x}As/GaAs$ single quantum wells (SQW) or multiple quantum wells (MQW). The parameters of these samples are descibed in Table 2.1.

Sample	Substrate	x	Well width L_W (nm)	Barrier width L_B (nm)	Periods
MO33(SQW)	undoped	0.22	5	----------	----------
MO96(SQW)	Cr--doped	0.15	3.5	----------	----------
MO97(SQW)	Cr--doped	0.15	8	----------	----------
MO98(MQW)	Cr--doped	0.15	8	10	5

Table 2.1 Growth parameters of quantum well samples

(1) GaAs Substrate

This sample is an undoped semi-insulating GaAs substrate (100) with a dark resistivity ρ of about $10^7 \Omega cm$. It was cut in length of 7 mm, width of 2mm and thickness of 0.5mm. The sample was well polished in advance so that only chemical etching was performed; the etch solution components are H_2SO_4-H_2O_2-H_2O (1:8:160). For (100) GaAs, the etch rate is $43 Å s^{-1}$[2.6]. The sample was immersed into the solution for about 2 seconds and it was immediately washed in distilled water.

The ohmic contacts consisted of two clean indium drops, in parallel configuration on the top of the sample (Fig.2.2a), melted into the sample in a vacuum oven at a temperature of 300°C.[2.6] [2.7] The heating process lasts about 10 to 15 minutes. Gold wires were soldered on the two indium drops. The distance between two contacts is about 4 mm.

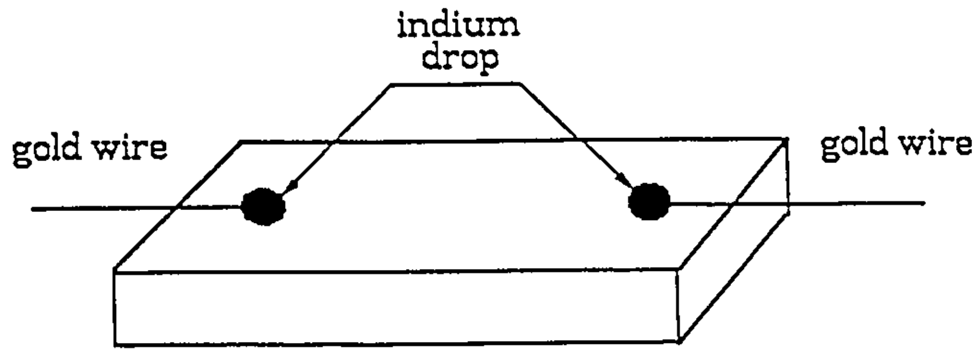

(a)

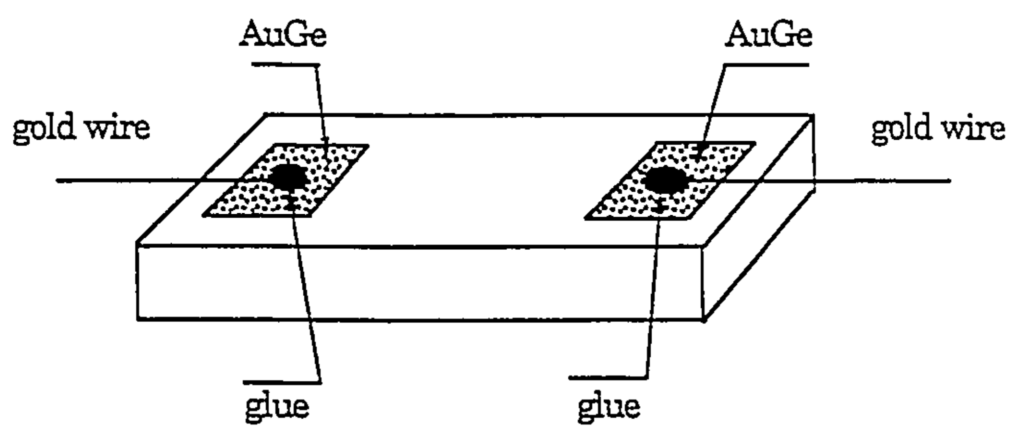

(b)

Fig. 2.2 Configuration of the contacts on the samples.

(2) GaAs Epitaxial Layer

The pure GaAs epitaxial layer was grown by MOCVD on the same substrate as above. The thickness of the layer is 3.4μm. The sample was cut into a parallelepiped of dimensions of $5.0 \times 1.5 \times 0.5 mm^3$. The surface of the layer is of optical quality so that no chemical etching is required. The two ohmic contacts of the sample consist of two evaporated AuGe layers of thickness 152Å (Fig. 2.2b). They were first deposited in a high vacuum environment, then annealed in a vacuum oven at temperature 450°C for about 4-5 minutes.[2.7] [2.8] After these, ABLEBOND 84-1LMI glue was used to connect two gold wires to the two electrodes by means of curing for 1 hour at a temperature of 150°C in a vacuum oven. The distance between two contacts is about 2.5 mm.

Some intrinsic data which come with the sample are given in Table 2.2.

	T=300K	T=77K
concentration n(cm^{-1})	2×10^{14}	1×10^{14}
mobility μ($cm^2V^{-1}s^{-1}$)	500	75,000

Table 2.2 Intrinsic data of the GaAs epilayer sample

(3) $In_xGa_{1-x}As$/GaAs Quantum Wells

As mentioned before, those quantum well samples are either SQW or MQW samples. They were cut into parallelepiped of 6mm×2mm. The

contacts to those samples are the same type as for the epilayer, but are made at NRC by the lift-off-Chlorobenzene process.[2.9]

2.2.2 Apparatus

The whole experimental set-up is shown in Fig. 2.3. It consists of an optical cryostat either the Janis cryostat (4.2-300K) or a smaller cryostat where the temperature can be adjusted only from room temperature to liquid Nitrogen temperature; a light source which can be a DIGIKROM 240 monochromator, a McPherson monochromator, a UNIPHASE He--Ne laser (2.5mW), a MELLES GRIOT He--Ne laser (7.7mW) or an Ion--Argon laser (5W); a magnetic--field generator with a KEPCO power supply or Solid State Model TR36--12M power supply, or a superconducting coil; an ITHACO//NF 3921, PAR. Model 122 or PAR. model 124 lock-in amplifier and a WATANABE WX4420 x-y chart recorder or a computer.

Also, a turbo--Alcatel pump was used to produce the high vacuum for the cryostats and a *Veeco* Model 7710 Cryo-Pumped vacuum evaporator system was used when making the contacts to the sample.

The small optical cryostat was made from plan of Dr. E. Fortin by the Physics shop of the University of Ottawa.[2.10] It was made of stainless steel and copper, with the lower outer portion of the cryostat having a detachable tail-piece fitted with a quartz window. The tail can easily fit within magnet poles. At liquid nitrogen temperature, the vacuum otained was about 10^{-6} Torr using the Turbo (Alcatel) pump. Fig. 2.4 shows a cross sectional diagram of the cryostat.

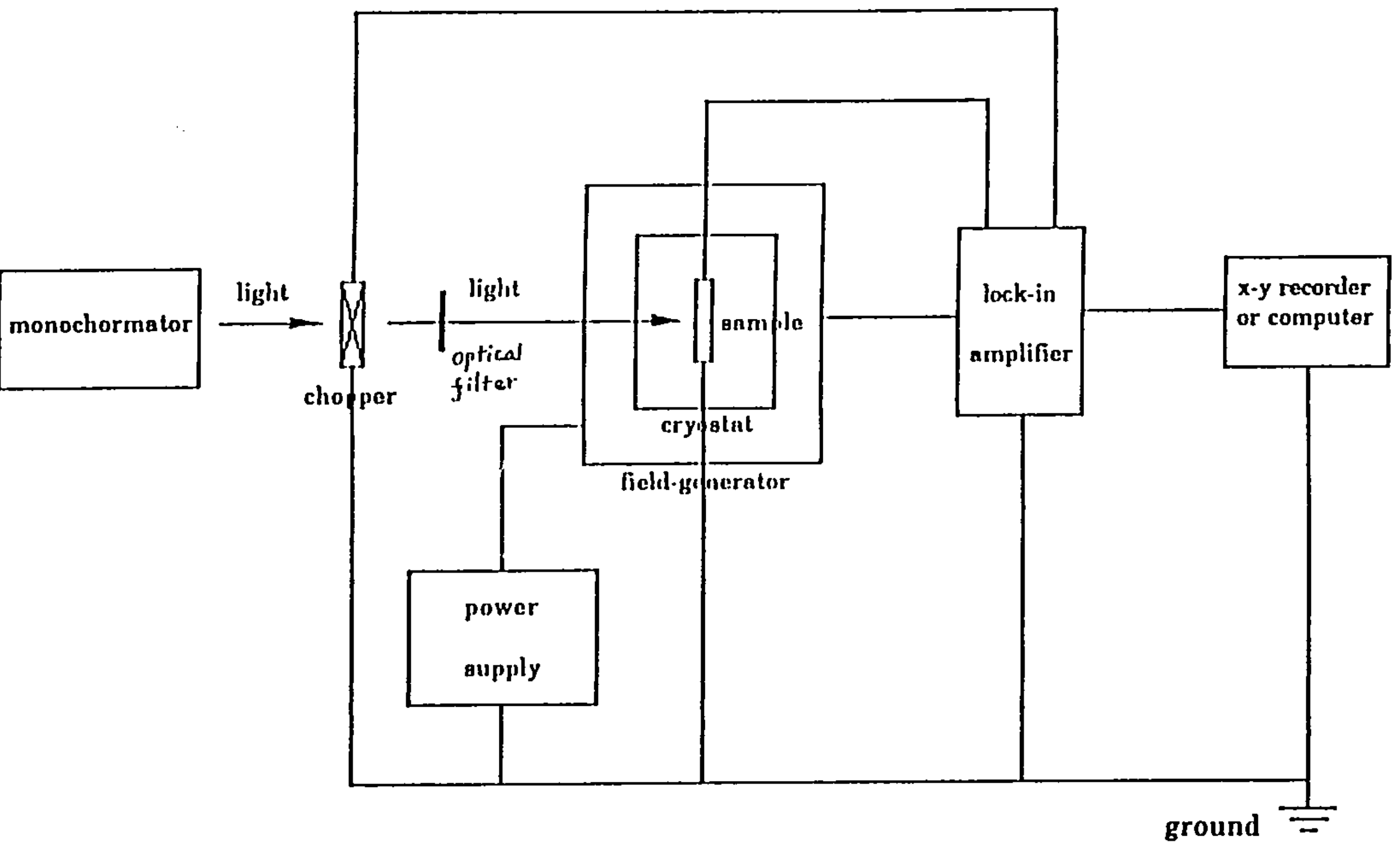

Fig. 2.3 The set-up diagram for PEM measurements

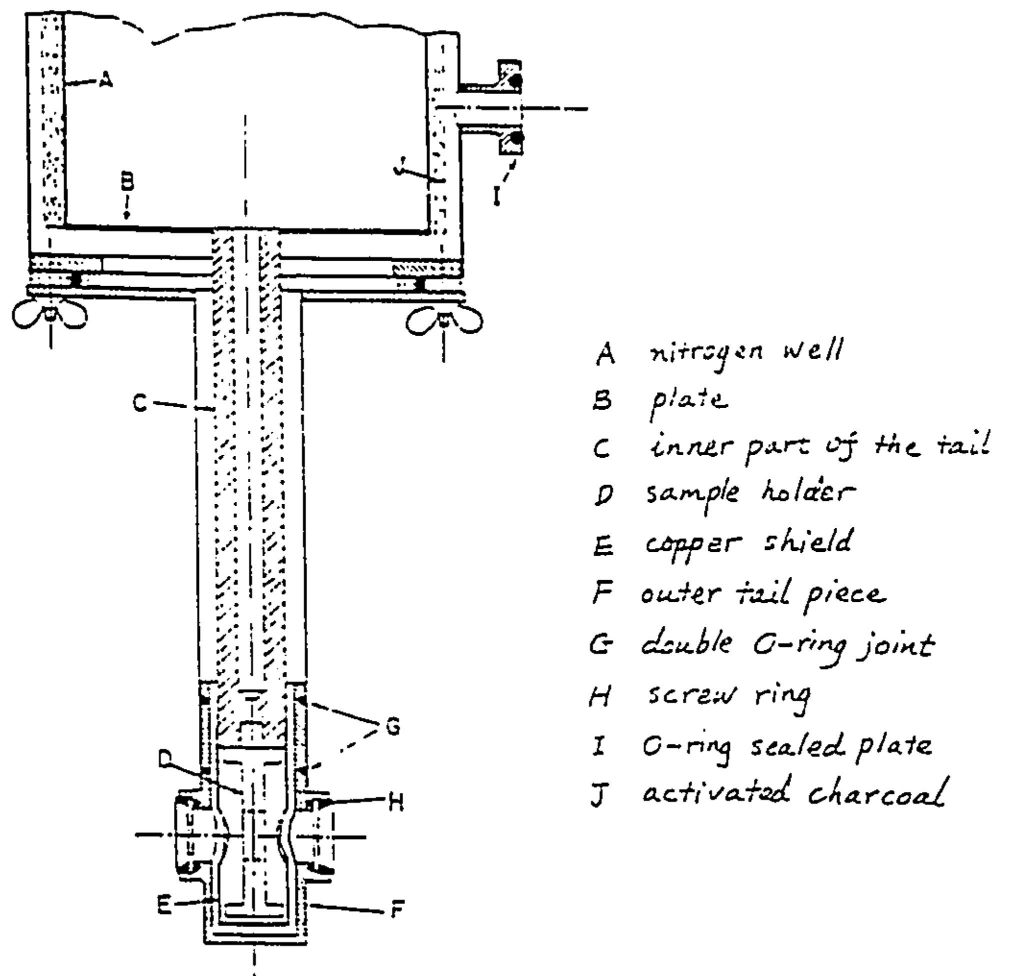

Fig. 2.4 The cross-section of the cryostat for PEM experiment.

A 30 Watts tungsten halogen projector lamp was used as an infrared source via a monochromator. The grating of the DIGIKROM 240 has 1200 grooves/mm, giving a reciprocal linear dispersion is 32Å/mm and a resolution of 0.6Å with 20 micron slits with the grating in first order. With respect to the McPherson monochromator, its grating has 1200 grooves/mm, the dispersion is 0.833nm/mm and the resolution is 0.01nm with slits of 8 microns. An optical filter with threshold at 0.66μm was placed between the lamp and monochromator to cut off the second order radiation, both the power and the wavelength of the Ion-Argon laser are adjustable and the wavelength used was chosen at 514nm.

Lock-in amplifier techniques were used to detect and amplify the PEM signal. The chopper produces A.C. light at a chosen frequency of 170Hz so that lock-in techniques can be used. The amplified signal was recorded on a x-y chart recorder or a computer.

The sample was put between two poles of the generator where the magnetic field was produced. A Gauss meter was used to calibrate the magnetic field. The field-current characteristics of the magnetic-field generator are shown in Fig. 2.5 and Fig. 2.6.

For liquid Helium temperature experiments, a Janis' optical cryostat was used. In this case, a small superconducting split magnet-coils was used and it was placed into the tail of the Janis to generate the magnetic field. A more complete description is given in Appendix (§2.5.2).

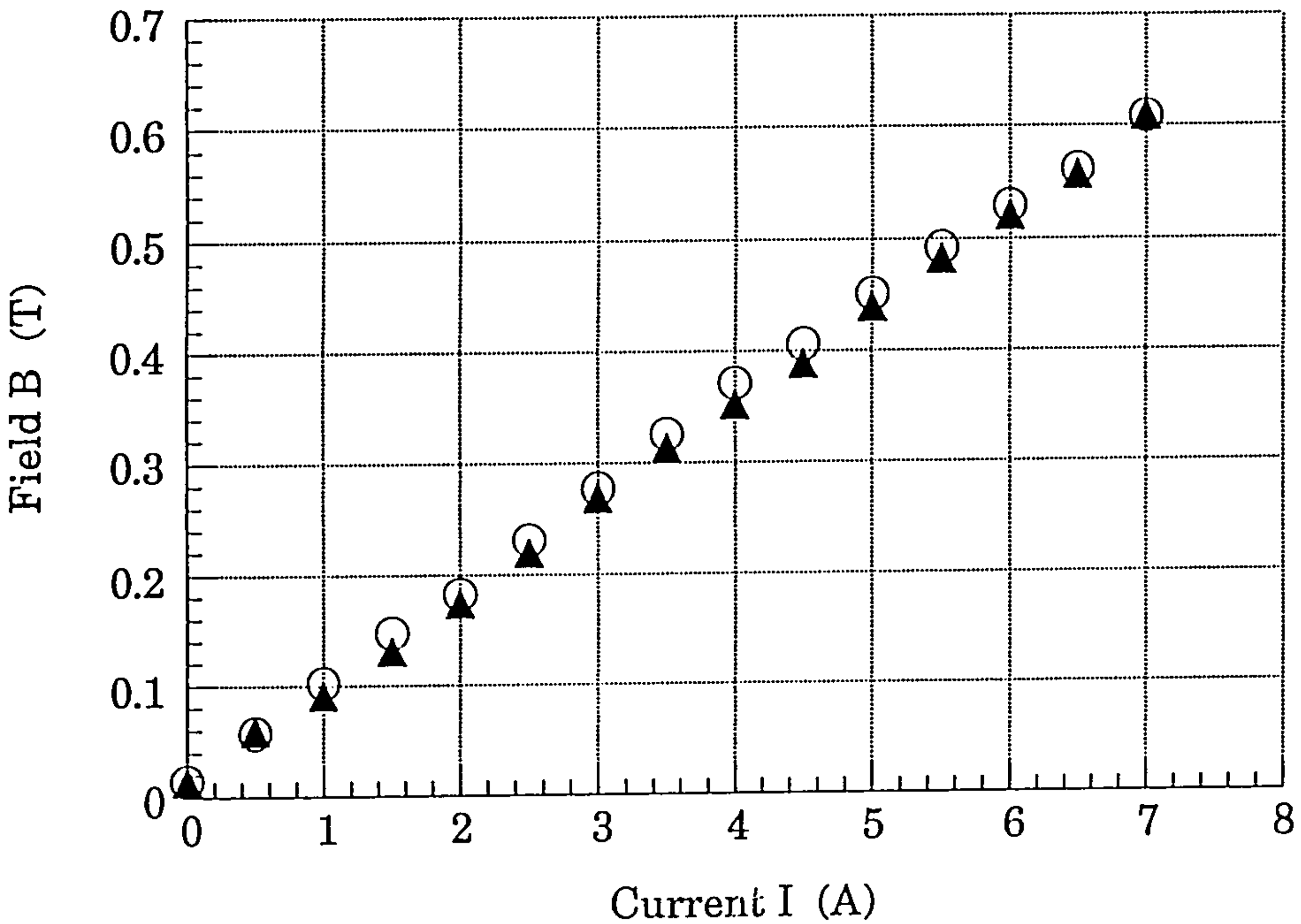

Fig. 2.5 Field-current characteristics of the magnetic-field generator with KEPCO power supply. ▲: current increases; ○: current decreases.

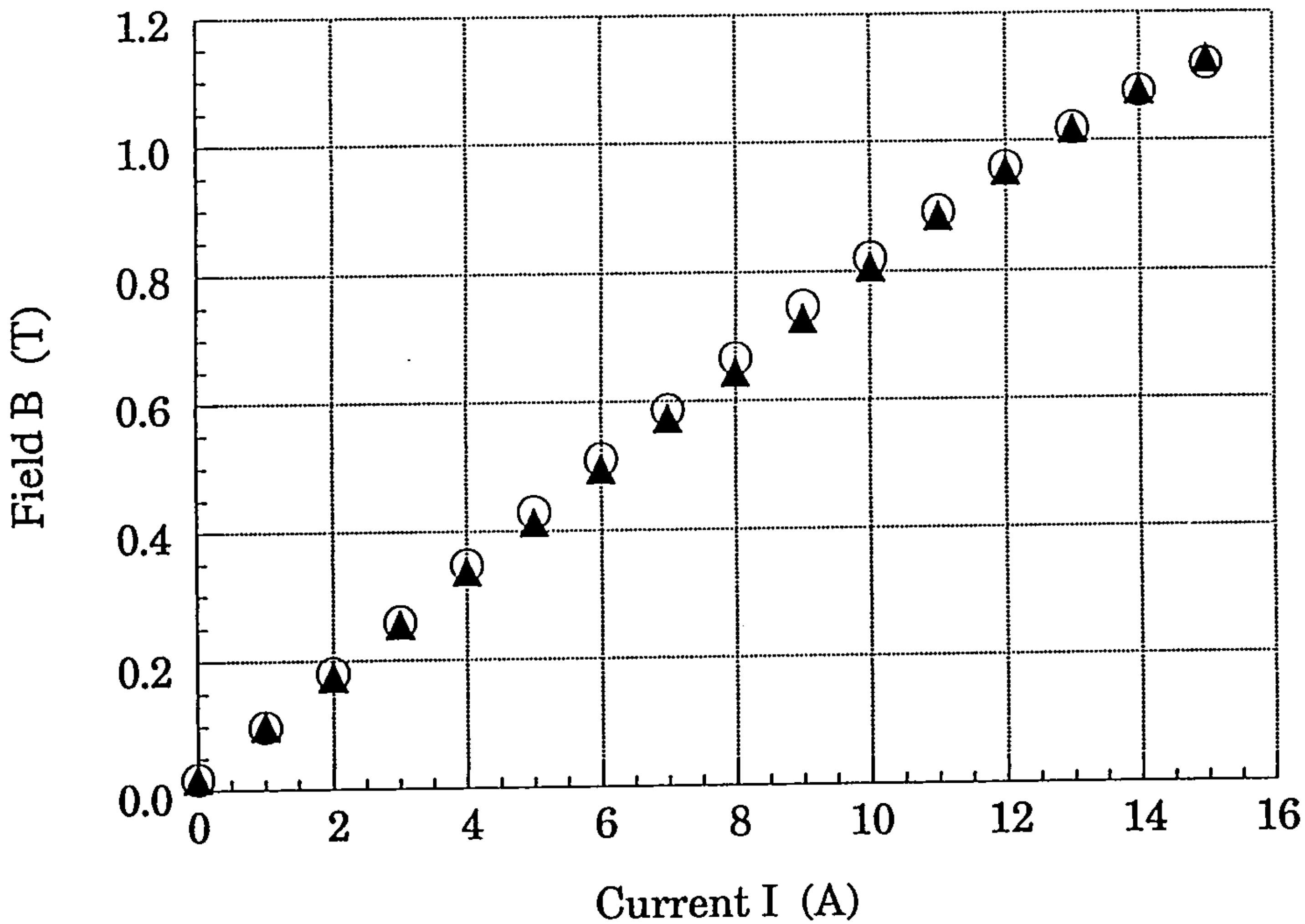

Fig. 2.6 Field-current characteristics of the magnetic-field generator with Solid State Model TR36-12M power supply. ▲: I increases; ○: I decreases.

2.2.3 Experimental procedure

In this part of the project, an extensive study of the PEM effect was carried out layer by layer. First, the undoped GaAs substrate was investigated , then the pure GaAs epitaxial layer on the same substrate was studied, finally, the quantum well samples grown on both undoped and Cr--doped substrates were tried.

In both substrate and epilayer measurements, at room and liquid Nitrogen temperatures, the tail of the cryostat was put between the two poles of the electromagnet and the sample was mounted into the tail of the cryostat shown in Fig. 2.4. If the sample's length is along the y axis, its width along the z axis, and its thickness along the x axis, then the magnetic field will be in the direction of z axis and the light will shine perpendicularly on the yz surface of the sample along the x axis as shown in Fig. 2.7.

In the epilayer measurements at liquid Helium temperature, the superconducting split-coils were put into the Janis' cryostat's tail in such a way that the magnetic field produced by the coils crosses the sample in the same direction as in Fig. 2.7.

(1) GaAs substrate

For the substrate measurements, the lock-in amplifier used was the ITHACO//Nf 3291. Its input impedance is 100KΩ. But the dark resistance of the sample is very high, about $10^9\Omega$ at T=300K and $10^{10}\Omega$ at T=77K. Therefore the lock-in amplifier acts as a current meter. The original data

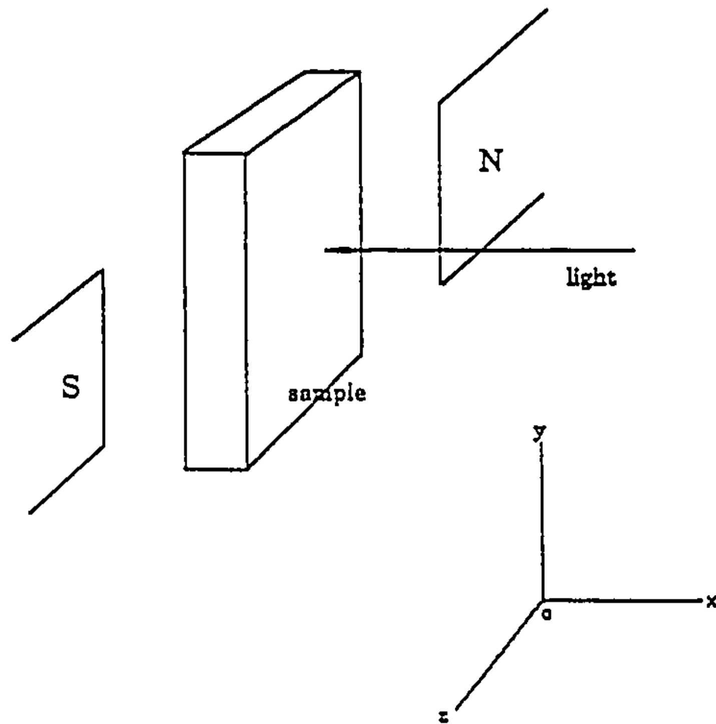

Fig.2.7 Schematic of the sample in a three dimensional coordinate system.

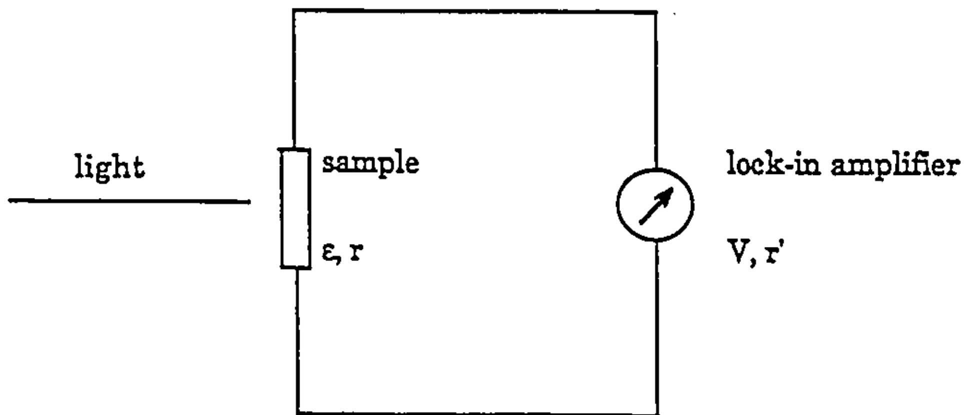

Fig. 2.8 Diagram of PEM measurement

from the experiment is the voltage across the lock-in amplifier. Suppose the impedance of sample is r, and the input impedance of the lock-in amplifier is r' (Fig.2.8), using the loop theorem: $\varepsilon = Ir+V$, the $V_{PEM}=\varepsilon$ can be obtained as $V_{PEM}=V(r'/r)$, with $r \gg r'$, and $V=2V_{measured}$, where $V_{measured}$ is the potential measured by the lock-in amplifier (Because the lock-in measures the average of the square wave).

The impedance of the sample depends on the wavelength and intensity of the stimulating light as well as the temperature. As the magnetic fields used are small, the change of impedance caused by the field is very small compared with that caused by the other two factors mentioned above.

All experiments were carried out in a dark room in order to reduce the effect of unnessary noise caused by stray light. The following measurements have been performed:

A. PEM spectra

$$V_{PEM}=f_{I,B}(\lambda) \quad \text{at } T=300K \text{ and } T=77K$$

In these measurements, the intensity of the light and magnetic field were fixed, the wavelength of the light was scanned by using the monochromator, from 850nm to 900nm at room temperature and from 800nm to 850nm at liquid Nitrogen temperature, i.e. from above bandgap energy to below bandgap energy. From the spectra, we can get a general overview of the sample characteristics useful for later measurements.

B. Change of PEM Voltage with Field B

$$V_{PEM}=f_{I,\lambda}(B) \quad \text{at } T=300K \text{ and } T=77K$$

The purpose of these experiments is to determine how the PEM voltage evolves with magnetic field so that a proper B value can be chosen in a linear part of the V_{PEM}--B curve for the use in subsequent measurements (step C). Both the intensity and wavelength of the light were fixed. The wavelength was chosen at different values: shorter than bandgap wavelengths and longer than bandgap wavelengths. The magnetic field B was raised from 0 to 0.6T.

C. Change of PEM Voltage with Intensity I

$$V_{PEM}=f_{\lambda,B}(I) \quad \text{at } T=300K \text{ and } T=77K$$

The intensity of the light was varied by inserting one or several calibrated neutral density filters in front of the sample. The wavelength of the light and the magnetic field were fixed. In this way the relationship between V_{PEM} and I was investigated. From this relationship, the sample's excitation state in this experimental condition can be known so that the carrier's diffusion length can be determined.

(2) GaAs epitaxial layer

Both A.C. and D.C. measurements were performed during this epilayer experiment. In A.C. measurements, the lock-in amplifier used was either the ITHACO//NF3921 or the PAR. Model 122. Their input impedances are 100KΩ and 10KΩ, respectively. The impedance of the sample is about 33KΩ at T=300K in darkness and about 8KΩ at T=77K in darkness, which is not

much different from the impedance of the lock-in amplifiers. Hence, both the impedances from the sample and look-in amplifier contribute to the equation $V_{PEM}=V(r+r')/r$ with $V=2V_{measured}$ (Fig. 2.8). In D.C. measurements, the 602 Keithley Solid State electrometer was used. It acts as a volt meter as its impedance is about $10^{14}\Omega$, much greater than sample's impedance. In that case $V_{PEM}=V_{measured}$.

At liquid Helium temperature, the sample's impedance is about $2.5M\Omega$ in darkness. The PAR. Model 124 Lock-in amplifier with an input impedance of $100M\Omega$ was used. In this case the amplifier acts as a volt meter and $V_{PEM}=2V_{measured}$. All measurements were carried out in a dark room.

As for the substrate, three types of experiments have been done for this sample: PEM spectra, PEM dependence on field B as well as on the intensity of the light I. The purpose was the same as for the substrate experiment.

2.3 Results and Discussions

In this section, the experimental results of the PEM effect for the samples of substrates, epilayers and quantum wells will be presented and discussed. Also from the relationship between V_{PEM} and I, or between V_{PEM} and B, the carriers' diffusion length in both samples (undoped GaAs substrate and undoped GaAs epitaxial layer on same substrate) will be estimated.

2.3.1 GaAs Substrate

(1) PEM spectra

As shown in Fig. 2.9, at room temperature, there is only one absorption peak at λ=871 nm or E_g=1.424eV which is just the GaAs intrinsic energy gap at T=298K. At liquid Nitrogen temperature (Fig.2.10), it was found that there are four broad peaks. Among them, A may be the effect of LO phonon related oscillations (it will be observed again in the PEM spectra of the epilayer at both T=77K and T≈5K), B (λ=822.3 nm or E_g=1.508 eV) of course is the intrinsic energy gap of GaAs at T=77K, C (λ=827 nm or E=1.449 eV) and D (λ=832 nm or E=1.490 eV) which are about 9 meV and 18meV lower than E_g and are possibly caused by the impurity levels in the band gap. The energy binding the electron to the impurity can be calculated out as: $E_i \approx 13.6\times(m^*/m_0\varepsilon^2 n^2)$eV which is smaller than 0.1eV with $m^*/m_0 \le 1$, $n \ge 1$ and ε of the order of 10, (m^* is the effective electron mass, m_0 is the free electron mass, n is the quantum number and ε is the dielectric constant of the crystal).

(2) Dependence of V_{PEM} on B

Fig. 2.11 and Fig. 2.12 present the relationship between V_{PEM} and B at room temperature. The incident light wavelength was kept at either λ=871 nm (from the monochromator) or λ=632.8 nm (from the He-Ne laser). From

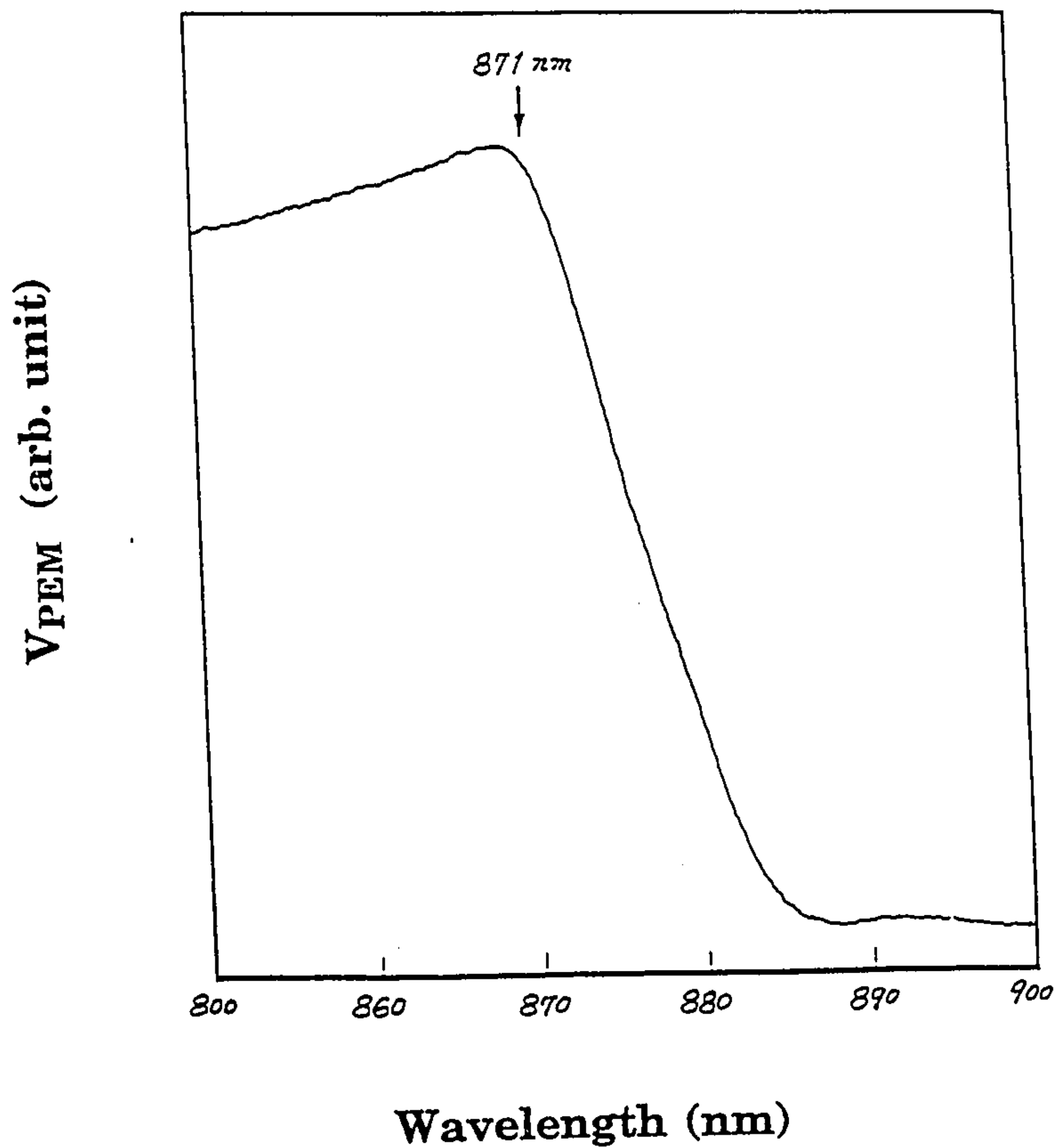

Fig. 2.9 PEM spectrum for undoped GaAs substrate at T=300K

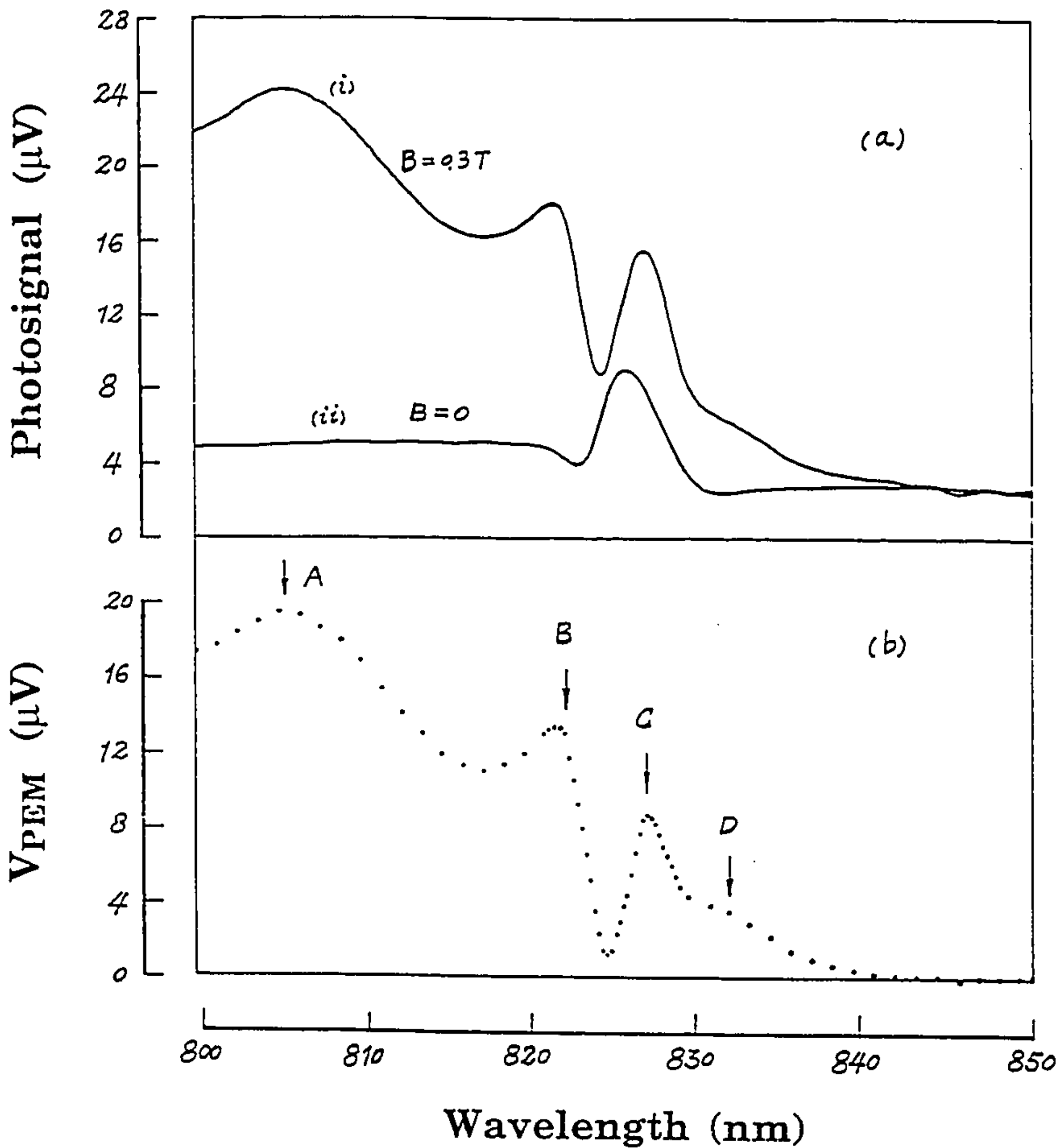

Fig. 2.10 PEM spectra for undoped GaAs substrate at T=77K. Graph (a) are the photosignal spectra with (i) B=0.3T and (ii) B=0 (background). Graph (b) is PEM spectrum which was obtained from subtracting the value of (i) and (ii) in graph (a).

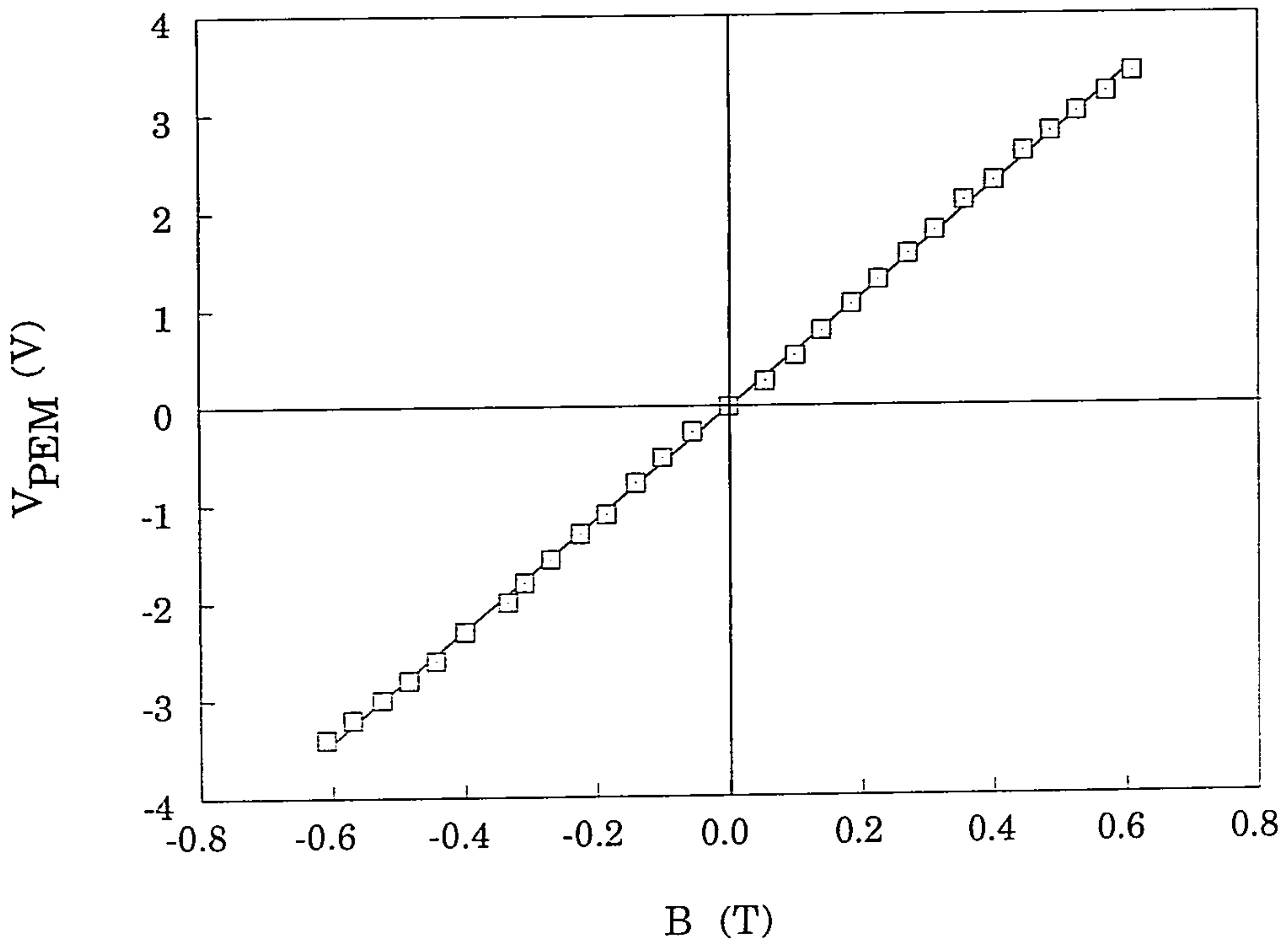

Fig. 2.11 V_{PEM} vs B at T=300K with λ=871 nm for undpoed GaAs substrate

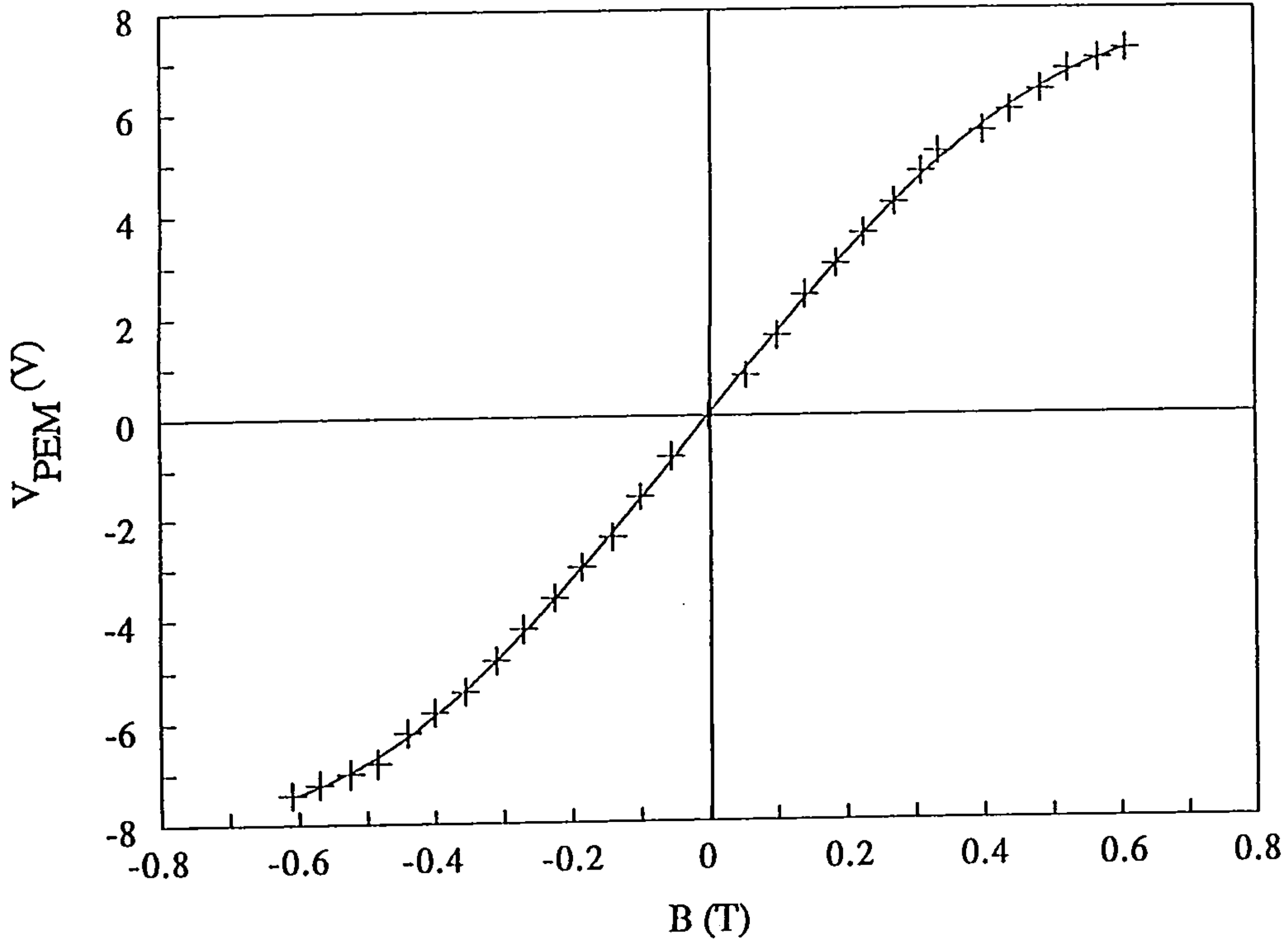

Fig.2.12 V_{PEM} vs B at T=300K with λ=632.8 nm for undoped GaAs substrate

Fig. 2.12 one can see that at low B, V_{PEM} is linear in B. This is in agreement with equation (2.27) and (2.28) at small B value. As B is increased, the straight lines start to level out. This is probably because as B increases, μB or $\omega\tau>1$ so that the carriers go through a significant part of an orbit between collisions: in this situation the PEM effect will decrease. That also follows from the theoretical considerations expressed in equations (2.27) and (2.28).

Fig. 2.13 and 2.14 show the relationship between V_{PEM} and B at liquid Nitrogen temperature. Again, the wavelength of the incident light was fixed at either λ =822.3 nm or at λ =632.8 nm. Fig. 2.13 is for illumination at λ =822.3 nm, and shares similar features with Fig. 2.12 and can be explained from analogous arguments. The more interesting thing is that in Fig. 2.14 which gives the graph of V_{PEM} vs B at T=77K and λ=632.8 nm (from He-Ne laser), the PEM effect increases linearly with B at the beginning, then starts to level out and eventually decreases. If we take the derivative of equation (2.27) and let it equals to zero, we can find that at $B=\pm 1/\mu$, B reaches maximum. When $|B|<1/\mu$, V_{PEM} is proportional to B, and when $|B|>1/\mu$, V_{PEM} is proportional to 1/B. This is the case for the result of Fig. 2.14. Since equation (2.27) is the one under condition of high carriers' surface recombination, we can assume that the results of Fig. 2.14 indicate a high surface recombination for this sample. But in the other three graphs that have been discussed, there is no maximum. Those are relevant with equation (2.28) in which V_{PEM} only reaches a saturation.

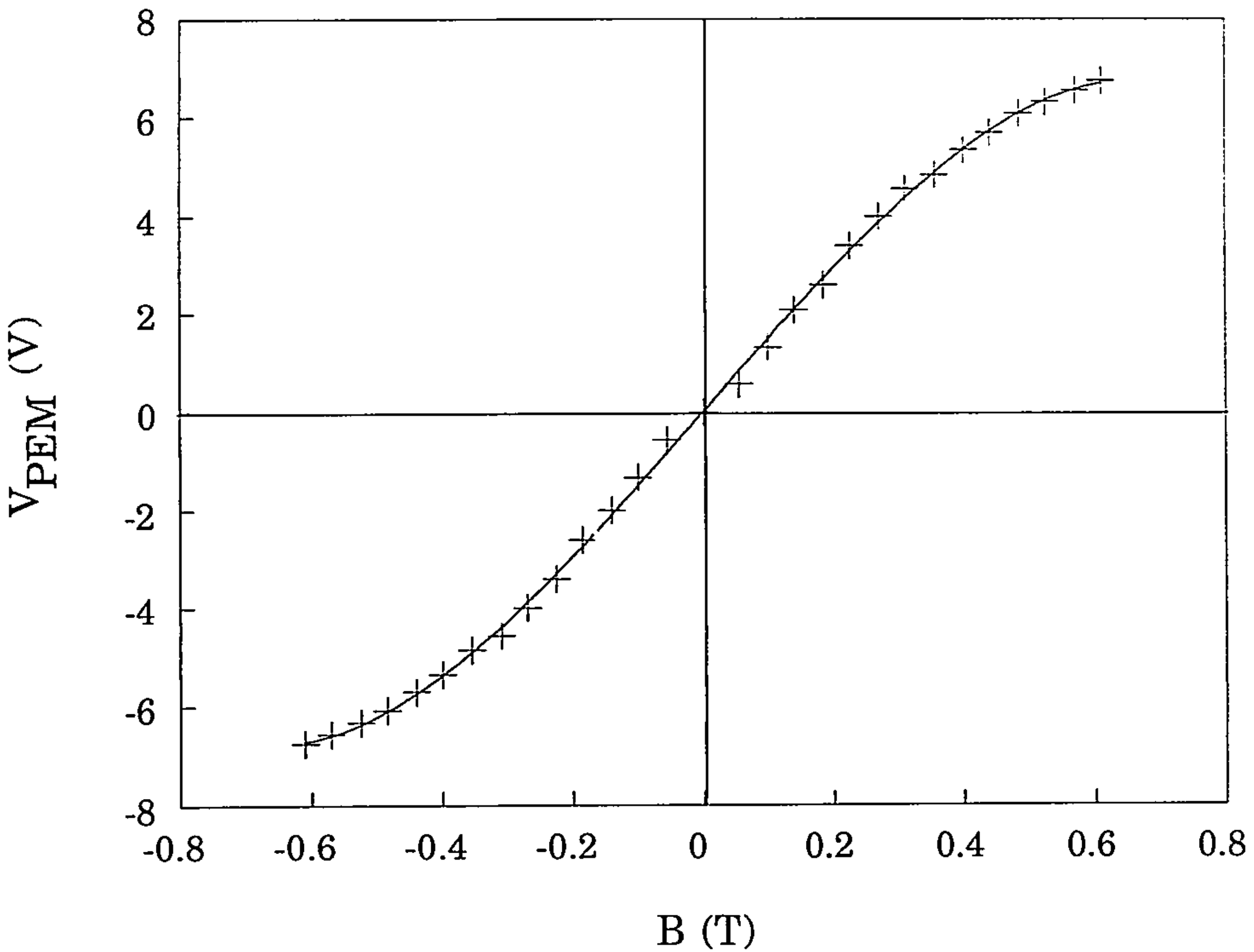

Fig. 2.13 V_{PEM} vs B at T=77K with λ=822.3 nm for undoped GaAs substrate

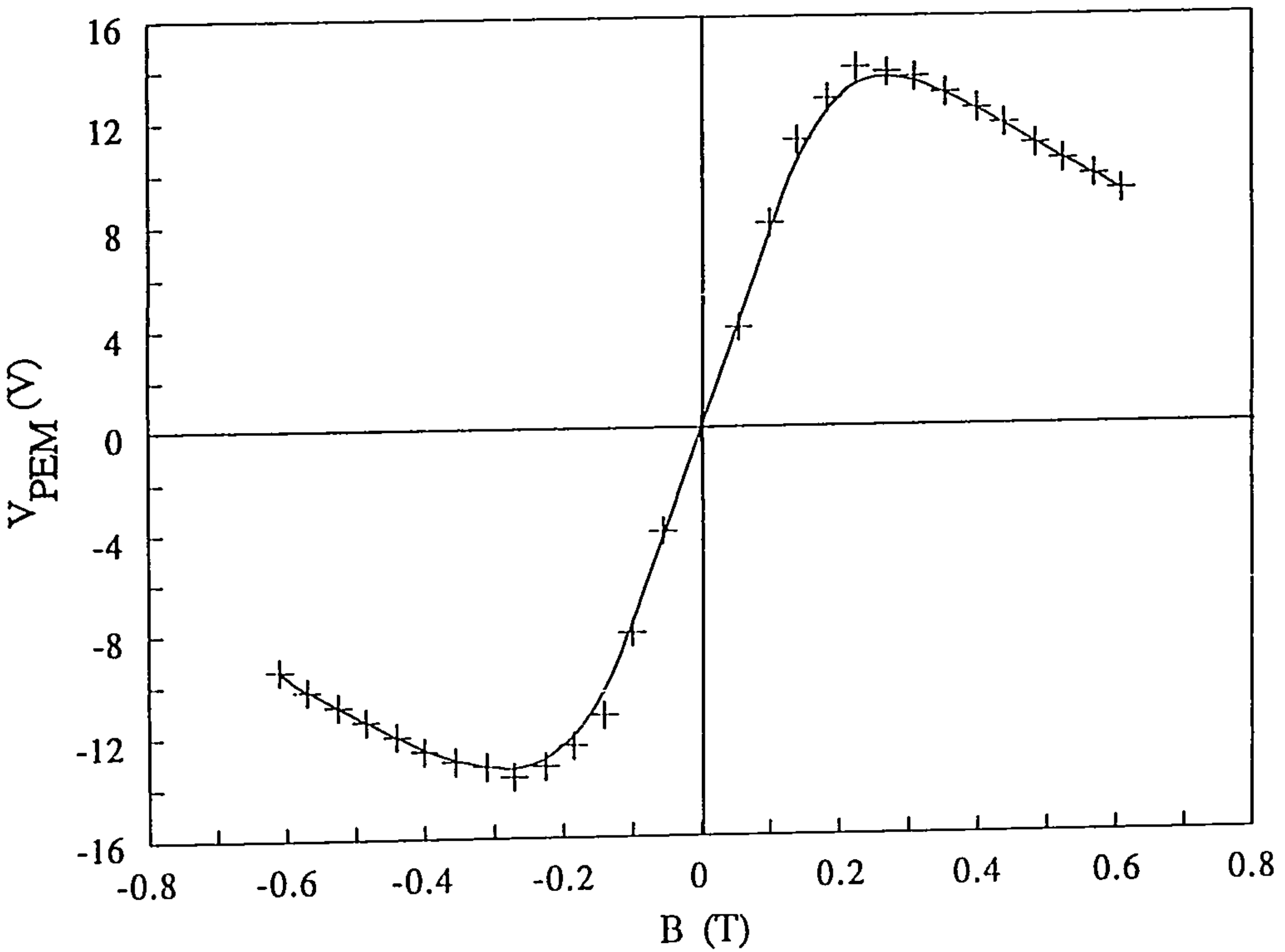

Fig.2.14 V_{PEM} vs B at T=77K with λ=632.8 nm for undoped GaAs substrate

Hence the sample may be in a low surface recombination situation at room temperature and liquid Nitrogen temperature for λ=822.3 nm (from monochromator). From Fig. 2.14, the B value at maximum V_{PEM} is about 0.25T. Therefore, the mobility of carriers for the sample at T=77K can be determined as $\mu=|1/B|$=40,000 $cm^2V^{-1}s^{-1}$.

(3) Dependence of V_{PEM} on I

From theoretical discussions [equation (2.26)], one can see that either low or high excitation levels can occur. At low excitation level, the dark conductivity of the sample (σ_0) is comparable with that of the illuminated one σ_l, i.e. $\sigma_0 \sim \sigma_l$, the PEM effect is always found to have a linear relationship with the intensity of light. At high excitation level, the dark conductivity of the sample (σ_0) is much smaller than that under illumination σ_l, i.e. $\sigma_0 \ll \sigma_l$. V_{PEM} tends to saturate with respect to the increase of intensity of light, i.e. V_{PEM} does not vary with the intensity at high excitation level. Fig.2.15, 2.16, and 2.17 show the PEM voltage changes with intensity of light at both room and liquid Nitrogen temperatures and at different wavelengths of illumination. Fig. 2.15 and 2.17 show that the excitation in this substrate sample can go from low to high level. From the result of the dependence of the V_{PEM} on I at high excitation level, the value of the carriers' diffusion length L_D can be calculated out (§2.3.4). It is L_D=0.27 μm at T=300K and L_D=0.44 μm at T=77K. These values are

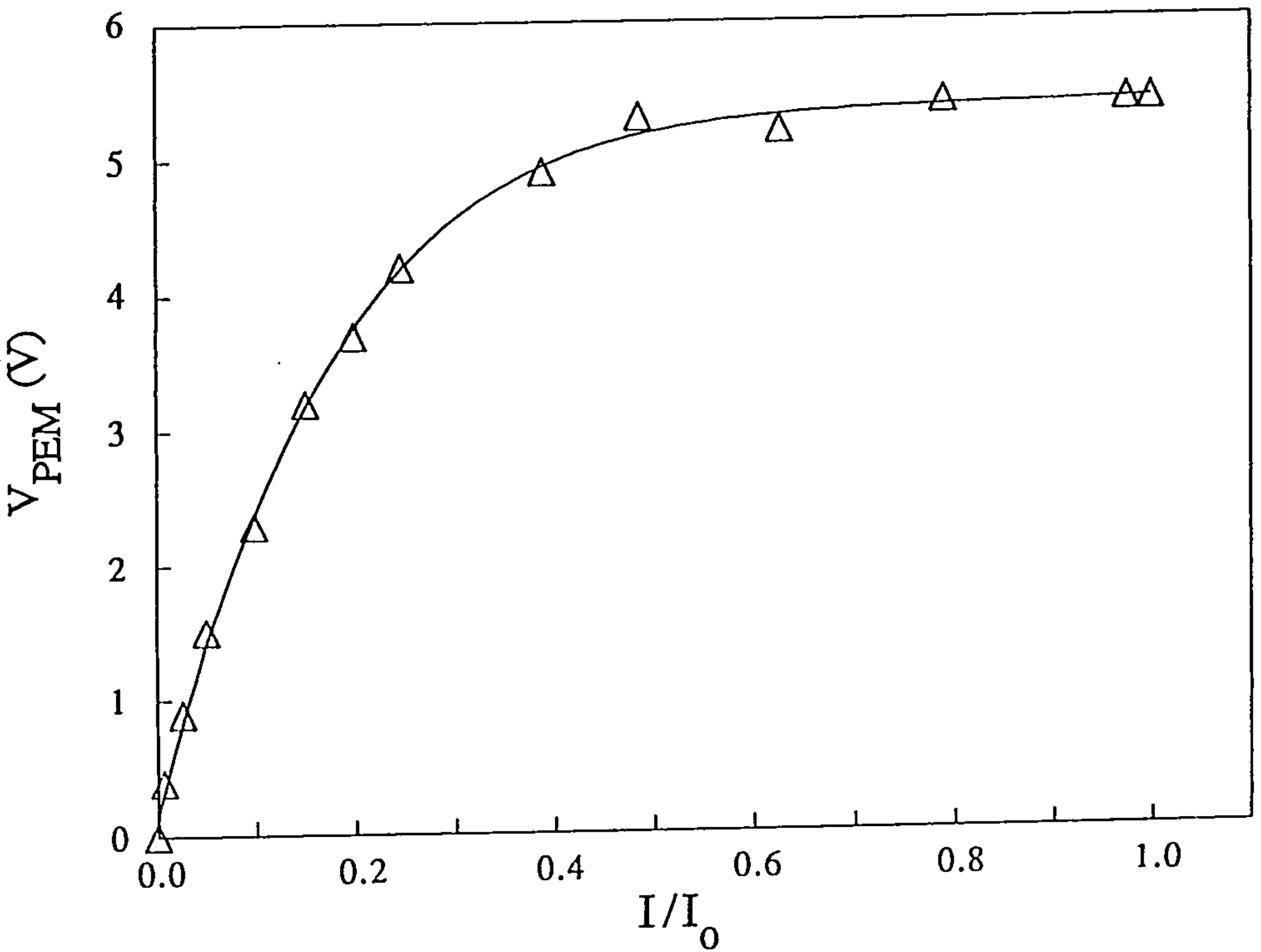

Fig.2.15 V_{PEM} vs I/I_o (I_o=2450W/m^2) at T=300K with λ=632.8 nm and B=0.4T for undoped GaAs substrate

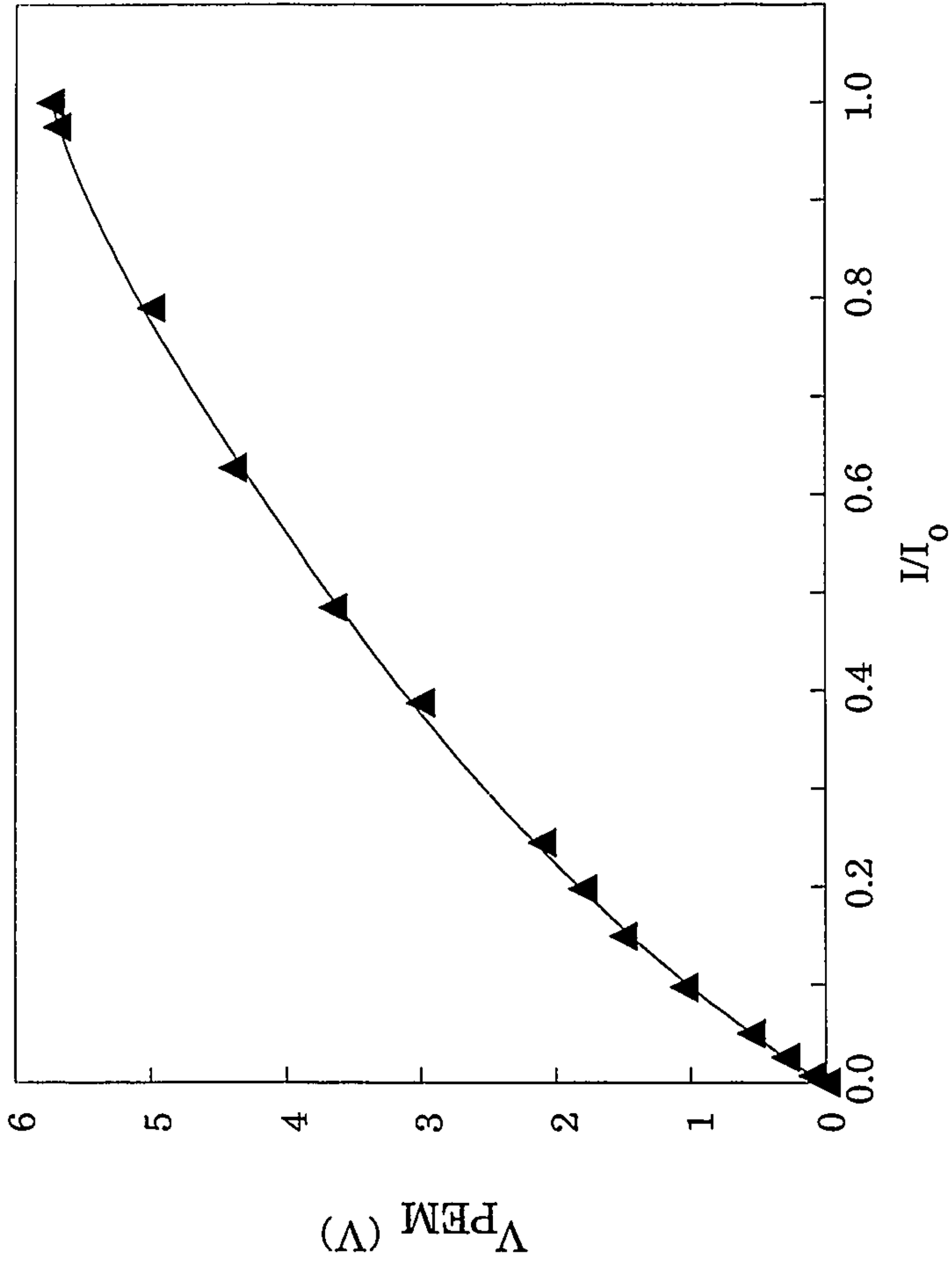

Fig. 2.16 V_{PEM} vs I/I_o at T=77K with λ=822.3 nm and B=0.4T for undoped GaAs substrate

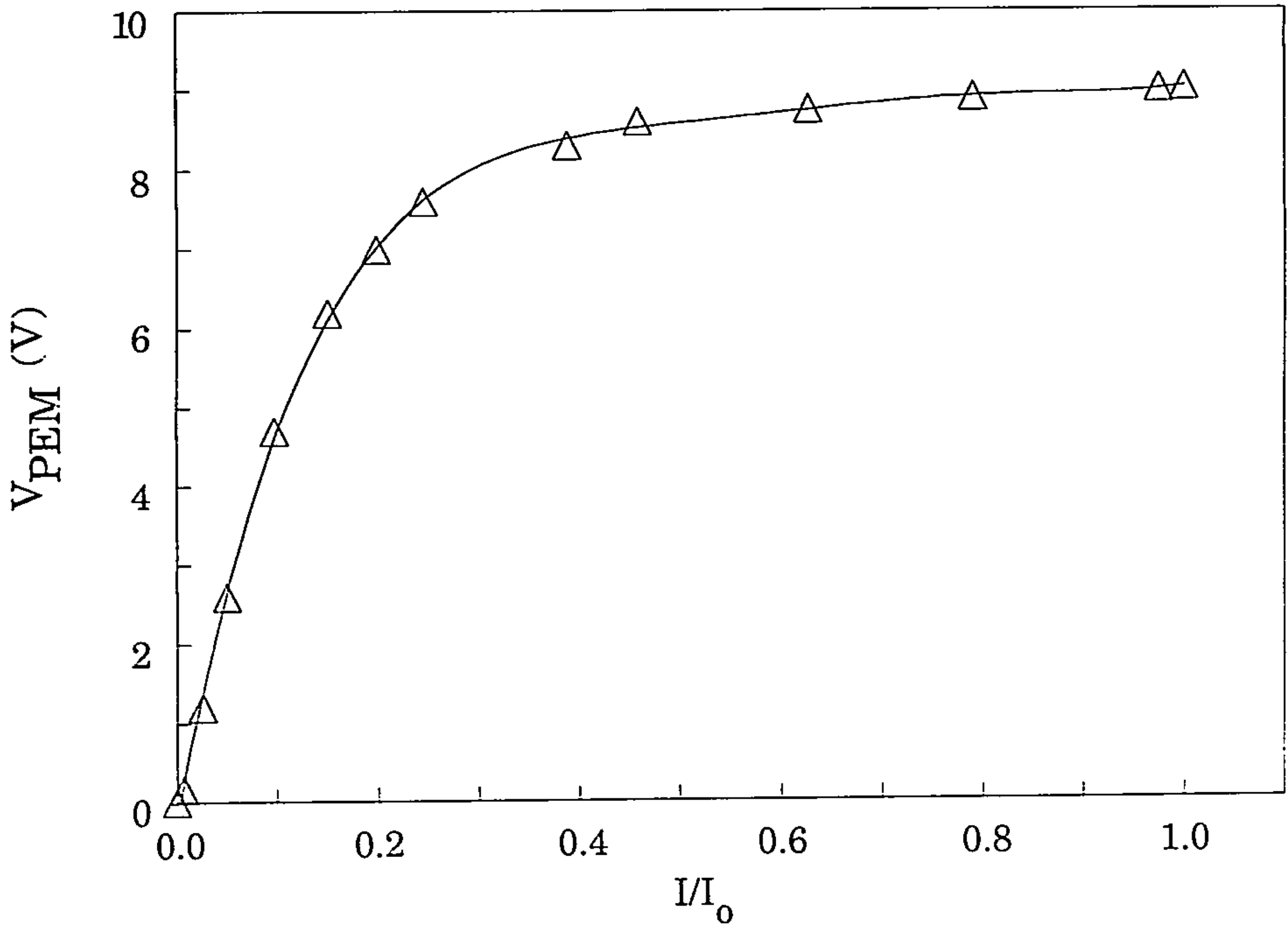

Fig. 2.17 V_{PEM} vs I/I_o (I_o=2450W/m^2) at T=77K with λ=632.8 nm and B=0.4T for undoped GaAs substrate

reasonable for semi--insulating undoped GaAs substrate and agree with others' results from other measurement methods.[2.11] [2.12]

2.3.2 GaAs Epitaxial Layer

(1) PEM Spectra

Fig. 2.18 shows the relationship at room temperature between V_{PEM} and λ. One can see that there is an intense broad peak (λ =877 nm) just below the bandgap (λ=871 nm). This phenomenon can be explained as that under the present experimental conditions, the sample has a high surface recombination velocity.[2.13]

Fig. 2.19 shows the V_{PEM} spectrum at liquid Nitrogen temperature T=77K. In the region of photoenergies higher than the GaAs bandgap (i.e. $E_{photon}>E_g=1.508$eV or $\lambda<822.3$nm), there is a strong PEM signal. Below the bandgap ($\lambda>822.3$nm), the PEM effect diminishes to zero. This is because when the photon energy is higher than the bandgap energy, many electron-hole pairs are created near the surface. These electrons and holes will diffuse from the illuminated surface to the dark surface with different mobility. As described in section §2.1 (theory), there is a carrier density gradient build up along the thickness of the sample. Under the presence of the magnetic-field, the PEM effect occurs. When the photo energy is lower than bandgap energy, fewer electron-hole pairs are created and they are created more uniformly across the sample so that $\nabla_n = \nabla_p = 0$ and

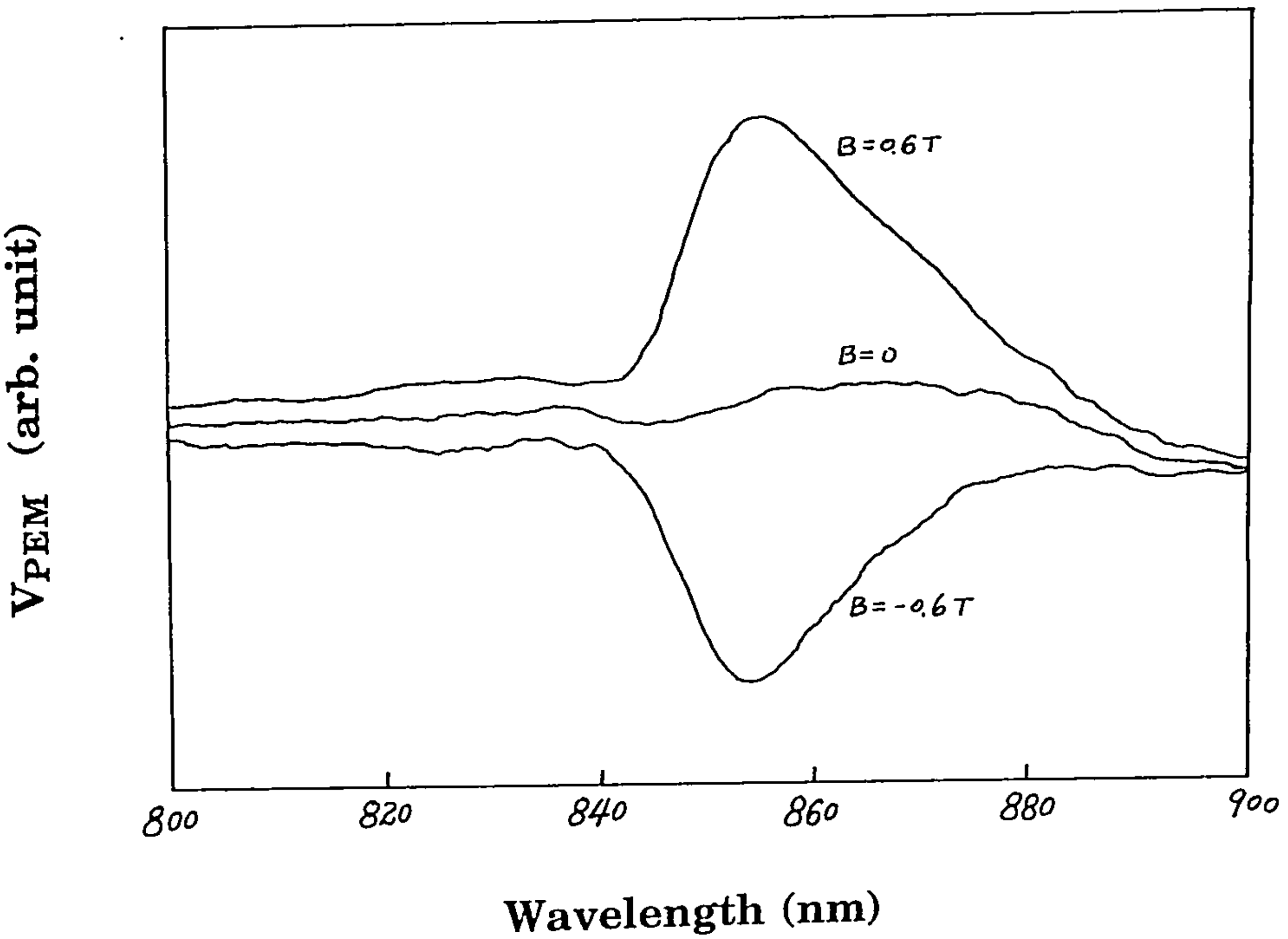

Fig. 2.18 PEM spectra for GaAs epilayer at T=300K.

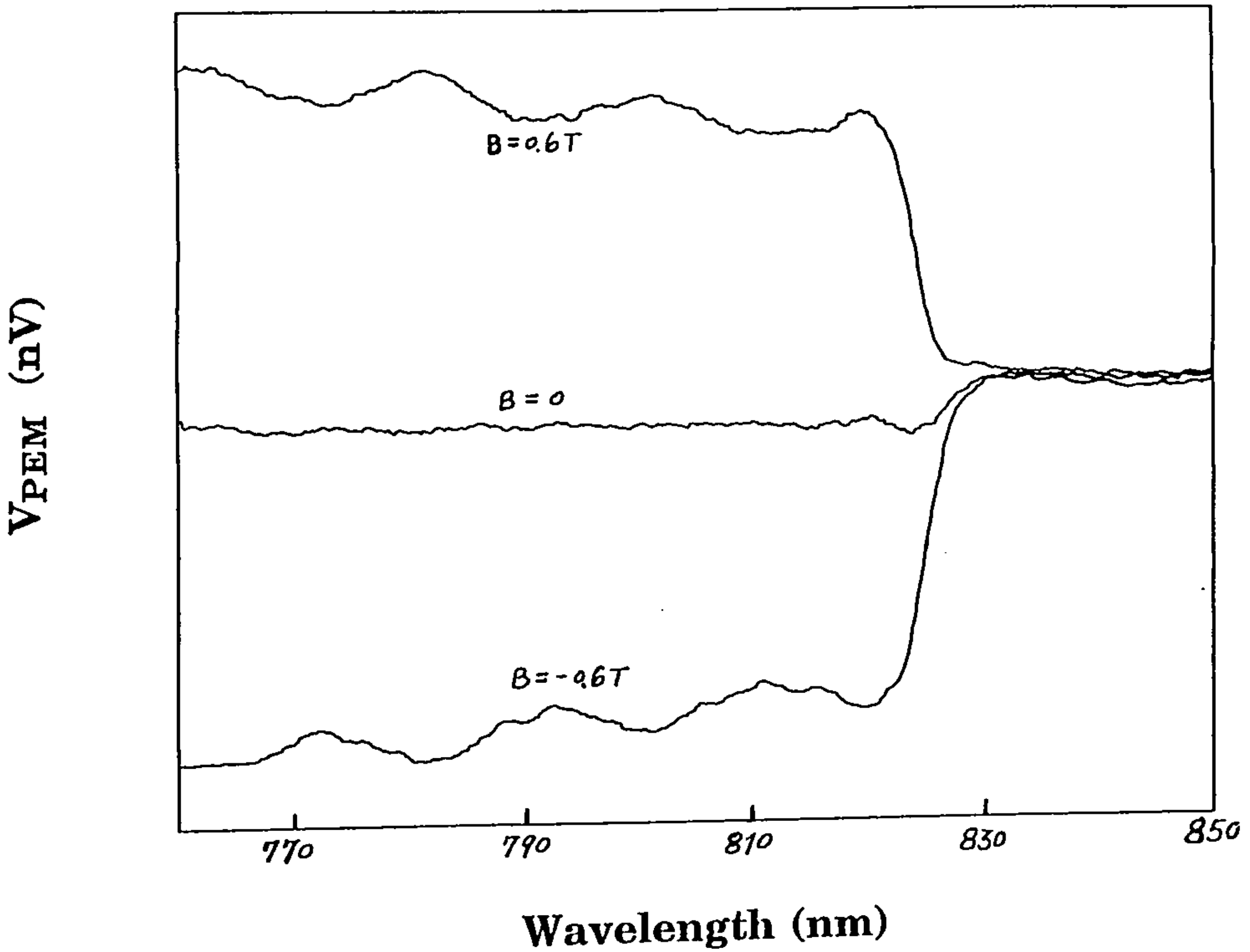

Fig. 2.19 PEM spectra for GaAs epilayer at T=77K.

consequently, no PEM effect occurs. Under field reversal, the direction of Lorentz force is reversed: the sign of the accumulated charge at both side of the sample a and b (Fig. 2.1) will change and so will the sign of the PEM signal. The PEM spectra with reversed field B are symmetric with respect to those without B reversed.

Fig. 2.20 and 2.21 show the experimental results at 5K. As for the liquid Nitrogen experiment, Fig. 2.20 presents two PEM spectra corresponding to two opposite B fields. The oscillation in the spectra may be the LO phonon related since the energy difference between two neighbouring minima (or maxima) is about 42 meV which is the value of the LO phonon in GaAs (Fig. 2.21).[2.14] The energy gap of GaAs at this temperature is 816nm, but it can not be seen clearly in the graph because of its corresponding photoenergy just in the range of a phonon resonance.

(2) Dependence of V_{PEM} on B

At room, liquid Nitrogen or liquid Helium temperatures, the PEM voltage is proportional to the field B (Fig. 2.22, 2.23, 2.24, 2.25, 2.26). This agrees with equation (2.27) and equation (2.28) at low B case. Fig. 2.22 and 2.23 show the relationship between V_{PEM} and B at room temperature with illuminating light wavelengths of λ=871 nm and λ=514 nm. Fig. 2.24 and 2.25 show the cases at liquid Nitrogen temperature with illuminating light wavelengths of λ=822.3 nm and λ=514 nm. At T=77K, the dependence of the PEM voltage on B does not have the features observed in the substrate at the same temperature, i.e. in the epilayer case, the PEM voltage is also linear

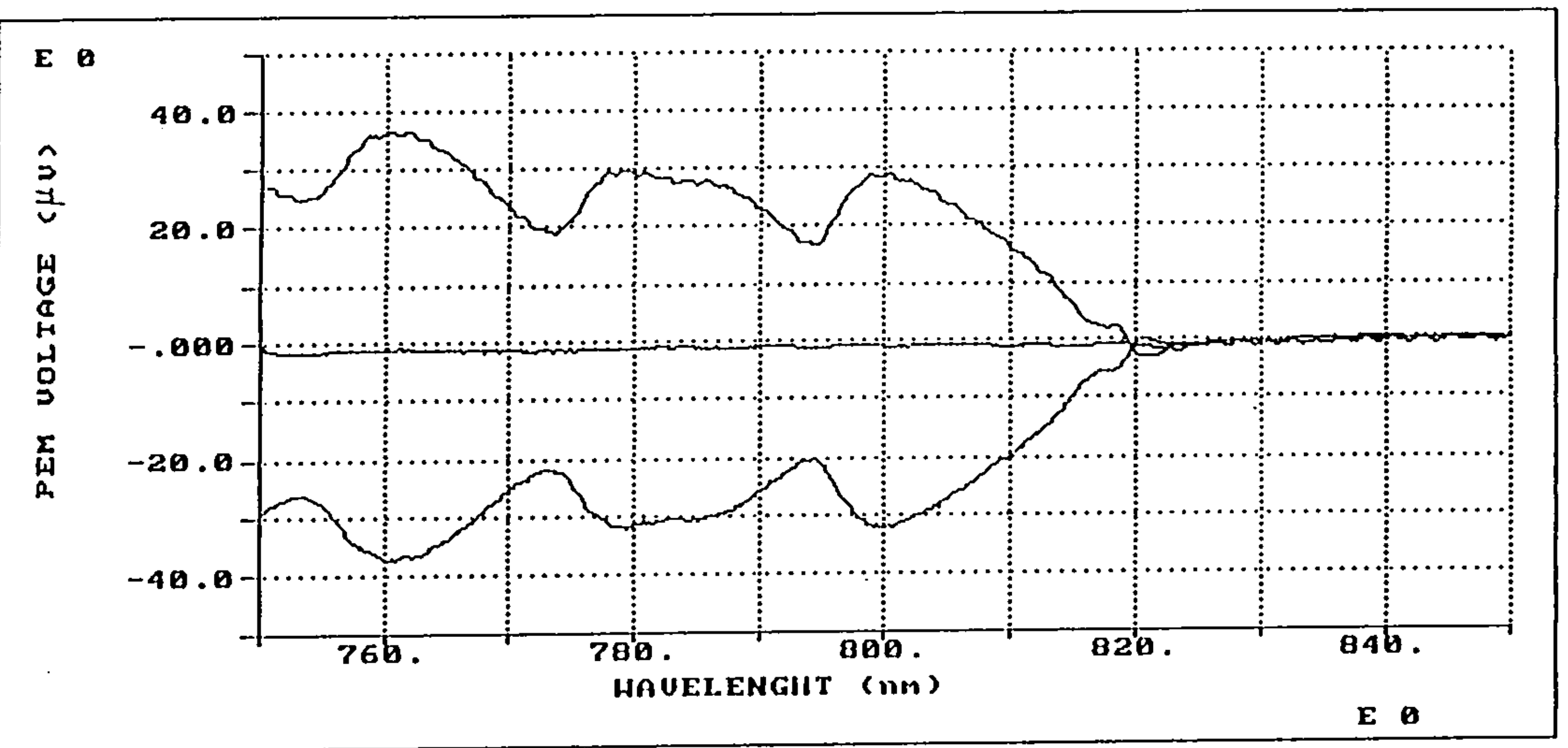

Fig. 2.20 PEM spectra for GaAs epilayer at T=5K.

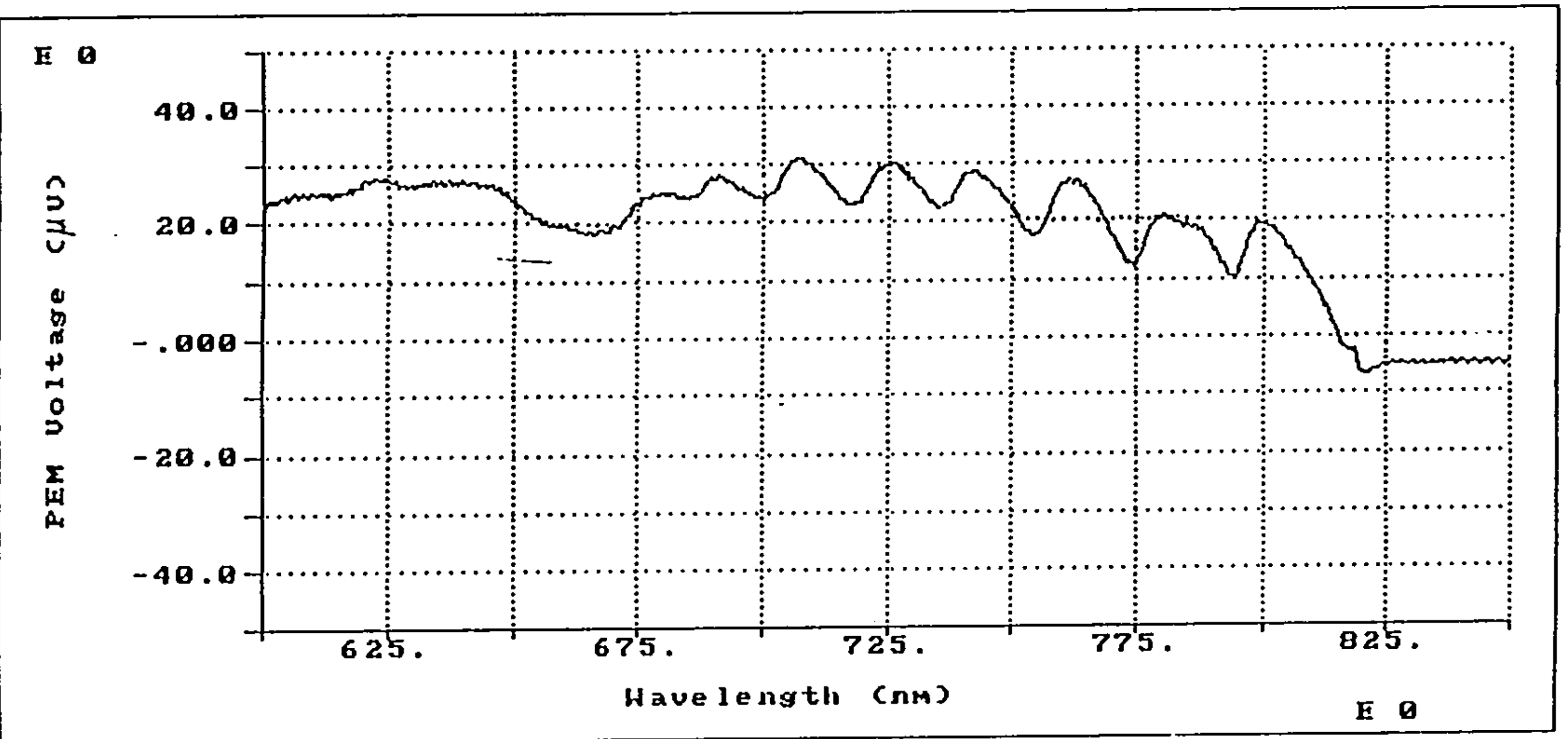

Fig. 2.21 PEM spectrum for GaAs epilayer at T=5K with wavelength from 600 nm to 850 nm.

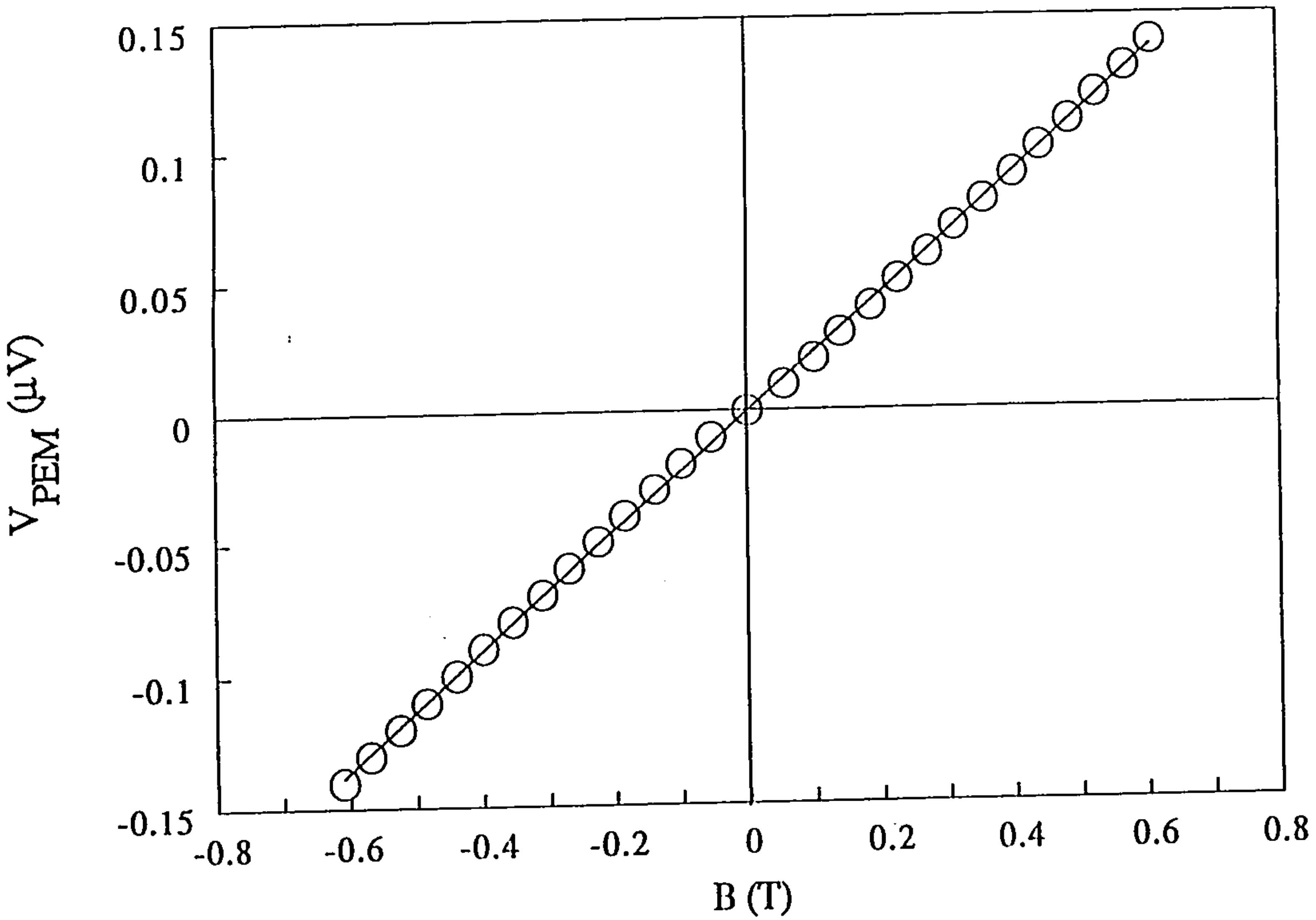

Fig.2.22 V_{PEM} vs B at T=300K with λ=871 nm for undoped GaAs epitaxial layer

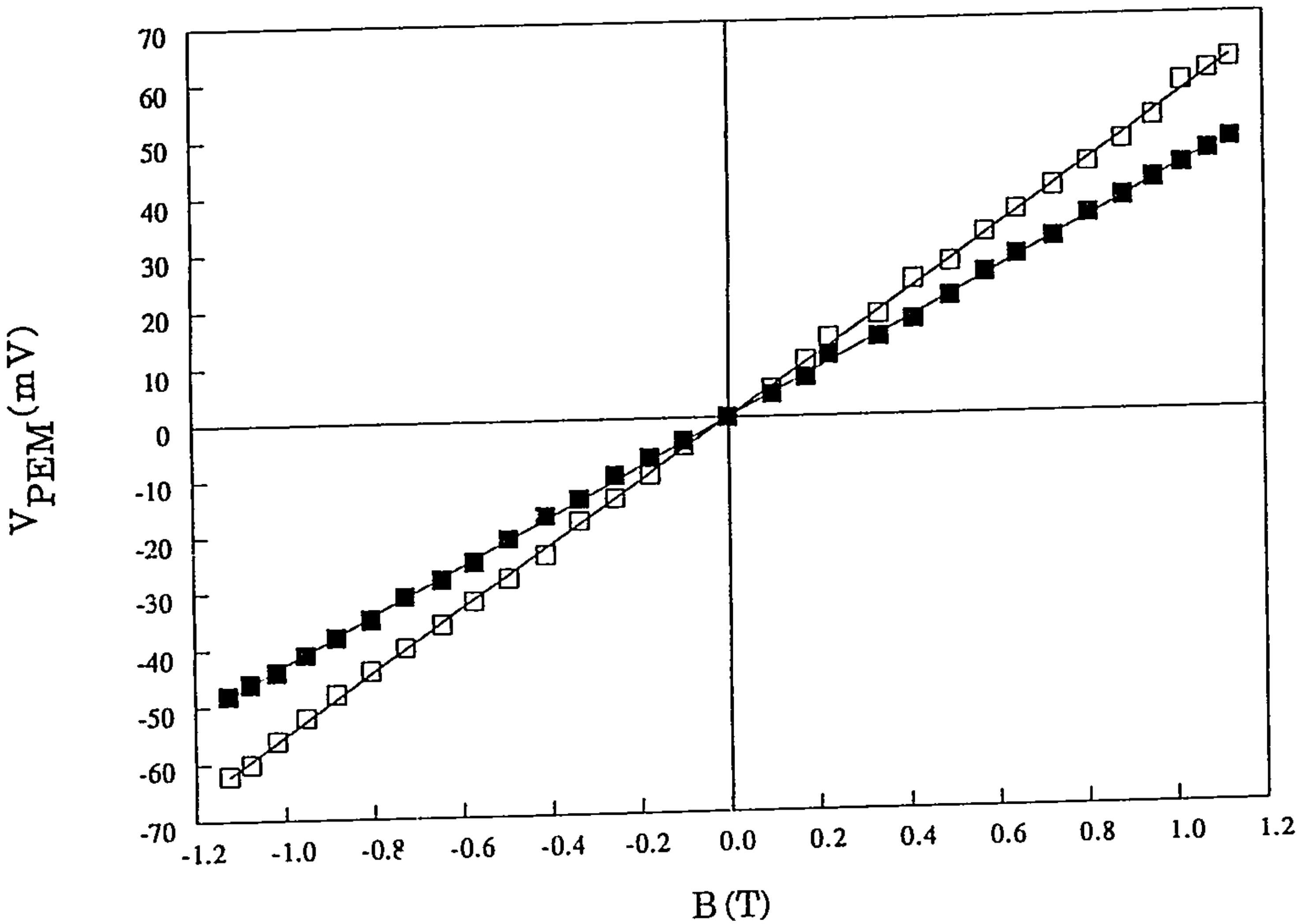

Fig.2.23 V_{PEM} vs B at T=300K with λ=514 nm for GaAs epilayer

□ : P=1W, ■ : P=0.5W

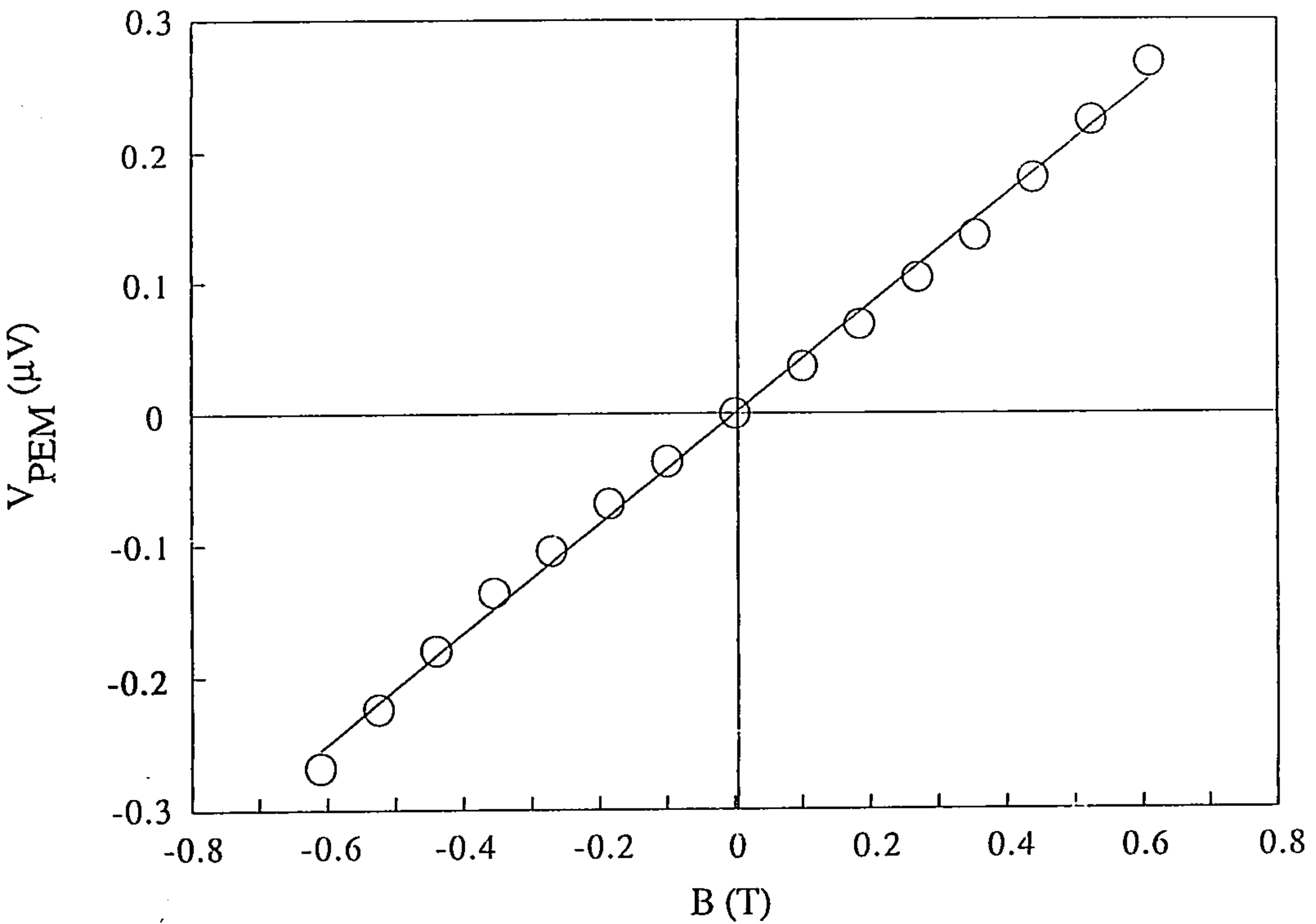

Fig.2.24 V_{PEM} vs B at T=77K with λ=822.3nm for undoped GaAs epitaxial layer

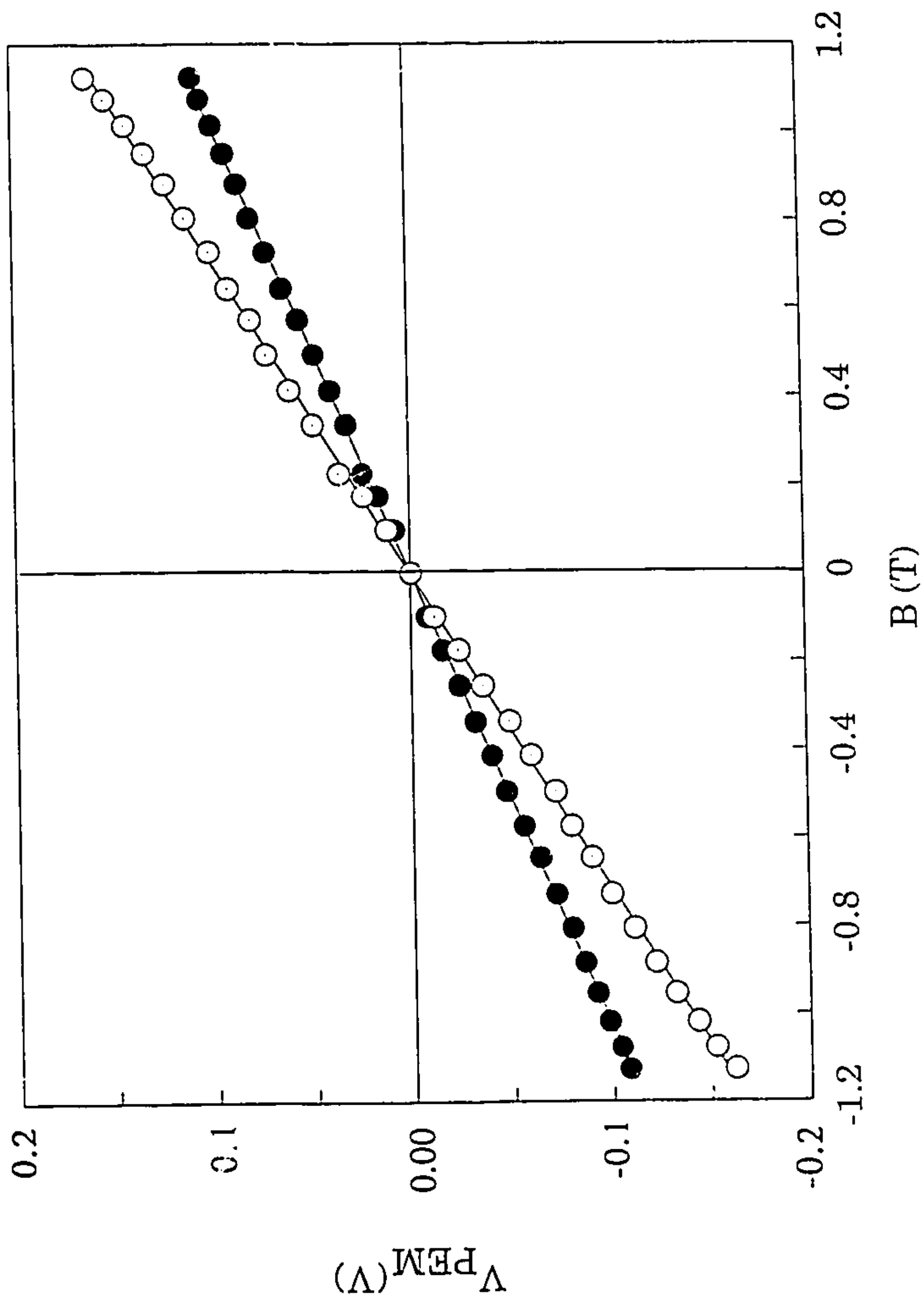

Fig.2.25 V_{PEM} vs B at T=77K with λ=514nm for GaAs epilayer

⊙: P=1W, ●: P=0.5W

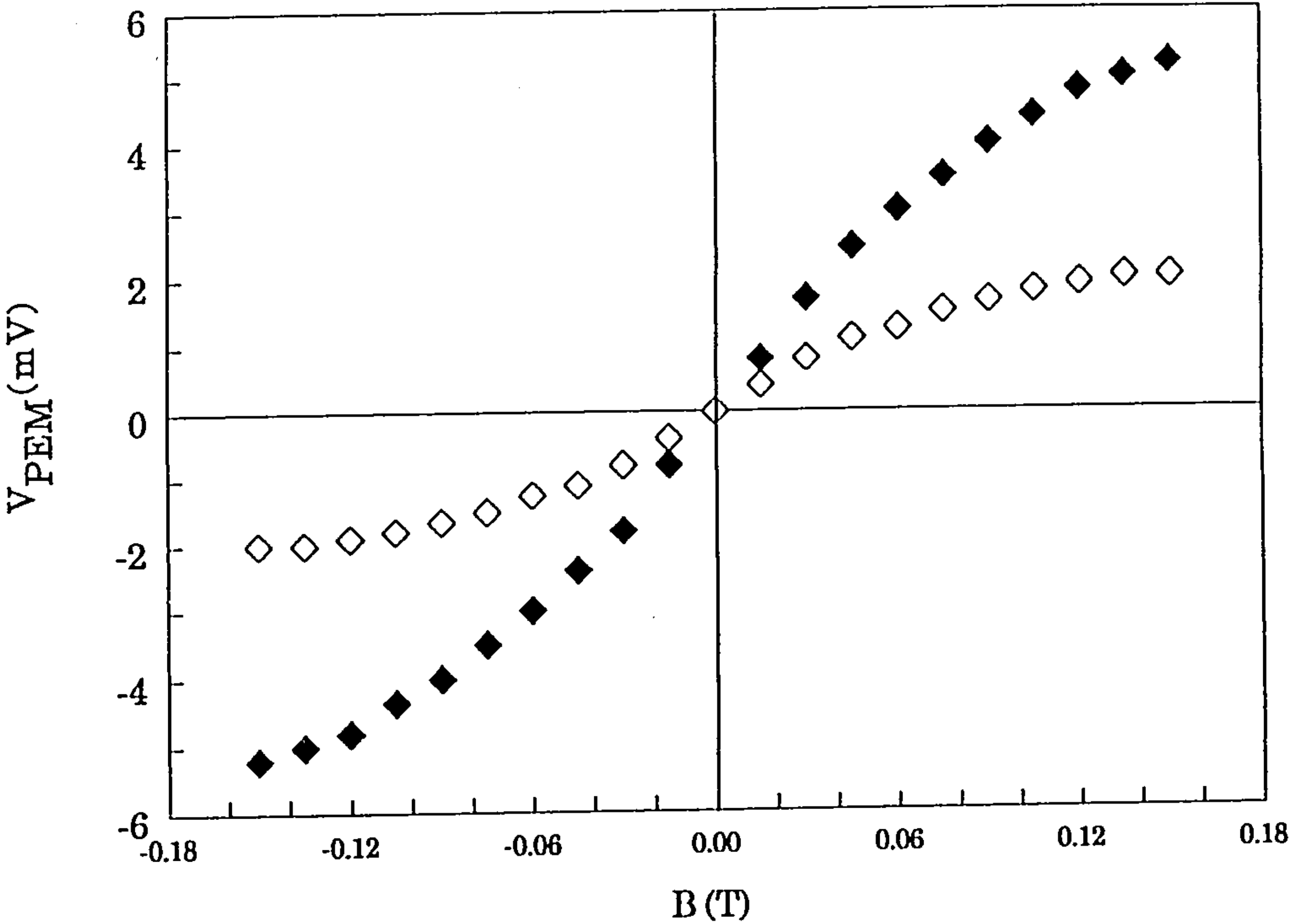

Fig.2.26 V_{PEM} vs B at T=5K with λ=632.8 nm for GaAs epilayer

◆: P=2.5mW, ◇: P=0.245mW

to the field B. This probably is because the epilayer sample has a much better surface than the substrate has.[2.15][2.16] Fig. 2.26 is the result at T=5.5K.

(3) Dependence of V_{PEM} on I

At both room and liquid Nitrogen temperatures, the monochromator and the He--Ne laser were used as light sources to conduct the experimental measurement of the dependence of the PEM voltage on light intensity I; the magnetic field was fixed at 0.6T. The results show that V_{PEM} is linearly dependent on I (Fig. 2.27) which means that the excitation state remains at low level. The high power Ion-Argon laser was used later as the light source, and a high range power supply was used to replace the small range one so that the field could be varied from 0--1.2T. The results then show that the excitation reaches the onset of the saturation (Fig. 2.28, 2.29). Since the resistance of the sample is so low (at T=300K R_{01}=33 KΩ, at T=77K R_{02}=8 KΩ) or the concentration of the carriers n_0 is relatively high ($10^{14}cm^{-3}$), the increase of the carrier concentration caused by illumination is not large enough compared with n_0 (i.e. it can not satisfy the relationship $\Delta n \gg n_0$). Hence the excitation did not reach high level even with Argon laser illumination, because in practice, too high an intensity of radiation will heat and even burn the sample.

In the vicinity of Helium temperature, the resistance of the sample quickly increases as the temperature decreases. At T=5.6K, R=2MΩ, at T=5K, R=2.5MΩ in darkness; these values are about three orders of

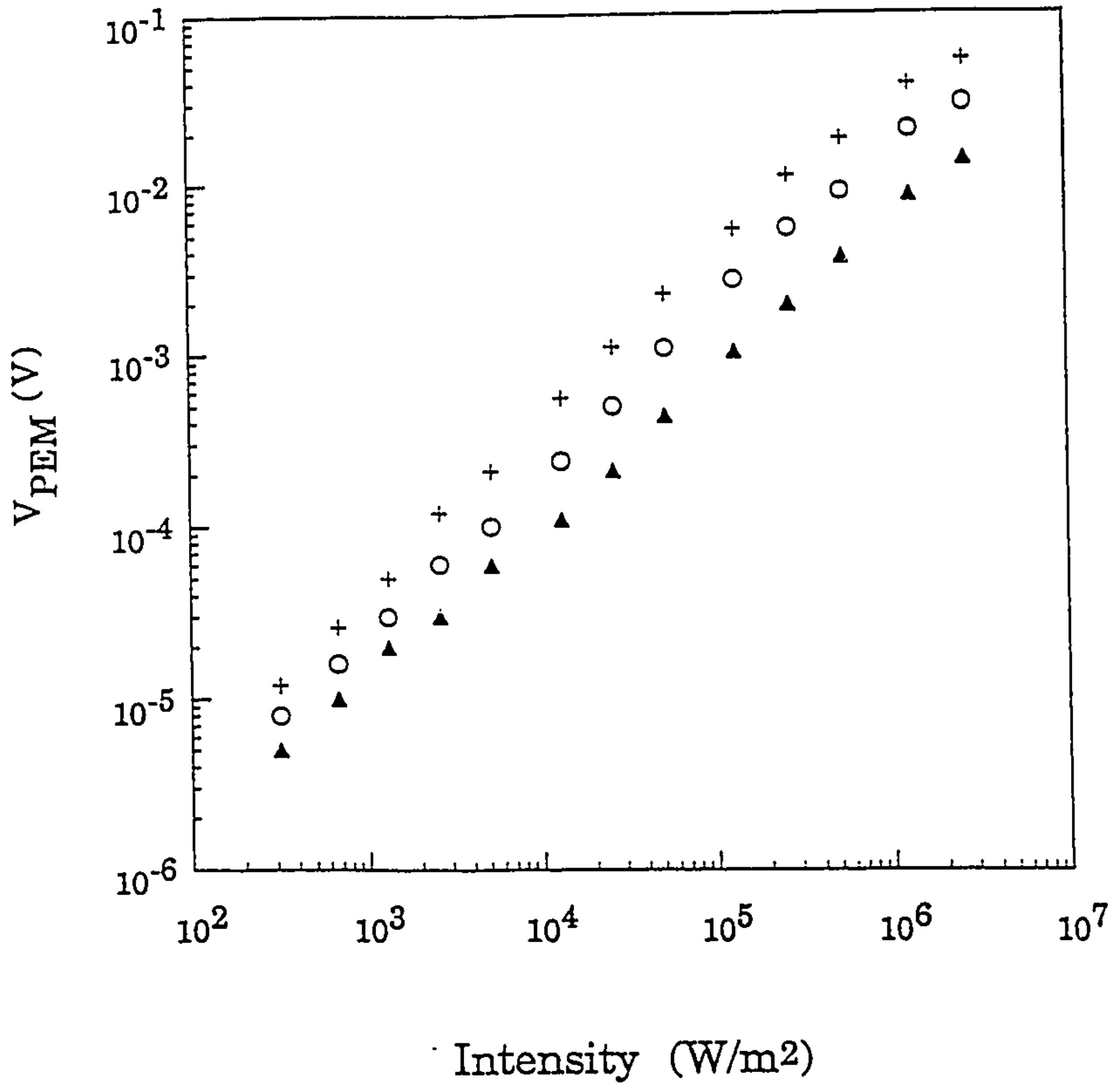

Fig. 2.27 V_{PEM} vs Intensity of the light with λ=514 nm at T=300K for epilayer.
▲: B=0.2T; o: B=0.5T; +: B=1.0T.

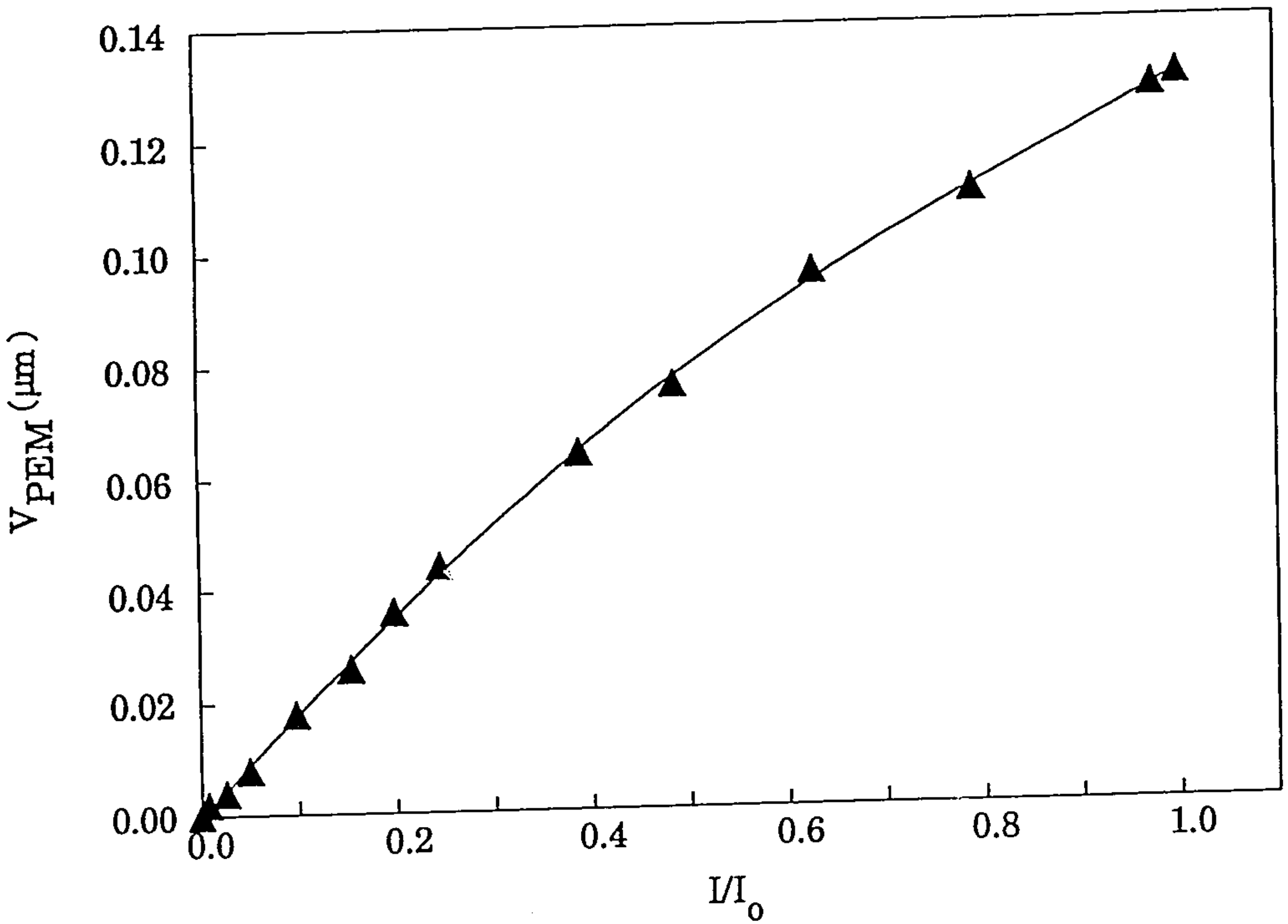

Fig. 2.28 V_{PEM} vs I/I_o at T=77K with λ=822.3 nm and B=0.4T for undoped GaAs epitaxial layer

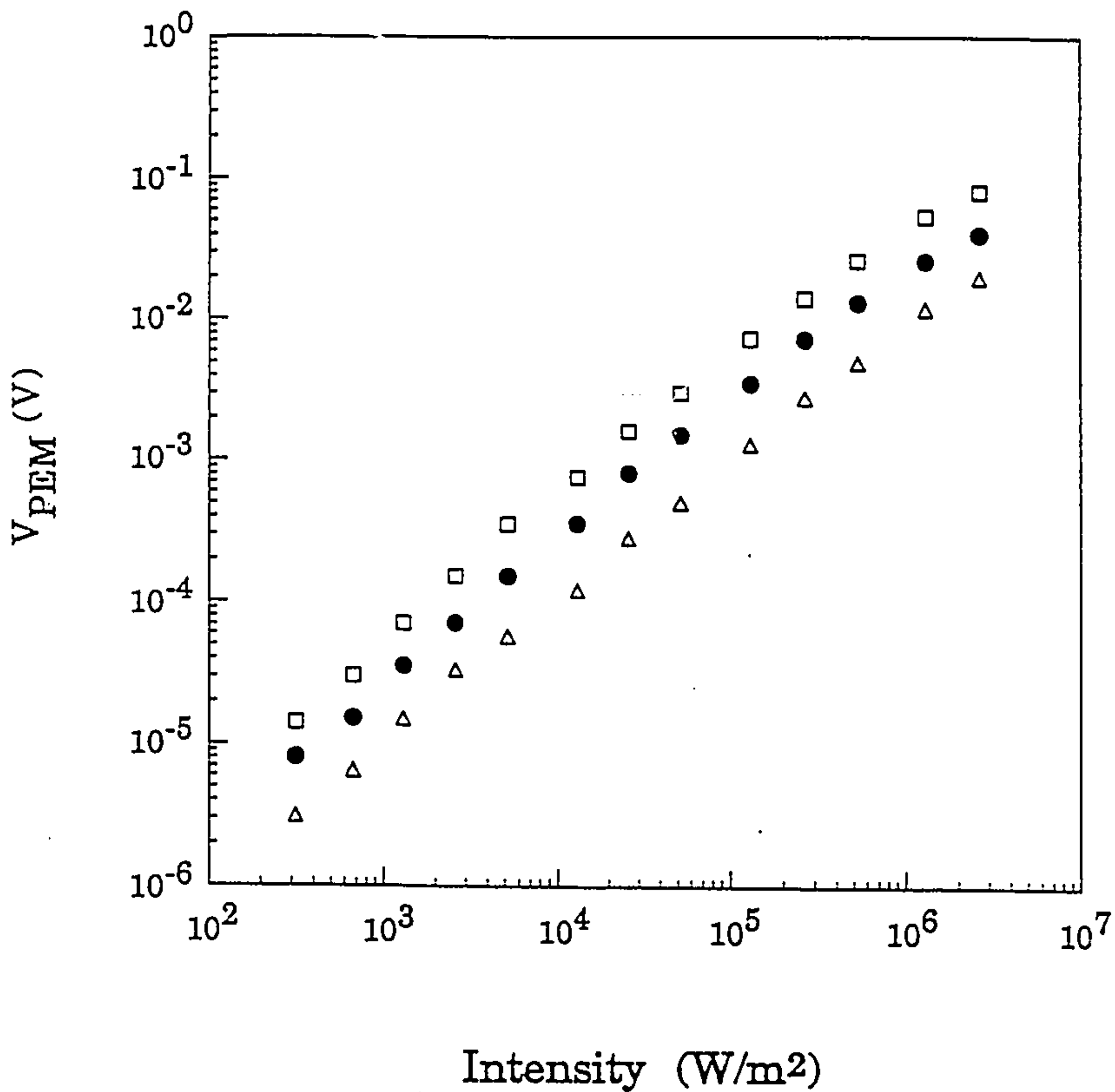

Fig. 2.29 V_{PEM} vs Intensity of the light with λ=514 nm at T=77K for epilayer.
△: B=0.2T; ●: B=0.5T; □: B=1.0T.

magnitude higher than the resistance at T=77K. In this case the concentration of the carriers n_0 is much lower and the increase Δn in the carriers concentration by the illumination of light can be larger than n_0. So the excitation can reach high level or the saturation of V_{PEM} at high I can happen. Fig.2.30 is the result of measurements of V_{PEM} vs I at T=5K which shows that V_{PEM} reached saturation at high I.

The carrier' diffusion length of this sample is calculated in section §2.3.4. The values are $L_D \geq 2.6$ μm at T=300K, $L_D \geq 3.1$ μm at T=77K, and $L_D \approx 3.5$ μm at T≈5K. Using PC spectroscopy methods, R. Muralidharan and K. Ploog measured carriers' diffusion length for epilayers with $n=10^{16}$ cm^{-3} at T=77K. They got $L_D \geq 3$ μm.[2.17] In our case, the carriers' concentration is $n=10^{14}$ cm^{-3} which means that the carriers' diffusion length for this material should be longer than 3 μm. Hence, our result $L_D \geq 3.1$ μm at T=77K is reasonable.

2.3.3 $In_xGa_{1-x}As/GaAs$ Quantum wells

The study of the PEM effect in quantum wells was one of the original purposes of this project. So far nobody has studied this subject yet. We tried the quantum well samples mentioned before (§2.2.2). Unfortunately, the experiment was unsuccessful. The PEM effect did not appear in the quantum well samples. This perhaps is because the diffusion length of the carriers is much longer (of the order of the micron; section §2.2.4) than the

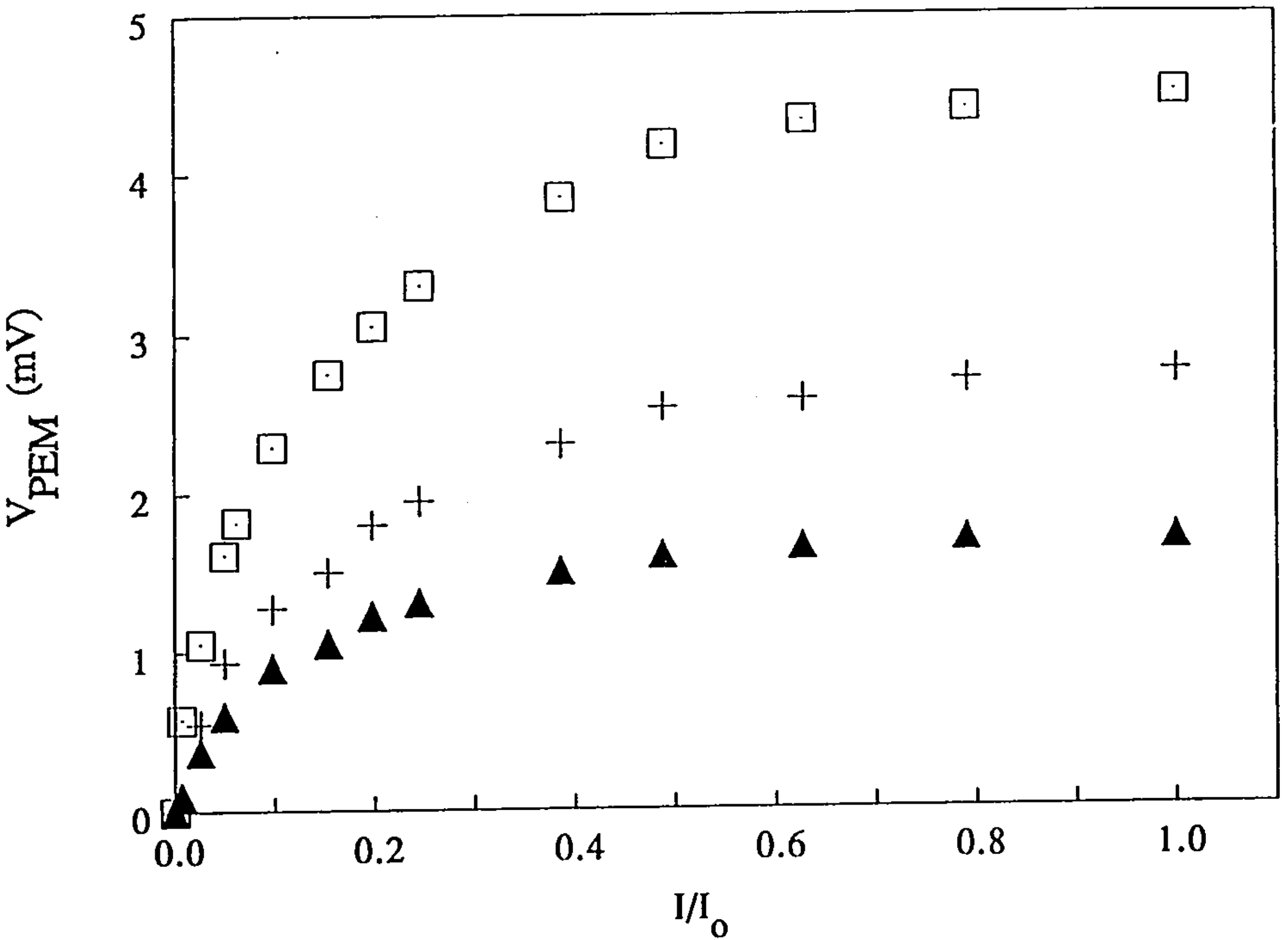

Fig.2.30 V_{PEM} vs I/I_o (I_o=2450W/m^2) at T=5K with λ=632.8 nm for GaAs epilayer.
⊡: i=5A(B=0.15T), +: i=2A(B=0.06T), ▲: i=1A(B=0.03T)

width of the well (10--20 nm). Because of that, there will be no carrier concentration gradient across the well and thus no PEM effect along the sample.

2.3.4 Estimation of the Diffusion Length of the Carriers for the Substrate and the Epitaxial Layer

(1) Substrate

Table 2.3 gives the resistances of the samples:

		darkness	with light		
			λ =632.8nm	λ=871nm	λ=822.5nm
			(with laser, 7.7mW)		
T=300K	R (Ω)	3.5×10^{9}	1×10^{8}	2.6×10^{8}	---------
	σ ($\Omega^{-1}m^{-1}$)	1.0×10^{-6}	3.5×10^{-5}	1.35×10^{-5}	---------
T=77K	R (Ω)	2.5×10^{10}	2×10^{8}	----------	1.9×10^{9}
	σ ($\Omega^{-1}m^{-1}$)	1.4×10^{-7}	1.8×10^{-5}	----------	1.8×10^{-7}

Table 2.3 Resistances and conductivities of the GaAs substrate samples under different conditions.

Since the conductivities of the sample satisfy: $\sigma_l \gg \sigma_0$, the exciations are

considered at high level. This is also in agreement with the experimental results (Fig.2.13, 2.14, 2.15). Therefore, use equation (2.25):

$$L_D = lDB/V_{PEM}$$

where $D=(kT/e)\mu'=(kT/e)\{2\mu_n\mu_p/(\mu_n+\mu_p)\}$. The value of μ and D are given below in Table 2.4[2.18][2.19] and the value of the ratio μ_n/μ_p was taken 10.[2.20][2.21]

		T=300K	T=77K
μ	μ_n ($cm^2V^{-1}s^{-1}$)	3,800	40,000
	μ_p ($cm^2V^{-1}s^{-1}$)	380	4,000
D	D (cm^2s^{-1})	17.8	48.2

Table 2.4 Values of μ and D of substrate at T=300K and T=77K

Inside the table, the value of μ_n(77K)=40,000 $cm^2V^{-1}s^{-1}$ is taken from the result of our measurement.

The carrier's diffusion lengths are (refer to Fig. 2.15 and 2.17):

at T=300K:

$$L_D = lDB/V_{PEM} = \mathbf{0.27\ \mu m}$$

at T=77K:

$$L_D = lDB/V_{PEM} = \mathbf{0.44\ \mu m}$$

(2) Epitaxial Layer

Table 2.5 gives the parameters of the sample:

		darkness	with laser	
			λ=632.8nm (2.5mW)	λ=514.5nm (500mW)
T=300K	R (Ω)	3.3×10^{4}	2.7×10^{4}	2.5×10^{4}
	σ ($\Omega^{-1}m^{-1}$)	1.6×10^{1}	1.9×10^{1}	2.1×10^{1}
T=77K	R (Ω)	8.1×10^{3}	7.3×10^{3}	7.0×10^{3}
	σ ($\Omega^{-1}m^{-1}$)	6.0×10^{1}	6.7×10^{1}	6.9×10^{1}
T=5K	R (Ω)	2.5×10^{6}	——	——
	σ ($\Omega^{-1}m^{-1}$)	9.8×10^{-2}	——	——

Table 2.5 Resistance and conductivity of the GaAs epilayer samples under different conditions

At both room and liquid Nitrogen temperatures, $\sigma_l \sim \sigma_0$, so that the excitations are considered at low level. This is also shown in Fig. 2.23, 2.24 and 2.25. The diffusion length can be determined by using equation (2.20)

$$L_D = V_{PEM} \frac{\sigma_0 d}{\beta I B e (\mu_n + \mu_p) l}$$

At liquid Helium temperature, $\sigma_l \gg \sigma_0$, and the experimental result show that the PEM voltage reaches saturation (Fig. 2.26), so in this case, the excitation can be treated as a high level excitation; using equation (2.25)

$$L_D = \frac{B}{V_{PEM}} / D$$

The values of μ_n and μ_p and n are given in Table 2.6,[2.21] and the value of the ratio of μ_n/μ_p is taken at about 10.[2.20] [2.21]

		T=300K	T=77K	T=5K
μ	$\mu_n(cm^2V^{-1}s^{-1})$	5,000	37,500	19,000
	$\mu_p(cm^2V^{-1}s^{-1})$	500	3,750	1,900
D	$D(cm^2V^{-1})$	23.4	45.2	1.5

Table 2.6 Values of μ and D in the GaAs epilayer
at T=300K, T=77K and T=5K

The value of μ at T=77K given by Dr. Roth is about 75,000 $cm^2V^{-1}s^{-1}$. But, in Table 2.5, a value of 37,500 $cm^2V^{-1}s^{-1}$ is taken. The reason of the modification is that if we use μ=75,000 $cm^2V^{-1}s^{-1}$ to calculate the resistance of the sample at T=77K, we will get R=4 KΩ. However, the measured value of R at T=77K is 8 KΩ. Therefore, the value of μ at T=77K should be half of

75,000 $cm^2V^{-1}s^{-1}$. At T≈5K, the value of μ is taken as $\mu_n(5K) \approx 0.5\mu_n(77K)$.[2.18] [2.22]

The useful intensity of the Ion--Argon laser at 500 mW is 0.84×10^{24} quanta·m^2s^{-1} with a beam diameter about 1.5 mm (see next section §2.5.1). The quantum yield coefficient can be chosen as β=1 in equation (2.20) in view of the good quality of the sample.

The diffusion length of the carriers for this sample are (refer to Fig. 2.23, 2.25 and 2.30):

at T=300K:

$$L_D = V_{PEM}\frac{\sigma_0 d}{IBe(\mu_n+\mu_p)l} \geq 2.6\ \mu m$$

at T=77K:

$$L_D = V_{PEM}\frac{\sigma_0 d}{IBe(\mu_n+\mu_p)l} \geq 3.1\ \mu m$$

at T=5K:

$$L_D = lDB/V_{PEM} \approx 3.5\ \mu m$$

2.4 Summary

The PEM effect method has been used to measure the carriers' diffusion length in GaAs materials in this experimental research. The results length for the different materials are summarized in the following table:

materials	carriers' diffusion length (μm)		
	T=300K	T=77K	T=5K
undoped semi-insulating GaAs substrate	0.27	0.44	-------
GaAs epilayer on same substrate above	2.6	3.1	3.5

Table 2.7 Summary of the results of the carriers' diffusion length from experiment

Since the carriers' diffusion length in $In_xGa_{1-x}As/GaAs$ quantum wells is much larger than the thickness of the well, there is no PEM effect. Therefore, using the PEM effect to measure carriers' diffusion length in single quantum well or in multiple quantum wells of total thickness $< L_D$ is meaningless.

2.5 Appendix

2.5.1 Estimation of the Intensity of the Laser Output

The output intensity of a laser operating in the TM_{00} mode is given by a Gaussian distribution as shown in Fig. 2.31:

$$I(r)=I_0(0)\, e^{-\alpha r^2} \tag{2.29}$$

The output power P can be written as:

$$P=\int I \cdot dA \tag{2.30}$$

where I is expressed by equation (2.29). A is the cross area of the beam and $dA=2\pi r \cdot dr$ Substituting I and dA into equation (2.29):

$$P=\int_0^{\infty} I_0 e^{-\alpha r^2} \cdot 2\pi r dr = -\frac{I_0\pi}{\alpha}\int_0^{\infty} e^{-\alpha r^2} d(-\alpha r^2)=\frac{\pi I_0}{\alpha} \tag{2.31}$$

If we assume that at the edge of the beam $I/I_0=1/e^2$, from equation (2.29), we have $\alpha=2/r^2$. For the Ar+ laser, r=0.75mm,hence $\alpha=3.6\times10^6 m^{-2}$. Bringing this back into equation (2.31), we have $I_0=\alpha P/\pi=1.13 \times 10^6 P (W/m^2)$. In the case of λ=514.5nm, one quantum has a photoenergy: $h\nu=h\cdot c/\lambda =3.96 \times 10^{-19}J$. For example, in the unit of quanta$\cdot m^{-2}s^{-1}$, $I_0=0.29 \cdot P \times 10^{25}$quanta$\cdot m^{-2}s^{-1}$. Or $I_0=1.45\times10^{24}$quanta$\cdot m^{-2}s^{-1}$ with P=0.5W. Considering the reflection from the cryostat's window and the sample, which can be taken as about 42%, the useful intensity will be: $I_0=0.84\times10^{24}$quanta$\cdot m^{-2}s^{-1}$.

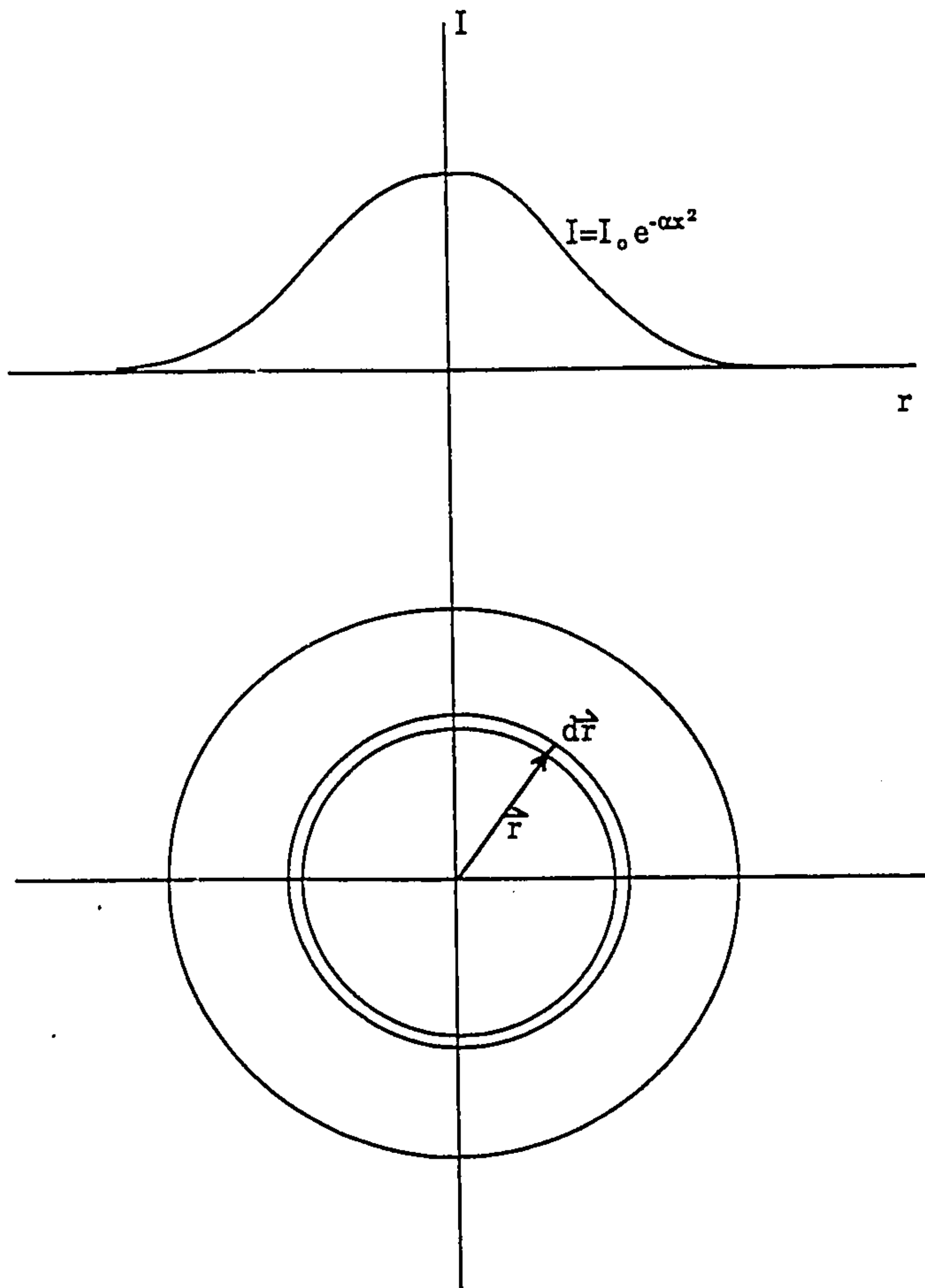

Fig. 2.31 Light intensity distribution for laser beam

2.5.2 Design and Performance of a Superconducting Coil for PEM Measurements at Low Temperatures

In order to measure the photoelectromagnetic effect at liquid Helium temperature, using the "Janis cryostat", a magnetic field is needed. There are two kinds of magnetic field devices that can be used. One is the magnetic field generator with two poles: considering the dimensions of the cryostat, this kind of generator should be big enough so that the tail of the cryostat can fit between the two poles. The other one is a superconducting solenoid coil which can produce an uniform magnetic field inside the solenoid. This superconducting coil can be built in a small dimension and it can be placed inside cryostat around the sample. Comparing those two devices, the superconducting coil has more advantages. We chose a superconducting coil to be our magnetic field source.

Since the coil is going to be put inside cryostat and the space where the coil can be put is not plenty, the size of the coil is limited. Also because of the perpendicular relationship among the directions of incident light, magnetic field and the potential built up between the sample, the whole apparatus must be designed in a way to satisfy the requirements mentioned above; in particular, optical access in the Voigt configuration should be provided for.

(1) Design

A. Mechanical Design

The supporting apparatus consists of two parts, the copper frame and the plastic frame. The copper frame is the supporter of both sample and superconducting coil. On the plastic frame, the superconducting wire is wound into two separated solenoid coils. The plastic frame itself is made of DELRIN which functions well at liquid Helium temperature.

The copper frame has three pieces: the major body which can be screwed on the Janis cryostat's centre bar, the sample holder where the sample is placed on as well as the bottom piece which can be screwed on the major body piece. The bottom piece acts not only as a protector to prevent the sample from dropping into the bottom of the cryostat, but also as a clamp to fix the superconducting coils (Fig. 2.32).

The plastic frame is a hollow tube (Fig. 2.32). A length of wire is twisted around the tube in such a way as to form two separate solenoid coils on it. There is a 10mm×2mm rectangular hole between the two coils on the plastic to let the incident light pass through the gap and shine on the sample. The sample is placed at the centre position inside the tube between the coils. The magnetic field created by the superconducting coils passes through the sample and its direction is perpendicular to the direction of the incident light. In the third direction which is both perpendicular to the field and light, the PEM potential is built up inside the sample. This PEM signal is detected from the two ends of the sample via external leads.

A current of 5A was available to produce a design maximum magnetic

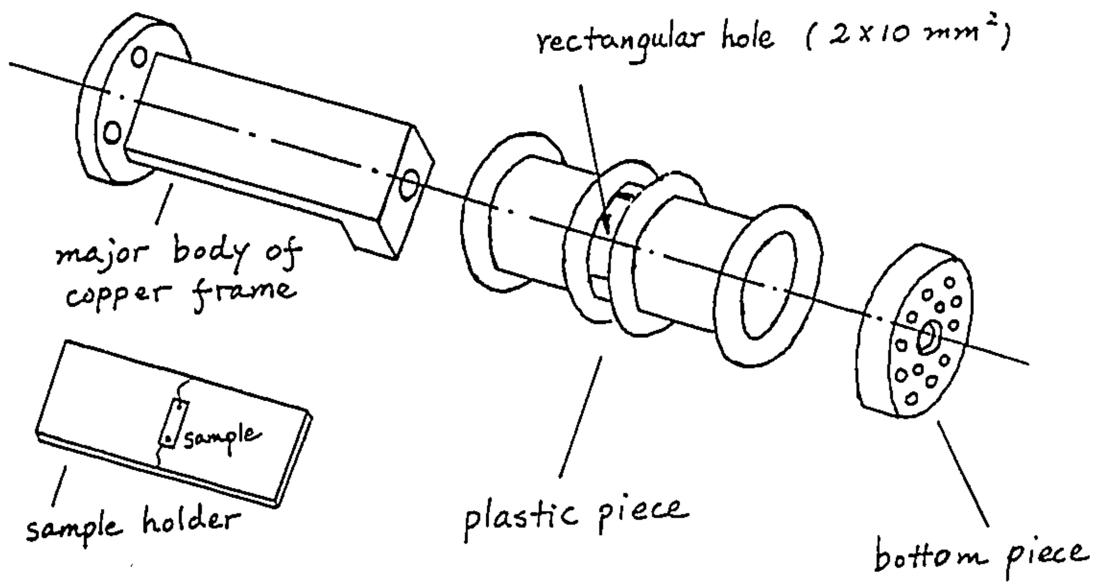

Fig. 2.32 A three dimensional schetch of the superconducting coils' frame.

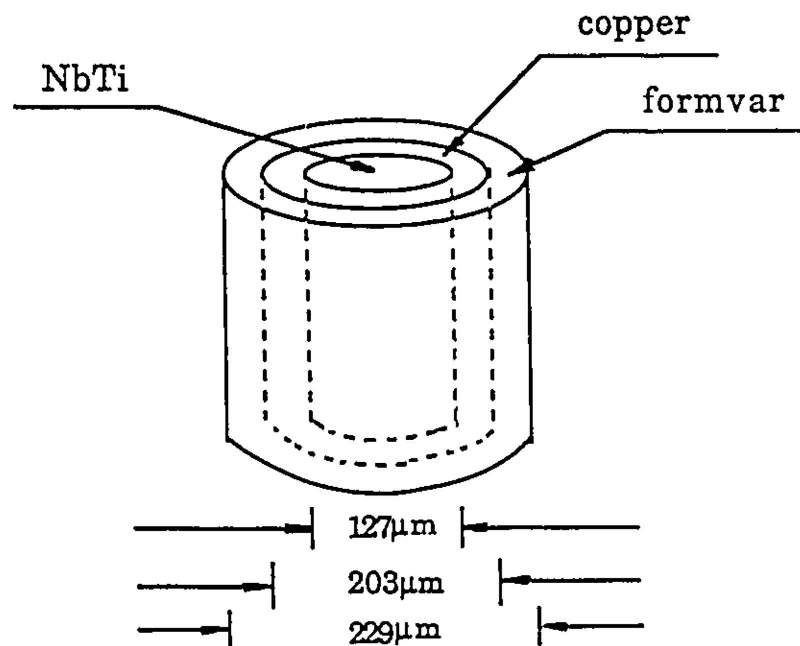

Fig. 2.33 The configuration of the superconducting wire.

field of 0.15T. The dimensions of the coil were chosen according to this requirement.

The superconducting wire is made of copper-clad NbTi, 127μm in diameter. The diameter of the wire including the copper is 203μm, and an insulation layer (formvar) covers the copper. The total diameter of the wire is 229μm. The configuration of the wire is shown in Fig. 2.33. The lead (normal) wire which carries 5A current above 10K is a No.22 copper wire with formvar insulation. Since those two kinds of wire have very different diameters, a third piece of wire, a normal No. 24 copper wire with insulation which is thiner than the No. 22 wire and can carry 5A current below 10K was used to join the No.22 wire and the superconductor. It was soldered directly to the superconductor wire and twisted one or two turns on the coil. Between the No. 22 and No. 24 wires, a small junction is used as a connector of these two wires. Two ends of these two wires are soldered individually to each end of the junctions and the junction itself can be separated easily by unplugging a hollow pin. In this way, one can easily connect or separate the coils with the normal lead wire as needed. A matching pair of clamps is designed in order to fix the junction beside the Janis centre bar. These clamps are also made of plastic.

The superconducting solenoid is placed around the copper frame and the sample is put on the copper frame inside the solenoid. The whole device solenoid must be isolated except for a small rectangular hole on the solenoid. This brings the problem of how to put the sample into or take the sample from the solenoid? To solve this problem, a bottom piece of copper frame is designed, which can be separated from the major body of the

copper frame. To separate the bottom piece, one can insert or pull out the copper section containing the sample, or, by separating the bottom piece, one can move the superconducting coils away by disconnecting the little junction and directly putting the sample on the copper frame.

The signal detecting wires (gold wires) from the sample can be connected through the hole between the two superconducting coils without removing the solenoid. Or one can first move away the tube in advance, putting the sample on the holder and then sliding back the solenoid to let the signal wires come out from the side of the solenoid, as illustrated in Fig. 2.32.

B. Field Design

The field at the centre point O (Fig.2.34) is: $B_0 \approx 0.7\mu_0 nI$ (see next section), where μ_0 is the permeability of free space, n is the number of turns of wire per unit length, and I is the current passing through the wire. If the maximum field needed is $B_{max}=0.15$Tesla and the maximum current is I=5A, with $\mu_0=4\pi\cdot10^{-7}=1.257\cdot10^{-6}$henry/meter, then we need n=34turns/mm. However, the diameter of the superconductor wire is 229μm, which gives:

$$\frac{1\text{turn}}{229\mu\text{m}}=4.37\text{turns/mm}$$

Considering of the space between the wires, we choose 4(turns/mm)·8(layers)=32turns/mm. Thus the thickness of 8 layers is ≤1.832mm

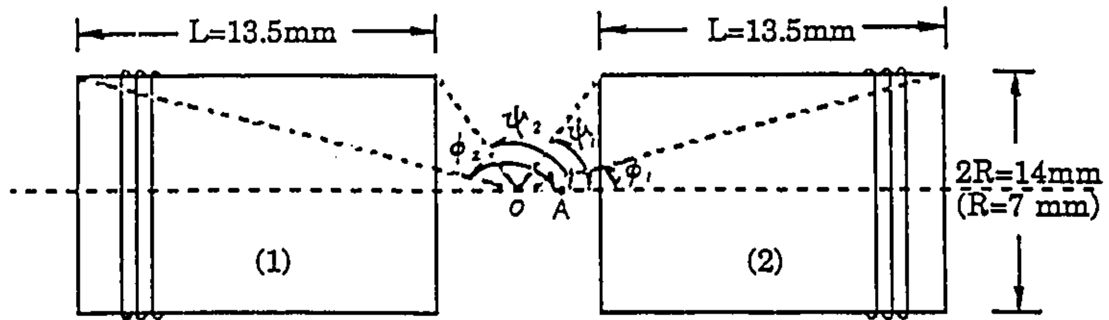

Fig. 2.34 Definition of angles ϕ, ψ for the finite coil.

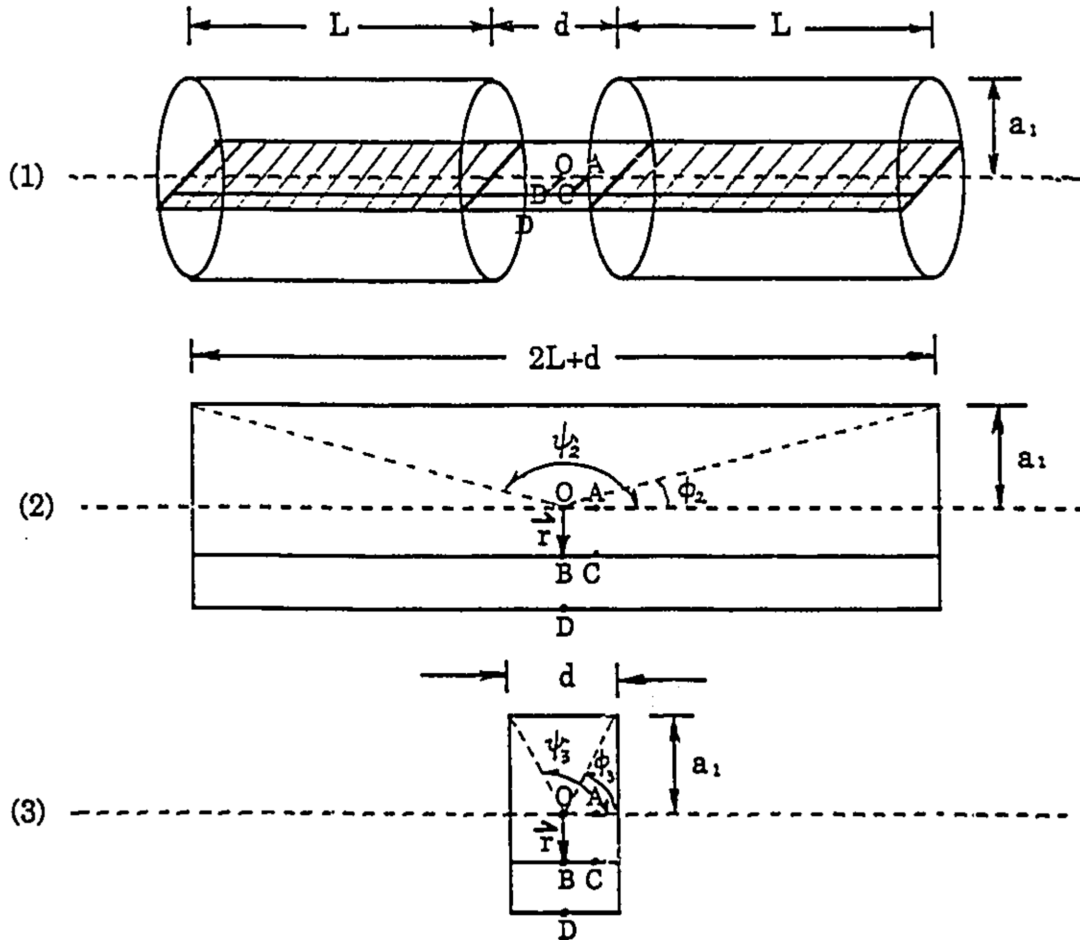

Fig. 2.35 Four points (O, A, B, C) in three different types of finite coils

(2) Field Calculation

The Magnetic field at four different points around centre of the gap between the two coils has been calculated {refer to Fig. 2.35 (1) }.

(a). Point O

Since point O is at the centre of axis Z, the field at this point is along the Z axis only . We can simple use the formula

$$B=0.5\mu_0 nI(\cos\phi - \cos\psi) \tag{2.32}$$

to calculate the field at point O. Here ϕ and ψ are the angles between the z axis and the two lines connecting the centre point O and the points at the edges of the coil (Fig.2.34).

At point O, the magnetic field B will be contributed by coils (1) and (2) :

$$B_{(1)}=0.5\mu_0 nI(\cos\phi_1-\cos\psi_1) \tag{2.33}$$

$$B_{(2)}=0.5\mu_0 nI(\cos\psi_2-\cos\phi_2)=0.5\mu_0 nI(-\cos\psi_1+\cos\phi_1) \tag{2.34}$$

with $\psi_2 = \pi - \psi_1$, $\phi_2 = \pi - \phi_1$

$$\therefore \quad B_O=B_{(1)O}+B_{(2)O}=\mu_0 nI(\cos\phi_1-\cos\psi_1) \tag{2.35}$$

where

$$\cos\phi_1=\frac{L+\frac{d}{2}}{\sqrt{(L+\frac{d}{2})^2+R^2}} \qquad \cos\psi_1=\frac{\frac{d}{2}}{\sqrt{(\frac{d}{2})^2+R^2}}$$

let L=13.5mm, R=7mm, d/2=1.5mm, equation (2.35) gives $B=0.697\mu_0 nI$ at point O.

(b). Point A

OA=1mm. The calculation is similar to that performed for point O; at point A,

$$B_A=B_{(1)A}+B_{(2)A}=0.5\mu_0 nI(\cos\phi_1+\cos\phi_2-\cos\psi_1-\cos\psi_2) \tag{2.36}$$

where

$$\cos\phi_1=\frac{L+0.5mm}{\sqrt{(L+0.5mm)^2+R^2}} \qquad \cos\phi_2=\frac{L+2.5mm}{\sqrt{(L+2.5mm)^2+R^2}}$$

$$\cos\psi_1=\frac{0.5mm}{\sqrt{(0.5mm)^2+R^2}} \qquad \cos\psi_2=\frac{2.5mm}{\sqrt{(2.5mm)^2+R^2}}$$

Sustituting the values of L, R into equation (2.36), we get $B=0.702\mu_0 nI$ at point A. Comparing to the field strength at point O, $B_A/B_O=1.007$ or $B_A \approx B_O$.

(c). Point B

OB=3.5mm. Since point B is not on the centre axis, equation (2.32) can not be simply applied because the direction of the field at this point is not along z only. Generally, at any point $P(\rho, \theta)$, where ρ and θ are conventional spherical coordinates. The axial and radial components of the field are:

$$B_z(\rho,\theta)=B_0\left[1+E_2(\alpha,\beta)\left(\frac{\rho}{a_1}\right)^2 P_2(u)+E_4(\alpha,\beta)\left(\frac{\rho}{a_1}\right)^2 P_4(u)+\cdots\right] \tag{2.37}$$

$$B_r(\rho,\theta)=B_0\left[0+E_2(\alpha,\beta)\left(\frac{\rho}{a_1}\right)^2 P'_2(u)+E_4(\alpha,\beta)\left(\frac{\rho}{a_1}\right)^2 P'_4(u)+\cdots\right] \tag{2.38}$$

where B_O is the field at centre point O, $P_n(u)$ are the Legendre Polynomials and their derivatives are $P_p'(u)$, u is the function of the angle θ, $\alpha(=a_2/a_1)$ and $\beta(=b/a_1)$ are the ratio constants and a_1, a_2, b are the interior radius, external radius and length of the coil respectively. The coefficients in $E_n(\alpha , \beta)$ are defined from the standard formula for the coefficients in a Taylor series:

$$E_{2n}=\left| \frac{1}{B_O} \frac{1}{(2n)!} \frac{d^{2n}B_z(z,0)}{dz^{2n}} \right|_{z=0} \qquad (2.39)$$

The Legendre polynomials and the values of cofficients E_n are given in Table 8.1 on P.234 and Table 8.12.1--8.12.25 on P.271--P.296 of ***Solenoid Magnet Design*** by D. BRUCE MONTGOMERY.[2.A]

Fig. 2.34 shows the four points being considered around the centre inside the solenoid. At points O, A, B, θ=0 or π/2, the field's radial components $B_r(\rho, \theta)=0$. This also can be seen from the symmetry. But it is not true at other points where θ≠0 or π/2 such as point C. Hence, at point B, only the axial component is considered. The field inside the gap (width d) between the two solenoids (L length for each) {Fig.2.35 (1) } can be calculated by subtracting the field for a solenoid coil of length d {Fig. 2.35 (2) } from that for solenoid coil of length 2L+d {Fig. 2.35 (3) }at the same point.

At point B with $\rho=r=a_1/2$, the field is

$$B_B^{(1)}\left(\frac{a_1}{2},\frac{\pi}{2}\right)=B_0\left[1-\frac{1}{2}E_2(\alpha,\beta)\left(\frac{1}{2}\right)^2-\frac{3}{8}E_4(\alpha,\beta)\left(\frac{1}{2}\right)^4-\frac{5}{16}E_6(\alpha,\beta)\left(\frac{1}{2}\right)^6+\cdots\cdots\right] \quad (2.40)$$

where the symbols $P_n(u)$ and $P'_n(u)$ are expressed by the value of Legendre Polynomial for $\rho=a_1/2$, $\theta=\pi/2$. Actually

$$B_B^{(1)}=B_B^{(2)}-B_B^{(3)} \quad (2.41)$$

where (1), (2), (3) indicate the different solenoid coils shown in Fig.2.35. And

$$B_B^{(2)}=B_0^{(2)}\left[1-\frac{1}{2}E_2(\alpha_2,\beta_2)-\frac{3}{8}E_4(\alpha_2,\beta_2)-\frac{5}{16}E_6(\alpha_2,\beta_2)+\cdots\cdots\right] \quad (2.42)$$

$$B_B^{(3)}=B_0^{(3)}\left[1-\frac{1}{2}E_2(\alpha_3,\beta_3)-\frac{3}{8}E_4(\alpha_3,\beta_3)-\frac{5}{16}E_6(\alpha_3,\beta_3)+\cdots\cdots\right] \quad (2.43)$$

in our case, the ratio constants α, β are:

$$\alpha_2=\frac{a_2}{a_1}=\frac{8.5\text{mm}}{7\text{mm}}=1.2$$

$$\beta_2=\frac{b}{a_1}=\frac{L+d/2}{a_1}=\frac{15\text{mm}}{7\text{mm}}=2.14$$

$$\alpha_3=\frac{a_2}{a_1}=\frac{8.5\text{mm}}{7\text{mm}}=1.2$$

$$\beta_3=\frac{b}{a_1}=\frac{d/2}{a_1}=\frac{1.5\text{mm}}{7\text{mm}}=0.24$$

The fields at centre point in case (2) and (3) are:

$$B_O^{(2)}=\frac{1}{2}\mu_0 nI(\cos\phi_2-\cos\psi_2)=\mu_0 nI\cos\psi_2=\mu_0 nI\frac{L+d/2}{\sqrt{(L+d/2)^2+R^2}}=0.9062\mu_0 nI$$

$$B_O^{(3)}=\frac{1}{2}\mu_0 nI(\cos\phi_3-\cos\psi_3)=\mu_0 nI\cos\phi_3=\mu_0 nI\frac{d/2}{\sqrt{(d/2)^2+R^2}}=0.2095\mu_0 nI$$

$$\therefore\ B_O^{(1)}=B_O^{(2)}-B_O^{(3)}=0.6967\mu_0 nI=0.697\mu_0 nI$$

Using Table 8.12.6 on P.277 of reference [2.A] which gives the value $E_n(\alpha,\beta)$,

we get

$$B_B^{(2)}=0.9125\mu_0 nI$$

$$B_B^{(3)}=0.2496\mu_0 nI$$

$$\therefore\ B_B^{(1)}=B_B^{(2)}-B_B^{(3)}=0.6629\mu_0 nI=0.663\mu_0 nI \quad \text{at point B.}$$

It gives

$$\frac{B_B^{(1)}}{B_O}=0.95 \quad \text{or} \quad B_B^{(1)}\approx B_0$$

4. Point C

At point C, both axial and radial components of the field exist.

$$B_{zc}=B_0[1+E_2(\alpha,\beta)\left(\frac{\rho}{a_1}\right)^2\left(\frac{1}{2}\right)(3u^2-1)+E_4(\alpha,\beta)\left(\frac{\rho}{a_1}\right)^4\left(\frac{1}{8}\right)(35u^4-30u^2-3)+$$

$$+E_6(\alpha,\beta)\left(\frac{\rho}{a_1}\right)^6\left(\frac{1}{16}\right)(231u^6-315u^4+105u^2-5)+\cdots\cdots] \quad (2.44)$$

$$B_{rc}=B_0[0+E_2(\alpha,\beta)\left(\frac{\rho}{a_1}\right)^2\left(\frac{1}{2}\right)(6u)u'+E_4(\alpha,\beta)\left(\frac{\rho}{a_1}\right)^4\left(\frac{1}{8}\right)(140u^3-60u)u'+$$

$$+E_6(\alpha,\beta)\left(\frac{\rho}{a_1}\right)^6\left(\frac{1}{16}\right)(138u^5-1260u^3+210u)u'+\cdots\cdots] \quad (2.45)$$

with

$$u=\cos\theta=\frac{1mm}{\sqrt{(3.5mm)^2+(1mm)^2}}=0.2747$$

$$u'=\sin\theta=\frac{3.5mm}{\sqrt{(3.5mm)^2+(1mm)^2}}=0.9615$$

$$\rho=\sqrt{(3.5mm)^2+(1mm)^2}=3.64mm$$

$$a_1=7mm$$

$$\frac{\rho}{a_1}=\frac{3.64mm}{7mm}=0.52$$

Using value for E(α , ß) from Table 8.12 in reference [2.A], we get:

The axial components are

$$B_{zc}^{(2)}=0.912\mu_0 nI$$

$$B_{zc}^{(3)}=0.237\mu_0 nI$$

$$\therefore \quad B_{zc}^{(1)}=B_{zc}^{(2)}-B_{zc}^{(3)}=0.675\mu_0 nI$$

The radial components are

$$B_{rc}^{(2)}=2.634\times10^{-5}\mu_0 nI$$

$$B_{rc}^{(3)}=0.088\mu_0 nI$$

$$\therefore \quad B_{rc}^{(1)}=B_{rc}^{(2)}-B_{rc}^{(3)}=-0.088\mu_0 nI$$

where "-" indicate the negative direction of radial component of the field.

Totally,

$$B_C^{(1)}=\sqrt{\left(B_{zc}^{(1)}\right)^2+\left(B_{rc}^{(1)}\right)^2}=0.681\mu_0 nI$$

Compared to B_O, it gives

$$\frac{B_C^{(1)}}{B_O}=0.98 \quad \text{or} \quad B_C^{(1)}\approx B_O$$

The field dircetion at these four points are given in Fig. 2.36.

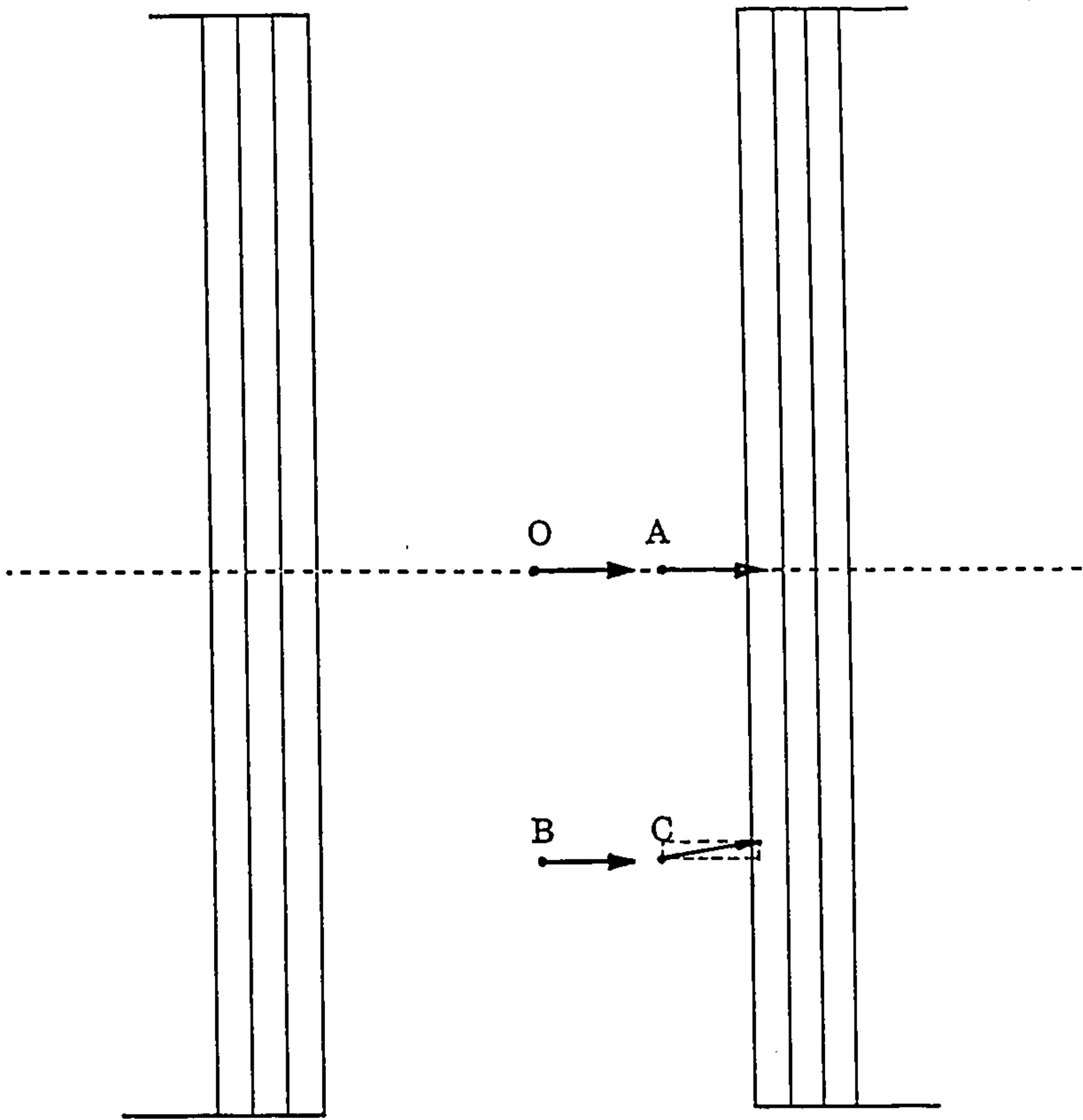

Fig. 2.36 Schematic of the fields at four points (O, A, B, C)

(3) Results

The superconducting wire used is #38 NbTi as mentioned before. There are 8 layers on each side of the split coils. the total number of turns is N=913 for both coils. The coils used about 44.7 meters of superconducting wire. The resistance of the coils was measured at both room and liquid Nitrogen temperatures. It is R=37.8Ω at T=300K and R=4.7Ω at T=77K. The maximum centre (point O) magnetic field is $B=0.7\mu_0 nI=0.15$Teslas.

Table A.1 lists the comparison between the practical parameters obtained from the coils we have made and the theoretical parameters.

parameters	actual	maxima
R ratio $(R_{(300K)}/R_{(77K)})$	8.04	8.07
field B (T)	0.15	10
current density i (A/m^2)	1.2×10^8	10^{11}

Table A.1 The practical and theoretical parameters of the copper-clad superconductor.

REFERENCES

2.1 Y. Marfaing, Photoconductivity, photoelectric effect, P. 471--9; 1980, Handbook on Semiconductors, Vol 2. Editor: Minko Balkanski; Amsterdon North Hollard.

2.2 Ryvkin, 1964, Photoelectric Effect on Semiconductor, P. 299--316, Consultants Bureau Enterprise Inc.

2.3 Richard H. Bube, 1967 Photoconductivity of Solid, P. 384-91, John Wiley

2.4 S. W. Kurnick and R. N. Zitter, J. of Appl. Phys. Vol 27 (3), 278--85 (1956).

2.5 Jack P. Dixon, Phys. Rev. Vol. 107 (2), 374--8 (1957).

2.6 E. Fortin, The Rev. of Scientific in Instruments, 41 (8), 1252 (1970).

2.7 Edited by M. J. Howes and D. V. Morgan, 1985, Gallium Arsenide Materials Devices and Circuits. P. 134, Wiley Sci.

2.8 A. Iliadis and K. E. Singer, Solid-State Electronic, 26 (1), 7--14 (1983).

2.9 Margaret Buchanan, Lab. of Microstructural Science, NRC, private communication.

2.10 P. H. Elder, April, 1968, A Study of the Properties of Au-Ge Ohmic Contacts to GaAs (Report of Physics Project in the Dept. of Phys., Univ. of Ottawa).

2.11 G. Duggan, G. B. Scott, C. T. Foxon and J. J. Harris, Appl. Phys.

Lett., 38 (4) 246--8 (1981).

2.12 R. M. Fletcher, D. Ken Wanger and J. M. Ballantyne, ibid, 41 (3), 256--8, (1982).

2.13 R. A. Smith, 1968, Semiconductors, P. 311, Cambridge.

2.14 A. J. Barbarie, E. Fortin, Solid State Communications, 14, 267--9, (1974)

2.15 S. W. Kuknick, R. N. Zitter, J. Appl. Phys., 27 (3), 278 (1956).

2.16 Jack R. Dixon, Phys. Rev., 107 (2), 374 (1957).

2.17 R. Muralidharan, K. Ploog, Appl. Phys. A, 49, 527-531 (1989).

2.18 H. J. Lee, D. C. Look, J. Appl. Phys. 54 (8), 4446 (1983).

2.19 A. L. Mears, R. A. Stradling, J. Phys. C4, L22 (1971).

2.20 D. C. Look, J. Phys. Chem. Solids, 36, 1311-1315 (1975).

2.21 H. A. Milner-Brown, Ph. D. Thesis, 1969, Photoconduction in a Magnetic-Field and Some Related Effects in Semi-Insulating Gallium Arsenide , Ottawa University.

2.22 Willardson and Beer, 1987, Semiconductor and Semimetal, Vol. 24, P. 78--90, United Kingdom Edition, Academic Press Inc. (London).

2.A D. Bruce Montgomery, 1969, Solenoid Magnet Design, P 234, 271-296, John Wiley & Sons, Inc..

CHAPTER 3

PC AND PV SPECTROSCOPY STUDY IN $In_xGa_{1-x}As/GaAs$ QUANTUM WELLS

Semiconductor heterojunctions have wide applications in practice. They can be used as high quality devices, which explains the great interest in material science in recent years. Since the previous attempt of using the PEM effect to study the quantum levels of these junctions was unsuccessful, and since the two electrodes on the samples are ohmic contacts which can be used both for PEM and PC measurements, a study of quantum levels in $In_xGa_{1-x}As/GaAs$ quantum wells using the photocurrent method was performed. Some photovoltaic spectra were also studied. This chapter begins with the theoretical review of band structure in quantum wells and the principle of PC and PV effects, followed by an experimental description which consists of experimental apparatus, methods and samples. The results and analysis are given last.

3.1 Theory

3.1.1 Quantum Well Energy Levels

The energy levels confined inside the quantum well can be calculated in the appoximation of the envelope wave function:[3.1] [3.2]

$$\psi=\sum_{A,B} e^{i\vec{k}_\perp \cdot \vec{r}} \cdot u_{c,\vec{k}}^{A,B}(\vec{r})\chi_n(z) \tag{3.1}$$

Where A and B indicate two materials with different bandgaps. These two energy bands are discontinuous, i.e. GaAs has larger bandgap forming an energy potential barrier and $In_xGa_{1-x}As$ has smaller bandgap forming an energy potential well; z is the material growth direction; $\vec{k}_\perp$ is the transverse electron wave vector; $u_{c,\vec{k}}(\vec{r})$ is the Bloch wave function in A or B material and $\chi_n(z)$ is the envolope wave function, determined to a good approximation by the Schrödinger-like equation:[3.3]

$$[-\frac{\hbar^2}{2m^*(z)}\frac{\partial}{\partial z^2}+V_c(z)]\chi_n(z)=\varepsilon_n\chi_n(z) \tag{3.2}$$

where $m^*(z)$ is the electron effective mass of the A or B material, $V(z)$ represents the energy levels of the bottom of the conduction band and ε_n is the so called confinement energy of the carriers. Using the Kane--model[3.4] including the strain effect for describing the electron and hole states in ternary layer, the conduction subbands and heavy--hole as well as light--hole subbands can be determined.

For electrons, in the case of bound states $\varepsilon_n<V_s$, where V_s is the barrier potential, the subbands are determined by the following equation:

$$\cos qd = \cos k_A L_A \cosh \kappa_B L_B + \frac{1}{2}(\xi - \frac{1}{\xi}) \sin k_A L_A \sinh \kappa_B L_B \qquad (3.3)$$

with and

$$\xi = \frac{m_A^* \kappa_B}{m_B^* k_A} = \sqrt{\frac{V_s - \varepsilon_n}{\varepsilon_n}} \qquad k_A = \sqrt{\frac{2m_A^* \varepsilon_n}{\hbar^2}} \qquad \kappa_B = \sqrt{\frac{2m_B^*(V_s - \varepsilon_n)}{\hbar^2}}$$

where L_A is the barrier width and L_B is the well width and q is the Bloch wave vector. The allowed energy bands are given as usual by $-1 \leq \cos qd \leq 1$. In case of unbound states $\varepsilon > V_s$, ε satisfies the following relation:

$$\cos qd = \cos k_A L_A \cos k_B L_B - \frac{1}{2}(\bar{\xi} + \frac{1}{\bar{\xi}}) \sin k_A L_A \sin k_B L_B \qquad (3.4)$$

with and

$$\bar{\xi} = \frac{m_A^* k_B}{m_B^* k_A} = \sqrt{\frac{\varepsilon - V_s}{\varepsilon}} \qquad k_A = \sqrt{\frac{2m_A^* \varepsilon}{\hbar^2}} \qquad k_B = \sqrt{\frac{2m_B^*(\varepsilon - V_s)}{\hbar^2}}$$

With the limit of noncommunicating wells ($\kappa_B L_B \rightarrow \infty$ or $k_B L_B \rightarrow \infty$), one can see that equations (3.3) and (3.4) which are for communicating multiple quantum wells or superlattices will lead to:

$$\cos k_A L_A + \frac{1}{2}(\xi - \frac{1}{\xi}) \sin k_A L_A = 0 \tag{3.5}$$

and

$$\cos k_A L_A - \frac{1}{2}(\bar{\xi} + \frac{1}{\bar{\xi}}) \sin k_A L_A = 0 \tag{3.6}$$

Rearrange equation (3.5):

$$\tan k_A \frac{L_A}{2} = \xi \quad \text{(even)} \tag{3.7}$$

$$\text{cotan}\, k_A \frac{L_A}{2} = -\xi \quad \text{(odd)} \tag{3.8}$$

These are the usual single quantum well solution which also can be directly solved from a single finite potential well.[3.5]

For the hole, the quantization problem is much more complicated in usual semiconductor materials. Reference [3.5] gives a detailed description of how to solve this kind of problem.

In the $In_xGa_{1-x}As/GaAs$ QW system, the lattice mismatch is accommodated by elastic strain in the layer. For a certain indium content, the ternary layer thickness should be smaller than the critical thickness L_C,[3.6] [3.7] to obtain a good--quality layer where the lattice mismatch is totally accommodated by elastic strain. In this elastic limit, only the ternary is strained with an amplitude independent of its thickness. Under this compressive strain, the InGaAs layer bandgap increases uniformly and its valence bandgap degeneracy is lifted at the Γ point, which result in

the heavy--hole valence band moving up an light--hole valence band moving down. In such a system, the relative position of the bands in the InGaAs wells and the GaAs barriers can lead to two possible configurations of the quantum wells potential as shown in Fig. 3.1a. In the configuration on the left--hand side, the electrons and both the heavy and light holes are confined in InGaAs wells. However, in the configuration on the right--hand side, the electron and heavy holes are in the InGaAs region, while the light holes are confined in the GaAs layer. Thus, the GaAs valence band lies between the InGaAs heavy--hole and light--hole valence band.[3.6] [3.8] Fig. 3.1b illustrates the possible transitions between valence and conduction bands.

For the calculation of quantum levels, the relevant parameters are given as follows:[3.8] [3.9]

$E_0(In_xGa_{1-x}As)=E_0(GaAs)-1.53x+0.45x^2$ at T=300K

$E_0(In_xGa_{1-x}As)=E_0(GaAs)-1.47x+0.375x^2$ at T=77K

$m^*_c=(0.0665-0.044x)m_0$

$m^*_{LH}=(0.094-0.062x)m_0$

$m^*_{HH}=(0.45-0.07x)m_0$

where x is the concentration of indium in the InGaAs material, m_0 is the free--electron mass, m^*_c, m^*_{LH} and m^*_{HH} are the conduction band electron effective mass, valence band light--hole effective mass and heavy--hole effective mass, respectively.

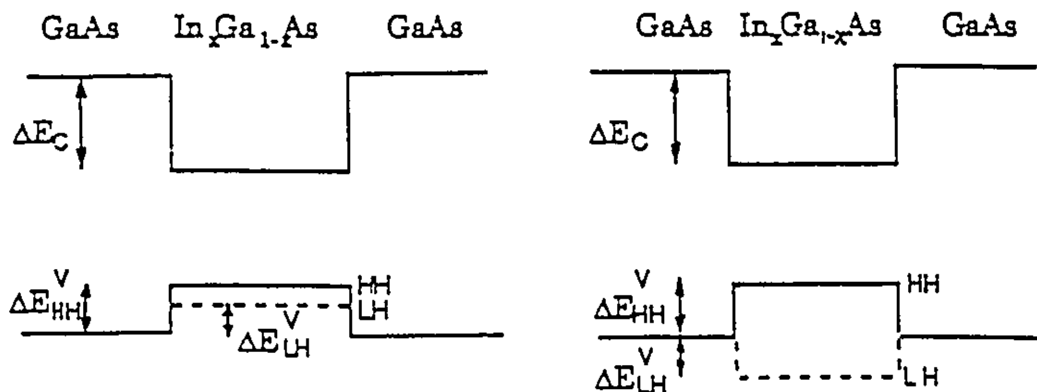

Fig. 3.1a Possible energy-band configuration in a strained-layer $In_xGa_{1-x}As/GaAs$ quantum well. In the InGaAs layer, the top of the valence is split into heavy- (HH) and light- (LH) hole bands as a result of the strain arising from the lattice mismatch between the two materials.

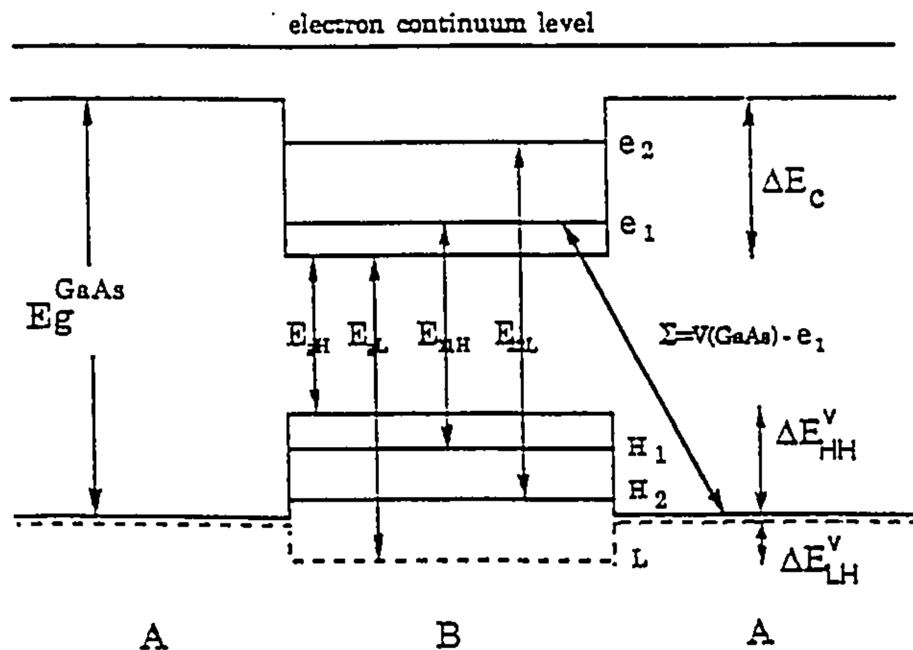

Fig. 3.1b Energy-band configuration of a strained $In_xGa_{1-x}As/GaAs$ QW and possible transitions between valence and conduction bands.

3.1.2 Photoconductivity and Photovoltage

The conductivity of a semiconductor is expressed as:

$$\sigma=e(n\mu_n+p\mu_p) \tag{3.9}$$

where n and p are the densities or concentrations of electrons and holes of the material, μ_n and μ_p are the mobilities of the electron and the hole, respectively.

Under the illumination of light with wavelength lying in the fundamental absorption region, the semiconductor will experience a process that the absorption of light quanta produces electron transitions from the valence band to the conduction band and consequently generates nonequilibrium electrons and holes. If Δn is the density of extra electrons and Δp the density of extra holes in the steady state, the resulting photoconductivity is given by:

$$\sigma=e[(n_0+\Delta n)\mu_n+(p_0+\Delta p)\mu_p] \tag{3.10}$$

or:

$$\Delta\sigma=e(\Delta n\mu_n+\Delta p\mu_p) \tag{3.11}$$

where n_0 and p_0 are the equilibruim carriers densities, giving a conductivity $\sigma_0=e(n_0\mu_n+p_0\mu_p)$ in darkness. The Photovoltaic effect constitutes a class of phenomena in which light generates a voltage across a portion of the semiconductor. This is due to inhomogeneities in the material or to surface barrier effects. The absorption of the photon results in the creation of an excess of free hole--electron pairs accumulating in regions where they produce a net space charge.

3.2 Experimental

3.2.1 Samples

Four $In_xGa_{1-x}As/GaAs$ quantum wells samples have been studied during the PC experiment. They were grown using metal organic vapor--phase epitaxy (MOVPE) method in a horizontal low--pressure reactor. Three of them were grown on Cr--doped semi--insulating GaAs (001) substrates. A micron thick GaAs buffer was first grown on the substrates before the quantum well was fabricated. Finally undoped GaAs cap layers with a thickness of 85nm were deposited to cover the top of the assembly. The four samples are numbered as MO96, MO97, MO98, and MO33. Fig.3.2 shows the cross--section of the quantum well samples. The growth parameters of the samples are summarized in Table 2.1 in Chapter 2.

All of the four samples were cut in rectangular shape as mentioned in §2.2.1 (Chapter 2). The two electrodes are in the paralled configuration on the top surface of the sample, about 3 mm apart. They were made by first using lift--off--chlorobenzene process to treat the samples, then evaporating AuGe on the well treated surface of the samples, finally annealing them in a vacuum oven at a temperature of about 450°C for 2--3 minutes.[2.9] After annealing, Ag--epoxy was used to connect two gold wires to the AuGe contacts and the epoxy was cured in the oven at 200°C for 5 minutes.

The samples studied in the PV experiment were MO96, MO98 and MO33. For sample MO96, one of the electrodes is the omhic contact made of AuGe with thickness of 200Å using the same method as mentioned in

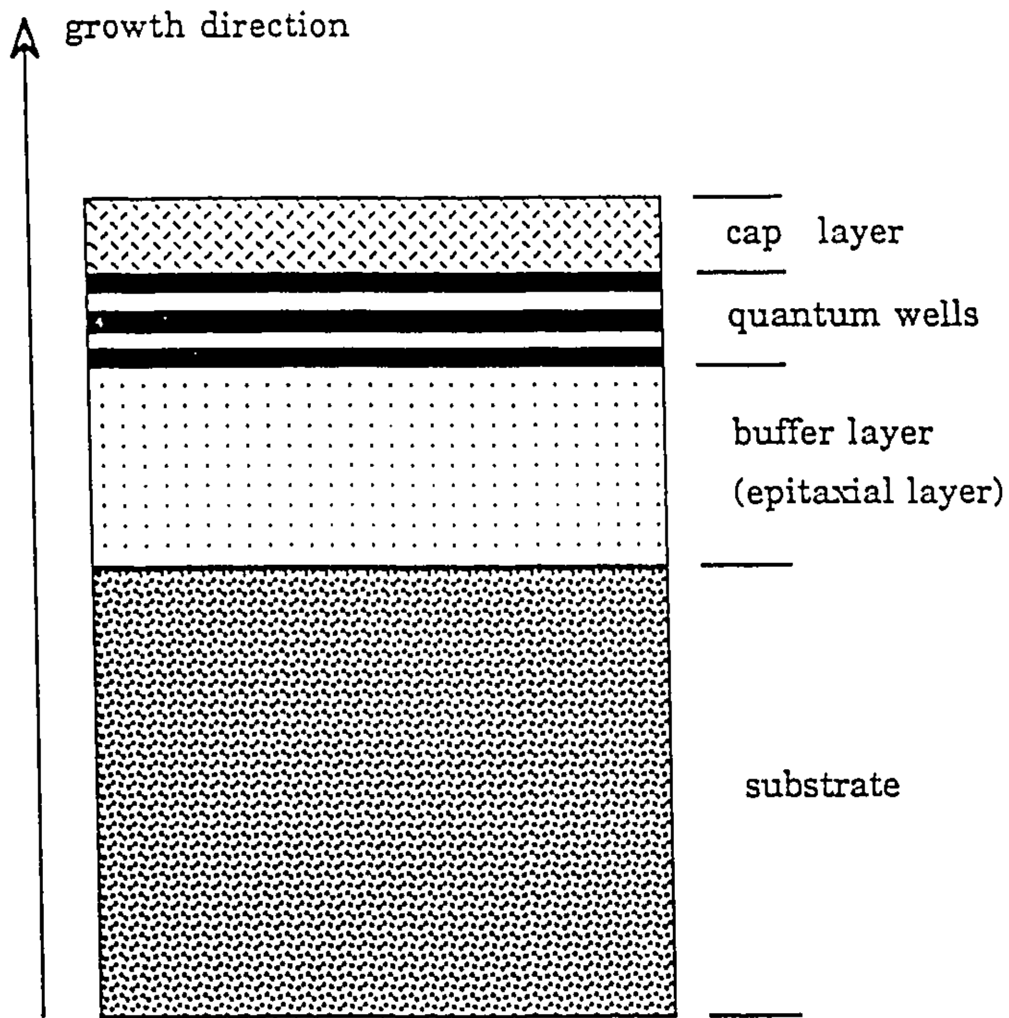

Fig. 3.2 Configuration of the QW samples' cross-section.

§2.2.1. Another electrode is simply made by putting a drop of silver paint directly on the surface of the sample and inserting a piece of gold wire at the same time and then leaving it to dry in the air at room temperature for 1 hour. This contact forms a Shottky barrier. The later two samples' contacts are omhic contacts as mentioned early in this section. Due to these samples' high impedance, the small barrier from the various heterojunctions can still contribute a sufficient PV signal to the measurement, but it is about 500 times lower than the PC signal.

All samples' impedance were measured at T=300K and T=77K, with values of about 10^8--10^{10} Ω at 300K and even much higher at 77K.

3.2.2 Apparatus

For the PC experiments, a 30W tungsten halogen projector lamp was used as the incident light source via the 2061 McPHERSON 1 meter scanning monochromator. An optical cryostat with temperatures adjustable from room to liquid nitrogen temperature was used as the sample holder. An ALCATEL turbomolecular pump was used to produce a high vacuum within the cryostat. A 9 volt battery or HEWLETT--PACKARD 6825A--BIPOLAR power supply, in series with a resistance box, was used as a bias supply. The lock--in amplifier was the PAR. model 124 and the signal recorder was a WATANABE WX4420 x--y recorder, or a computer with a data acquisition and analysis progam (Asystant+). The whole experimental set up is shown in Fig. 3.3.

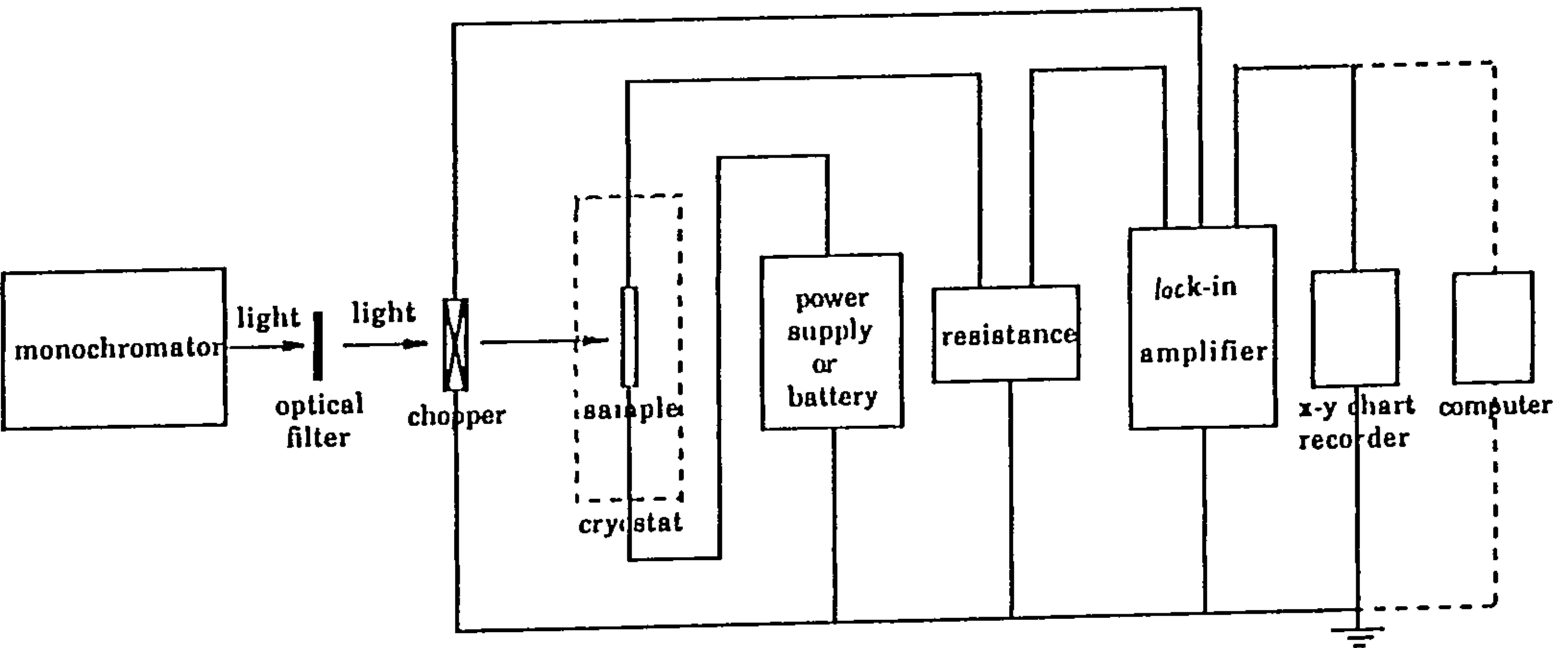

Fig. 3.3 Circuit diagram for PC measurement.

The 2061 McPHERSON monochromator has a grating of 1200 grooves/mm and a dispersion of 0.833nm/mm. its resolution is 0.01 nm with slits of 8 microns.

An optical filter was placed between lamp and monochromator to cut off the second order radiation. A chopper was adjusted at a suitable frequency to provide an AC light beam, and thus an AC photosignal.

The cryostat was made of the same materials as the one used in PEM effect measurements but with a different configuration. Fig. 3.4 shows a cross--sectional digram of the cryostat.

In the PV measurements, the apparatus were the same as that used in the PC experiment but without bias supply. The whole set-up of PV experiment is shown in Fig. 3.5.

3.2.3 Experimental Method

Fig. 3.6 shows the principle circuit diagram for PC measurements. The peak positions in the spectrum may be related to carrier's transitions between the conduction and valence subbands.

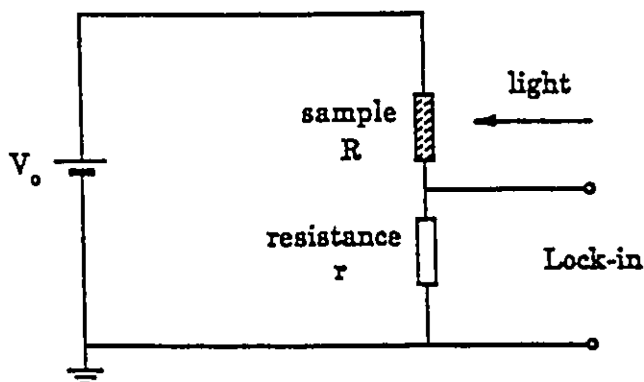

Fig. 3.6 The circuit for PC measurements

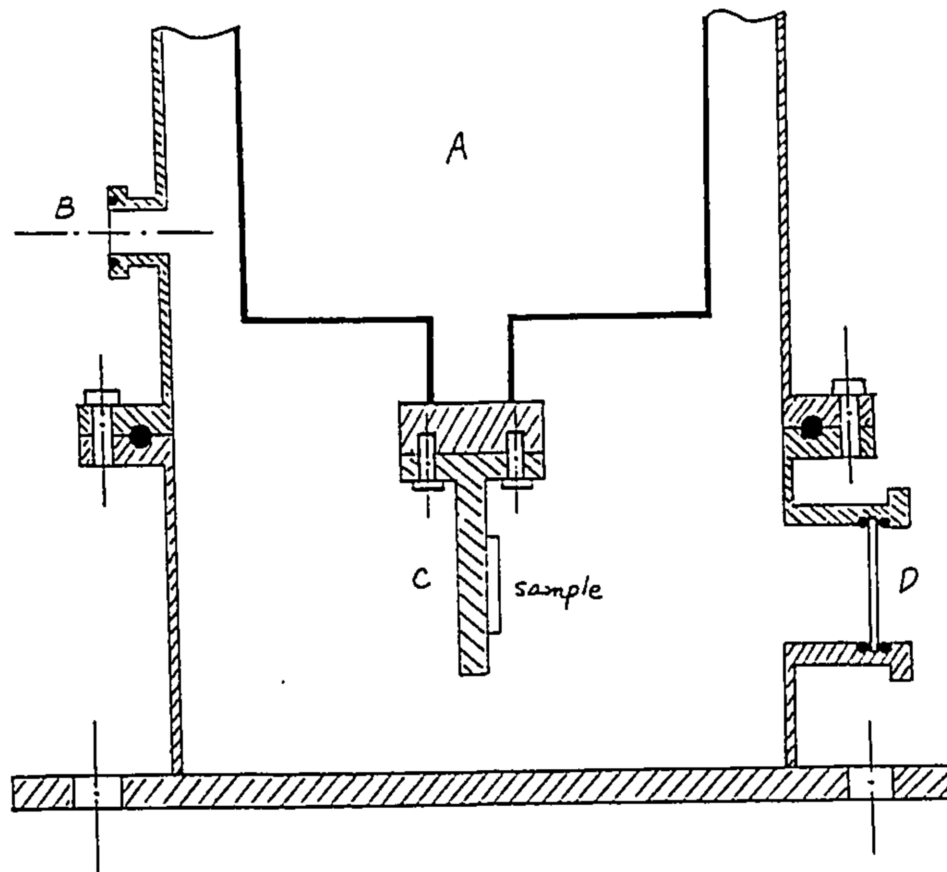

A nitrogen chamber
B electrical and thermal jack
C sample holder
D window
● O-ring

Fig. 3.4 Cross-section of the cryostat for PC mesurement.

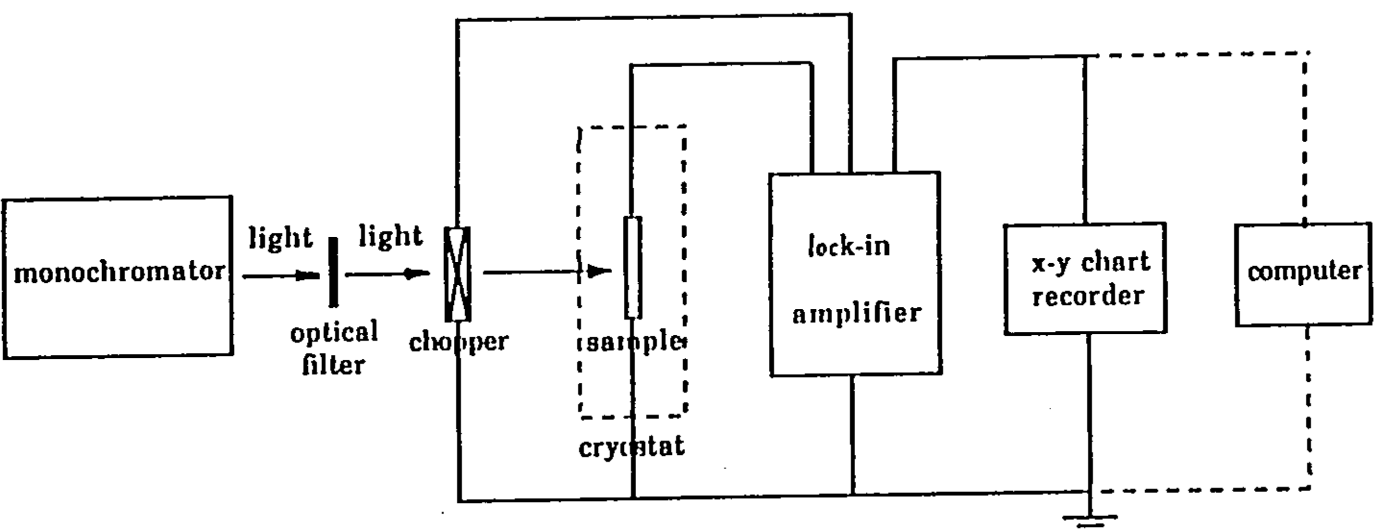

Fig. 3.5 A sketch of PV measurement set-up.

As shown in Fig. 3.6, a sample S (of impedance R) is connected to a resistance r ($r \ll R$) in series, which is supplied with a DC voltage V_0. A look-in amplifier is connected in parallel with the resistance r. Suppose the sample's impedance in darkness is R_0 and the impedance under illumination is R

$$R_0 - \Delta \leq R \leq R_0 \tag{3.12}$$

where the differential quantity Δ is dependent on the wavelength of the radiation. Neglecting the internal resitance of the power supply, the total resistance R_T of the loop is:

$$R_T=R+r \tag{3.13}$$

If the impedance of the lock--in amplifier is much larger than r, the current inside the circuit will be:

$$I=V_0/R_T=V_0/(R+r) \tag{3.14}$$

The value of R changes from R_0 to R_0-Δ due to the illumination and V_0 remains constant so that the current varies between:

$$V_0/(R_0+r) \leq I \leq V_0/[(R_0-\Delta)+r] \tag{3.15}$$

This current variation is called the photocurrent.

By detecting the voltage change V across the resistance r, one can monitor the current I through the sample since V is proportional to I:

$$V=rI \tag{3.16}$$

and the current I flowing through r is the same as that through R. Thus, the photocurrent can be detected.

In the PV measurement, the lock--in amplifier was directly connected to the sample to measure the photo--potential built up along the sample.

3.3 Results and Discussions

In this section, the photocurrent spectra of all four samples will first be presented and discussed. Then, photovoltaic spectra results of samples MO96, MO98 and MO33 are given out and discussed. Growth parameters of the samples obtained from matching of the experimental results with the theoretical calaulation are summarized in Table 3.1 and these values are different from those (given out by the crystal grower) listed in Table 2.1.

Samples	Substrate	x	L_W(Å)	L_B(Å)	Period
MO33(SQW)	undoped	0.24	60	----------	----------
MO96(SQW)	Cr--doped	0.154	38	----------	----------
MO97(SQW)	Cr--dpoed	0.166	85	----------	----------
MO98(MQW)	Cr--doped	0.167	90	100	5

Table 3.1 Samples' parameters for quantum wells

In the identification of the transitions, the notation mnH/L was used to indicate the transition between the nth valence and mth conduction subbands for heavy (H) or light (L) holes.

The calculated energies correspond to interband transitions whereas, at least for 11H transition, the experimental peak has an excitonic character. Since the binding energy of a free 11H exciton is of order of 5--8 meV, we select the values for x, L_W and L_B so that the calculation energies compared to the experimental ones should be larger in a value of the same order.

The band offset Q defined by equations:

$$\Delta E_{HH}=Q\cdot\Delta E_g \quad \text{and} \quad \Delta E_C=(1-Q)\cdot\Delta E_g \tag{3.14}$$

where $\Delta E_g=E_g(GaAs)-E_g(In_xGa_{1-x}As)$

or
$$Q/(1-Q)=\Delta E_{HH}/(\Delta E_{HH}+\Delta E_C) \tag{3.15}$$

was taken between 0.3--0.4, ΔE_{HH} and ΔE_C which are defined in Fig. 3.1a can be determined after the value of the band offset Q was taken.

3.3.1 PC Spectroscopy

(1) Sample MO96

Sample MO96 is a SQW with x=0.154±0.005, L_W=38±3Å. The band offset is Q=0.36, band parameters are shown in Table 3.2.

Energy (eV)	T=77K	T=300K
E_g(InGaAs)	1.290	1.202
ΔE_C	0.095	0.097
ΔE_{HH}	0.051	0.053
ΔE_{LH}	-0.208	-0.017
E_{gH}	1.362	1.272
E_{gL}	1.434	1.503

Table 3.2 Band parameters from theroetical calculation for Sample MO96

Fig. 3.7 to 3.10 present the photocurrent spectra at T=77K and T=300K. Among them, Fig. 3.8 gives the spectral dependence with different applied voltages V_0 at T=77K with only one AC light source. Fig. 3.9 is the spectrum recorded at T=77K using two light sources, i.e. one AC scanning light plus another DC white light during the measurement, to get rid of the effect from the Cr--doped substrate. Fig.3.10 shows the room temperature PC spectrum with one AC light.

From Fig. 3.7 and 3.8, three maxima labeled α, β and γ and one minimum ξ are displayed. They can be identified and matched with the theoretical calculation. The two peaks α and β reveal the QW transition between the valence and conduction subbands. The stronger one, α, is the transition between first heavy--hole level in valence band and first electron level in conduction band, named 11H. From numerical calculations, the broader β is found to coincide with the transition between the first electron level in conduction band and the GaAs valence band [e1--E_v(GaAs)]. Compared to the spectrum obtained from PC measurement on Cr--doped substrate (Fig. 3.11), it can be seen that the minimum ξ is related to the fundamental gap transition of GaAs and peak γ is the effect from the Cr--doped substrate. E. Fortin *et al* have studied the interference between substrate and layer in similar systems.[3.10] When the exciting light energy is smaller than the GaAs band gap at liquid nitrogen temperature (1.508eV), the photosignal is due to the absorption at the substrate material and not at the surface layer. The Cr--doped substrate interferes with the

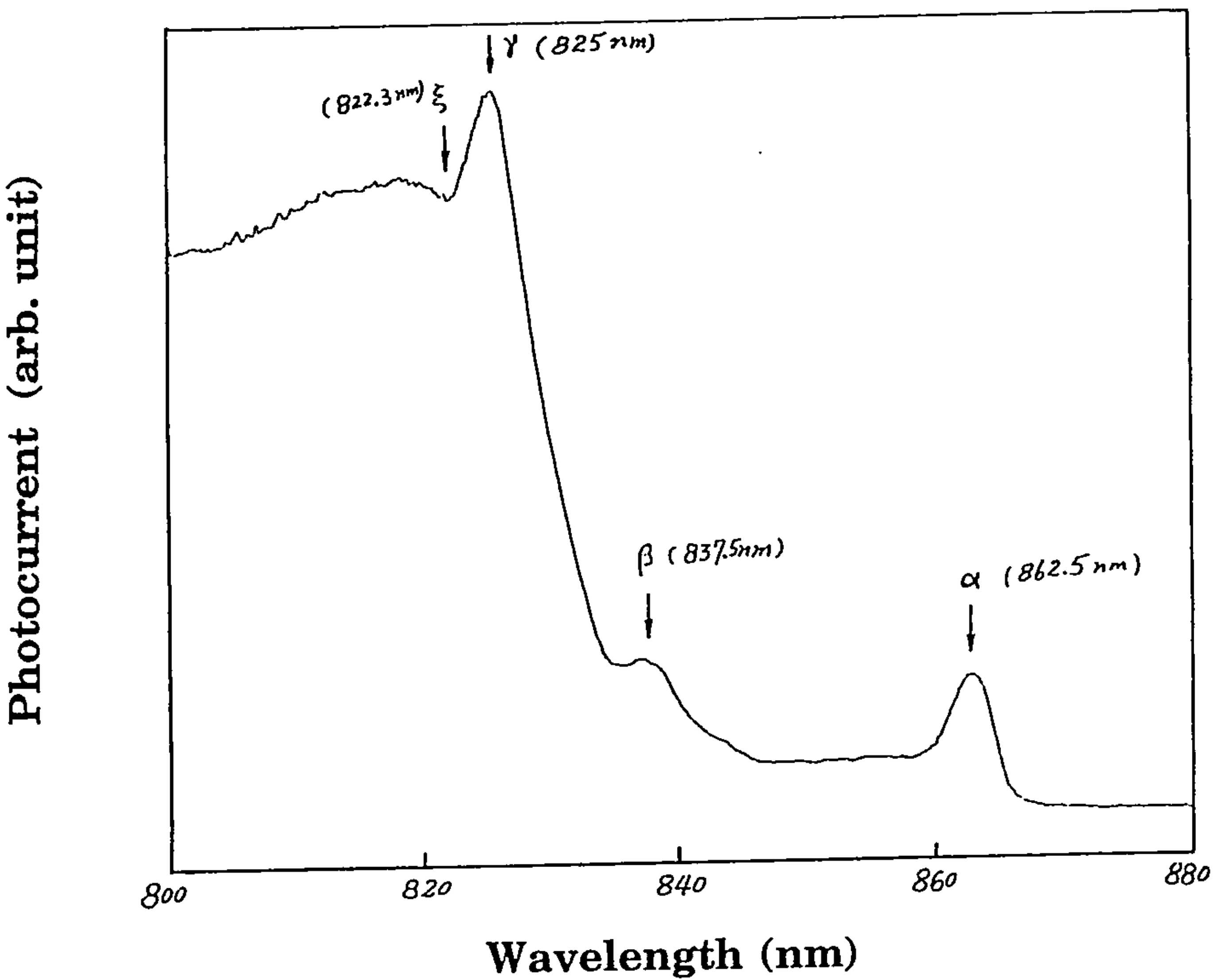

Fig. 3.7 PC spectrum for sample MO96 at T=77K in a dark environment.

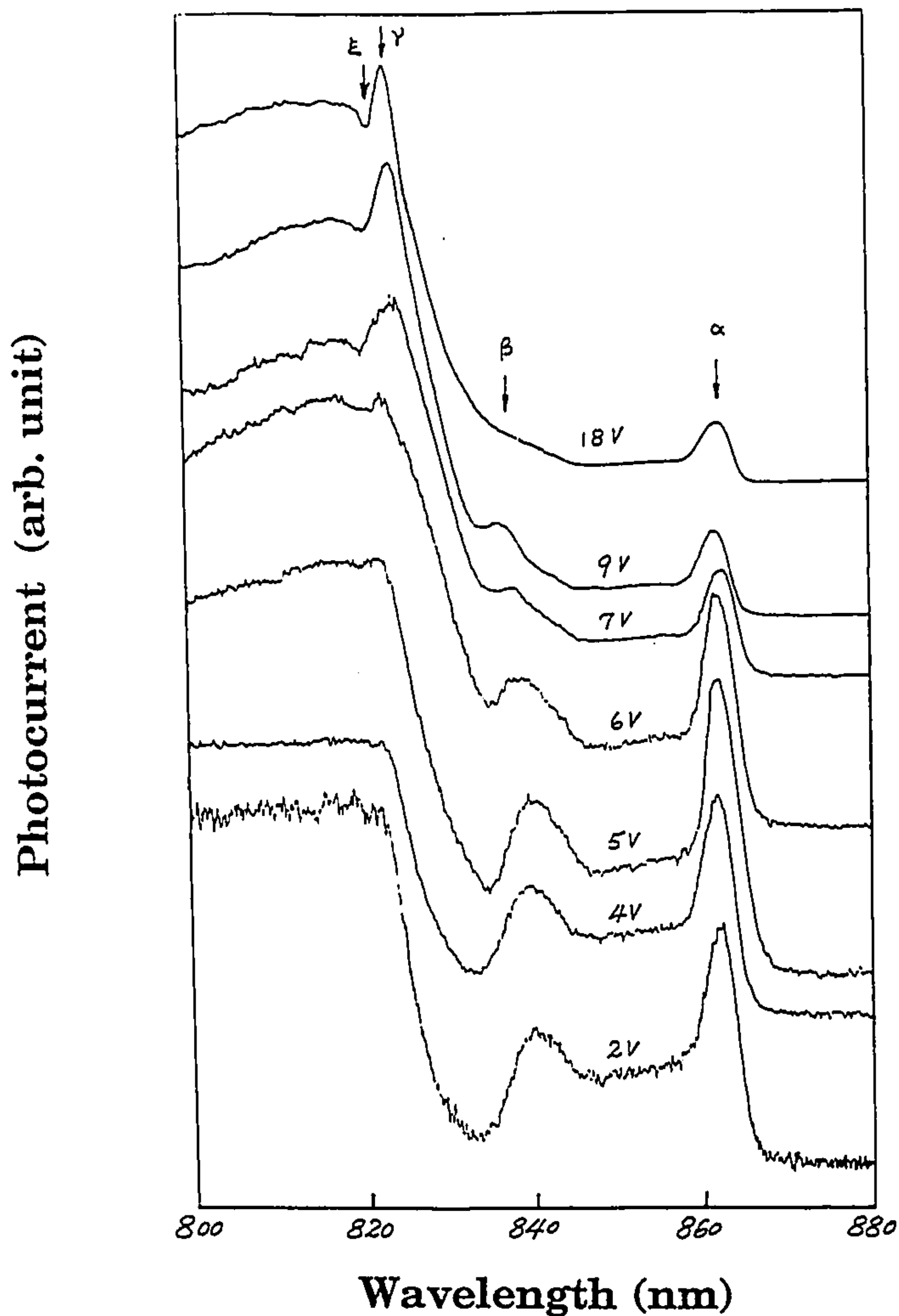

Fig. 3.8 PC spectra for sample MO96 at T=77K with different voltages applied (V=18volts--2volts) in a dark environment.

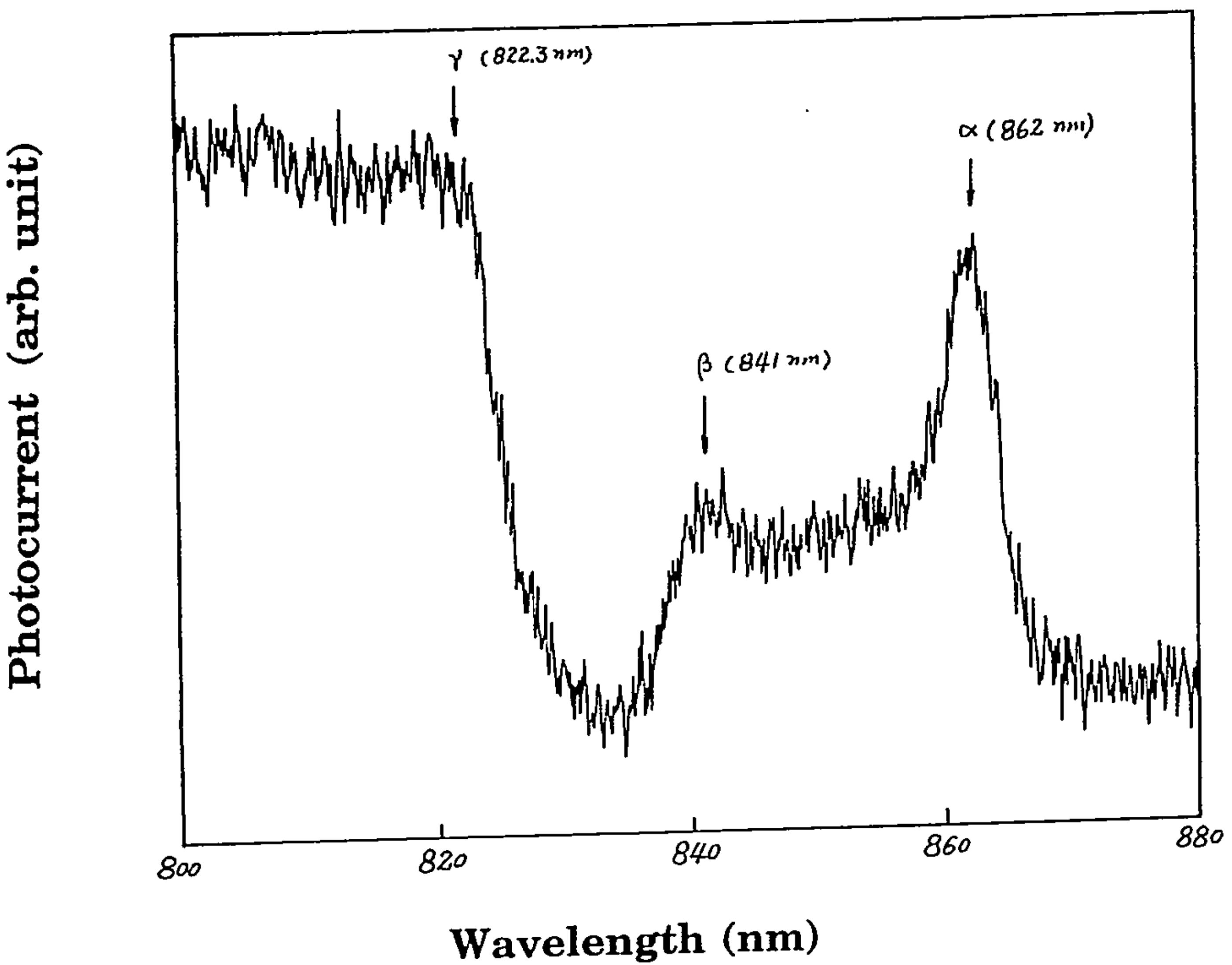

Fig. 3.9 PC spectrum for sample MO96 at T=77K with V=9volts and with a white DC light on.

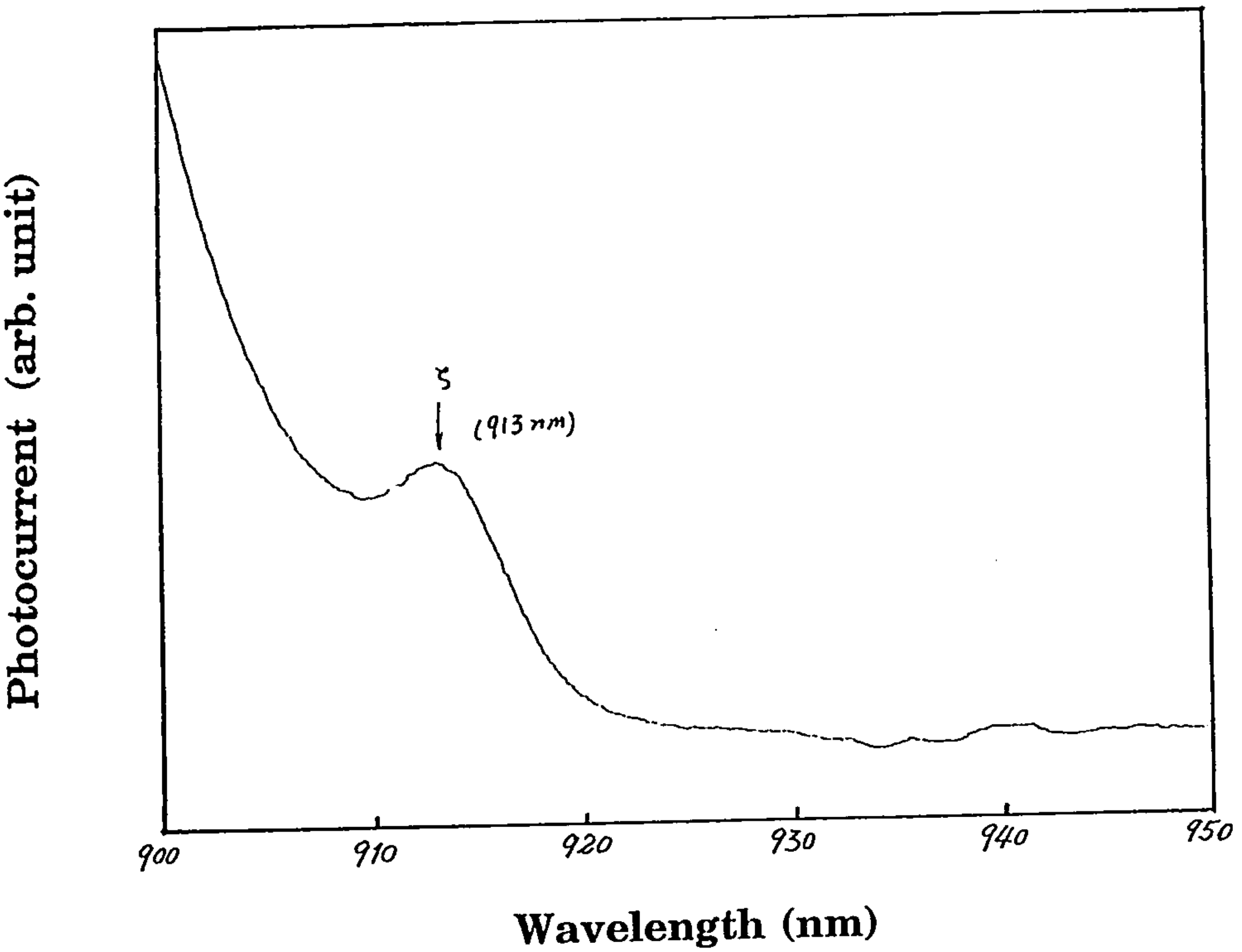

Fig. 3.10 PC spectrum for sample MO96 at T=300K.

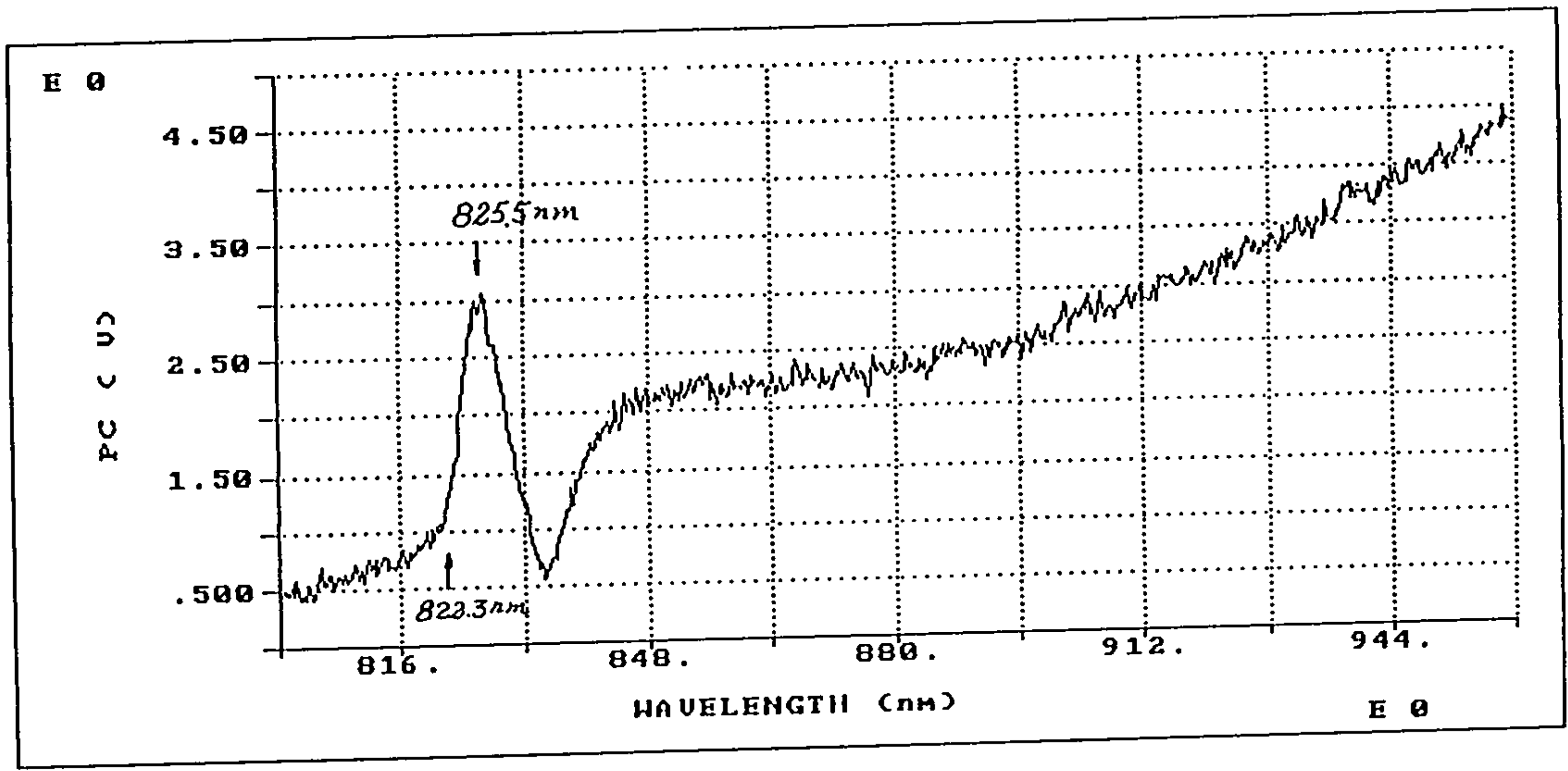

Fig. 3.11 PC spectrum for Cr--doped GaAs substrate at T=77K.

photosignal measurement on the structure above it. This causes the appearance of feature γ, and the GaAs energy gap (ξ) appearing as a minimum .

Table 3.3 gives the transition energies both from the experiment and from the calculation at T=77K and T=300K.

Temperatures	Transitions	Calculated Energies (eV)	Experimental Energies (eV)	wavelength (exp.) (nm)
	α 11H	1.446	1.438	862.5
	β e1--E_v(GaAs)	1.475	1.474	841
T=77K	γ effect from substrate			
	ξ E_g(GaAs)		1.508	822.3
T=300K	ζ 11H	1.365	1.358	913

Table 3.3 Identification of the PC spectral structures for MO96 at T=77K and T=300K

In real space, since both heavy--holes and electrons are confined within the InGaAs layer, the 11H is a direct transition and it is strong while the transition e1--E_v(GaAs) is indirect and it appears weak.

At the substrate and buffer interface, because of the high density of Cr impurities, electrons from the Cr--donor and holes from the Cr--acceptor levels fall into deep traps. Upon illumination of interface with the light of appropriate energy, electrons are excited from these traps into the conduction band and give rise to the photocurrent. Similarly, holes can be excited from hole traps into the valence band will contribute to the signal as well. With a strong illumination with DC light, all trapped elctrons and holes will be excited into the conduction and valence bands and we will approach a saturated condition. Therefore, with AC detection, the influence from the substrate is eliminated from the measured spectra. That is why the peak γ in Fig. 3.7 disappears in Fig. 3.9, the valley ξ in Fig. 3.7 becomes flat in Fig. 3.9, and the broader β in Fig. 3.7 rises to a peak and moves to longer wavelength in Fig. 3.9.[3.11]

Another interesting property is that in the case of one light source, the structures of the spectra change with the applied voltage V_0. When the applied voltage was decreased from 9 volts, the feature of the PC spectra (Fig. 3.8) are close to and eventually are identical to those obtained by using two light sources (one AC chopped scanning light plus a DC white light) (Fig. 3.9). But when the applied voltage is increased up from 9 volts, the changes of the structures of the spectra go in the opposite direction. This is especially obvious for feature γ and β. It can be argued that Cr--doped substrate influences the above structures and when we decrease the voltage V_0, we can also erase the effect from the substrate as we did by using a second DC white light source.

(2) Sample MO97

Sample MO97 is similar to sample MO96 except that the concentration and width of the well are different (x=0.166±0.005, L_W=85±3Å). Table 3.4 lists the calculated results for the relevant energies pattern at T=77K and T=300K. Table 3.5 displays the transition energies from the theoretical calculations and from the experimental results at T=77K and T=300K. The band offset was taken as Q=0.38 for the identification.

Energy (eV)	T=77K	T=300K
E_g(InGaAs)	1.274	1.189
ΔE_C	0.098	0.112
ΔE_{HH}	0.060	0.048
ΔE_{LH}	-0.017	-0.027
E_{gH}	1.350	1.263
E_{gL}	1.428	1.338

Table 3.4 Calculated band structure parameters of sample MO97

Fig. 3.12 shows the experimental PC spectra at T=77K. Fig. 3.14 shows the PC spectrum at T=300K. Fig. 3.12 is the record of the experimental results with one light source and Fig. 3.13 is the one with two light sources at T=77K, obtained by using the same measurement method as for sample MO96. As illustrated in Fig.3.12, the strong and sharp peak A identifies the

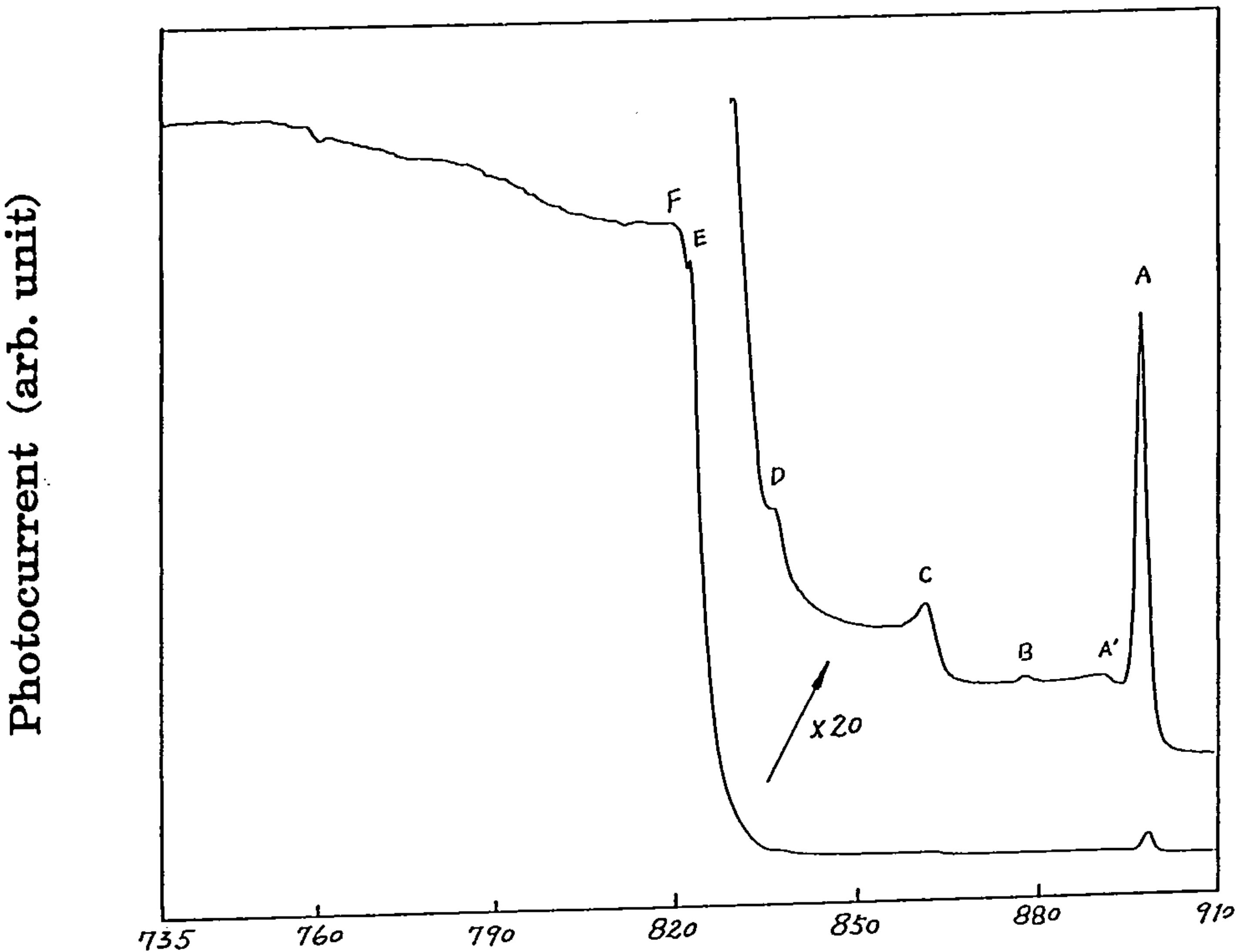

Fig. 3.12 PC spectra for sample MO97 at T=77K in a dark environment.

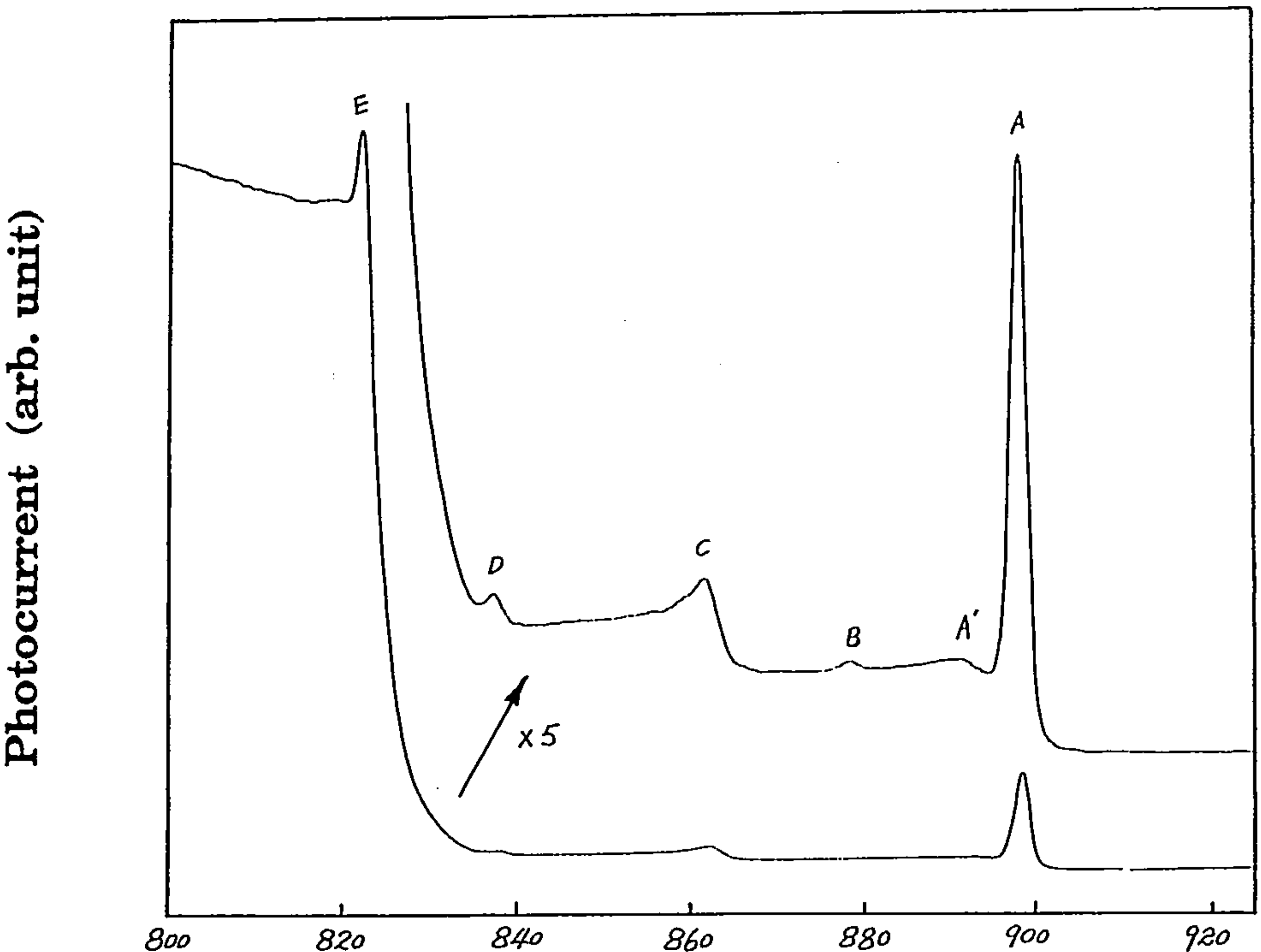

Fig. 3.13 PC spectra for sample MO97 at T=77K with DC white light on.

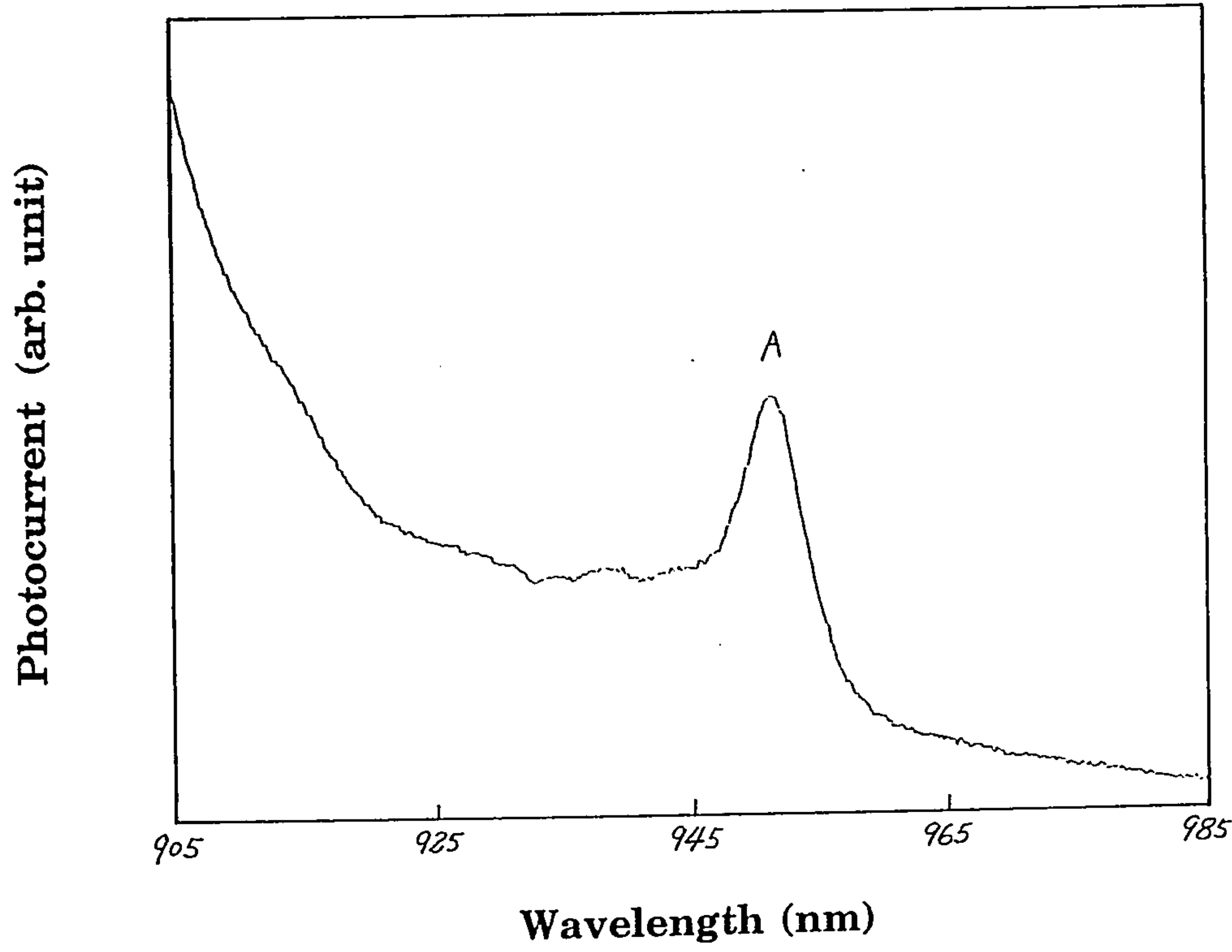

Fig. 3.14 PC spectrum for sample MO97 at T=300K.

exciton nature of the 11H transition. Peak C can be either e1--E_v(GaAs), 13H, or e1--cH and D is assigned to the transitions 22H, while peak E is related to the GaAs energy gap. Considering the energy difference between the excitonic peak A and the very weak feature A', to be about 9 meV, which is the approximate value for the excitonic binding energy, this feature A' can perhaps be identified as the excited state of the 11H exciton.[3.12] [3.13] The interesting thing is the weak broader B. According to theoretical fit, the broader peak B could be associated with transition 12H. But according to the selection rule $\Delta n=0$, this transition is forbidden. Perhaps, a weak barrier from the heterojunction or the metal contacts provides an electric field which changes the Hamiltonian as well as the envelope wave function so that some forbidden transitions become possible.

Comparing Fig. 3.12 with Fig. 3.13, one notes that feature F in Fig. 3.12 disappears in Fig.3.13, feature D in Fig. 3.12 changes its shape in Fig. 3.13. Same explanation here as for sample MO96: the Cr--doped substrate affects the buffer and QW structure. A second DC white light erases this influence.

Temperatures	Transitions	Calculated Energies (eV)	Experimental Energies (eV)	Wavelength (exp.) (nm)
	A 11H	1.389	1.381	898
	A' excited state of 11H exciton		1.391	892
	B 12H	1.411	1.411	878.6
T=77K	C e1--E_v(GaAs)	1.440	1.439	861.5
	or: 13H	1.440		
	or: e1--cH	1.440		
	D 22H	1.475	1.483	836
	E E_g(GaAs)		1.508	822.3
T=300K	A 11H	1.309	1.301	953.3

Table 3.5 Identification of the PC spectral structures for sample MO97 at T=77K and T=300K

(3) Sample MO98

MO98 is a 5 period MQW with x=0.166±0.005, L_W=90±3Å and L_B=100±3Å. Using a band offset Q=0.3 gives out the calculated energy parameters at T=77K and T=300K, summarized in Table 3.6.

Energies (eV)	T=77K	T=300K
E_g(InGaAs)	1.273	1.194
ΔE_C	0.111	0.110
ΔE_{HH}	0.048	0.047
ΔE_{LH}	0.030	0.026
E_{gH}	1.349	1.266
E_{gL}	1.427	1.340

Table 3.6 Energy Band structure parameters from theoretical calculation for sample MO98

The calculation (Table 3.6) shows that $\Delta E_{HH}>0$ and $\Delta E_{LH}>0$. This means that both split heavy--hole and light--hole valence bands are above zero potential (GaAs valence band, Fig. 3.1). In this case, the light--holes are confined within the InGaAs layer.

Fig. 3.15--3.19 illustrate for PC spectra at T=77K and T=300K. In those figures, peak "a" is identified as the 11H transition, peak "b" is the 11L transition, and shoulder "c" is associated with 21H transition. Feature "d" may be due to the Cr--doped substrate because it changes its shape and becomes weak upon illumination with two light sources (AC and DC) illuimnation or after the applied voltage has been decreased. This is the same situation as mentioned for sample MO96. Clearly, feature "e" is due

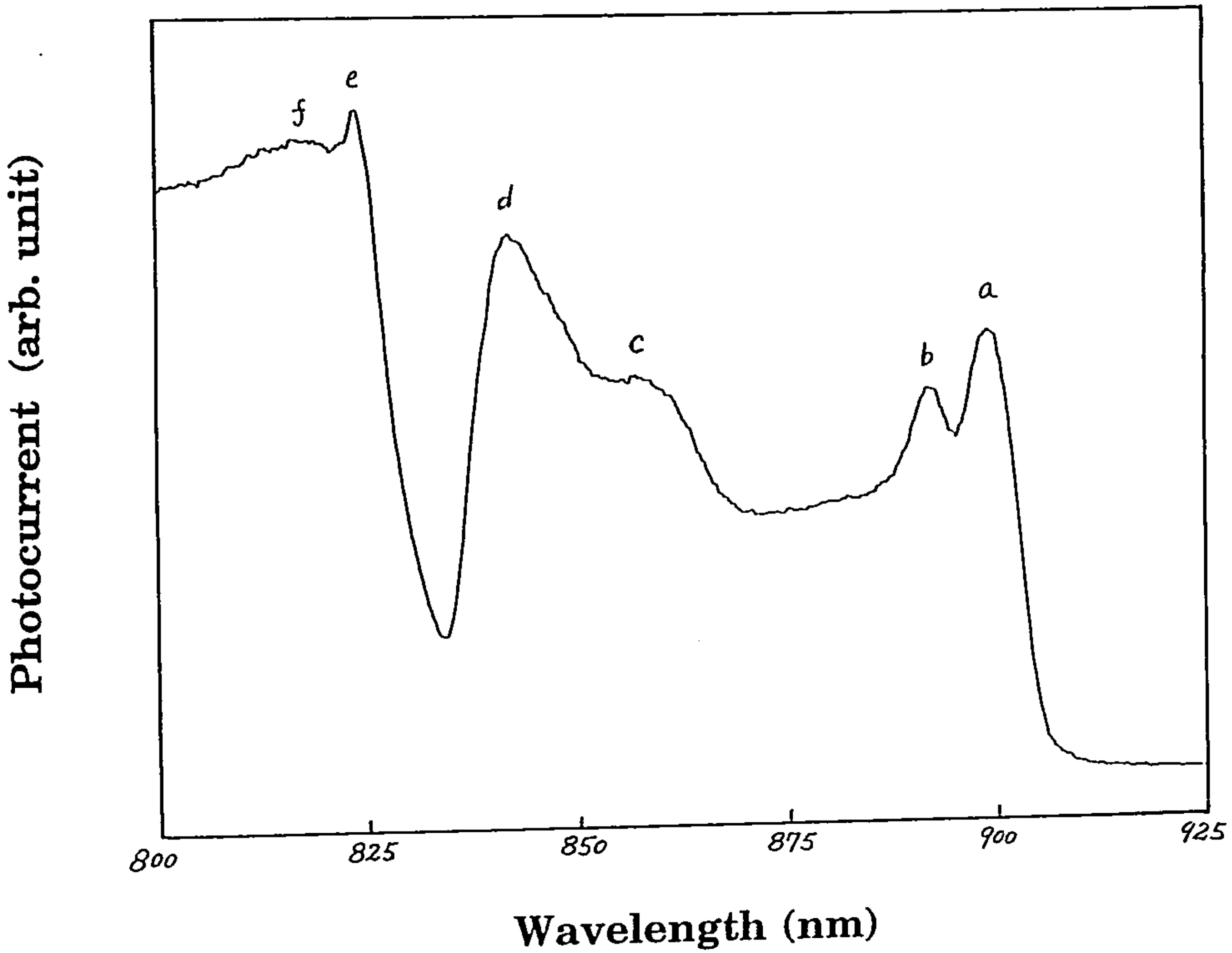

Fig. 3.15 PC spectrum for sample MO98 at T=77K in a dark environment.

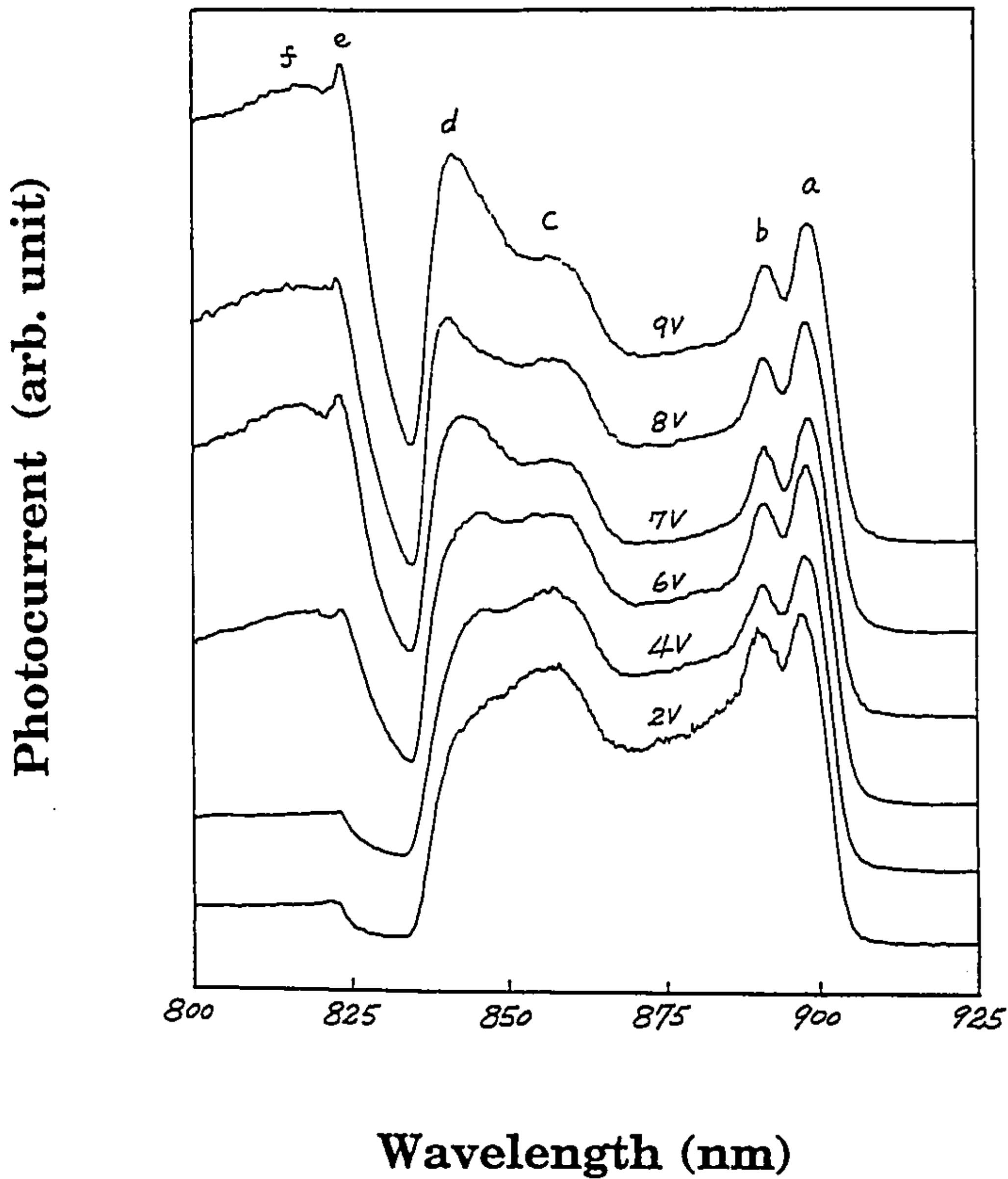

Fig. 3.16 PC spectra for sample MO98 at T=77K with different voltages applied (V=9volts--2volts) in a dark environment.

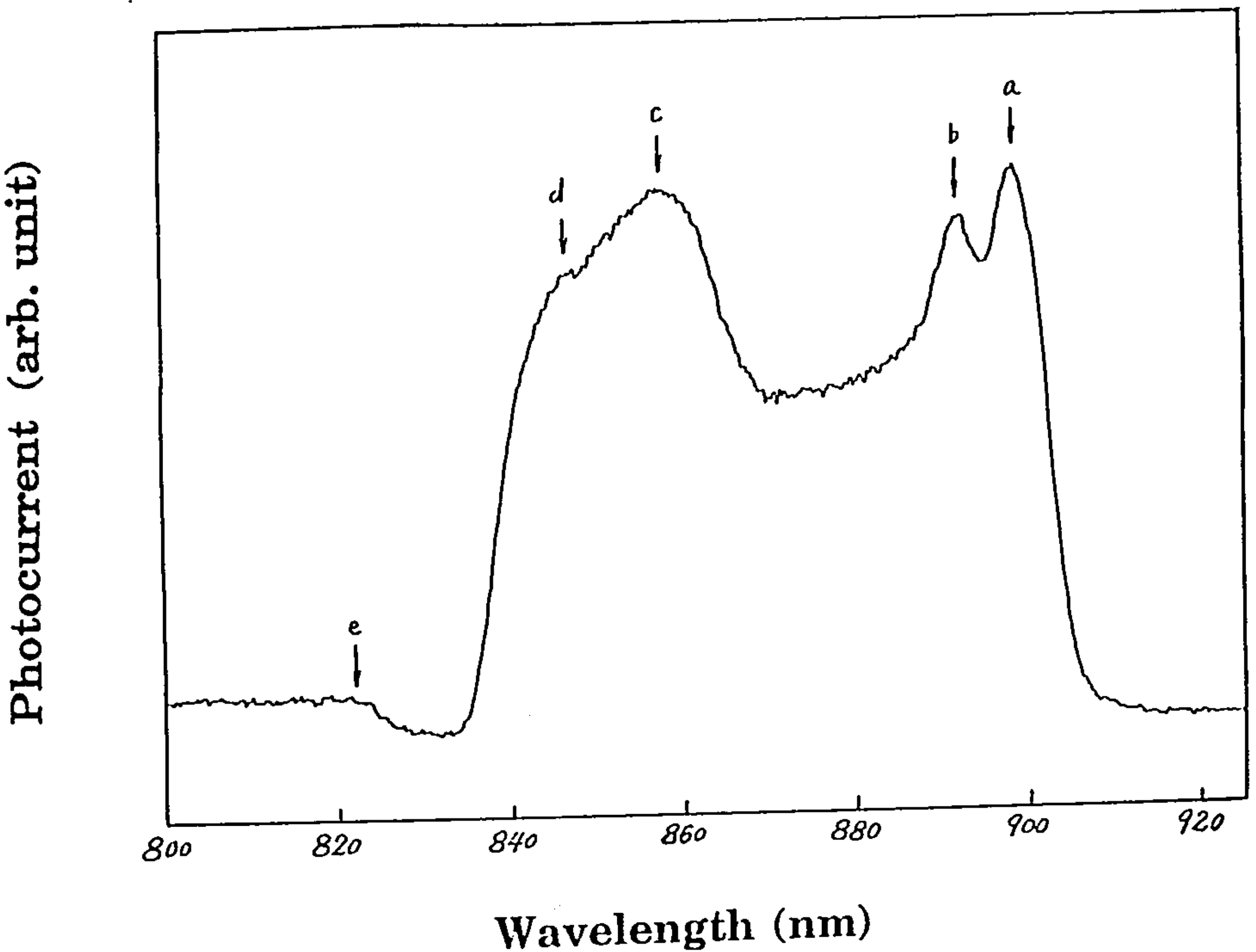

Fig.3.17 PC spectrum for sample MO98 at T=77K with DC white light on

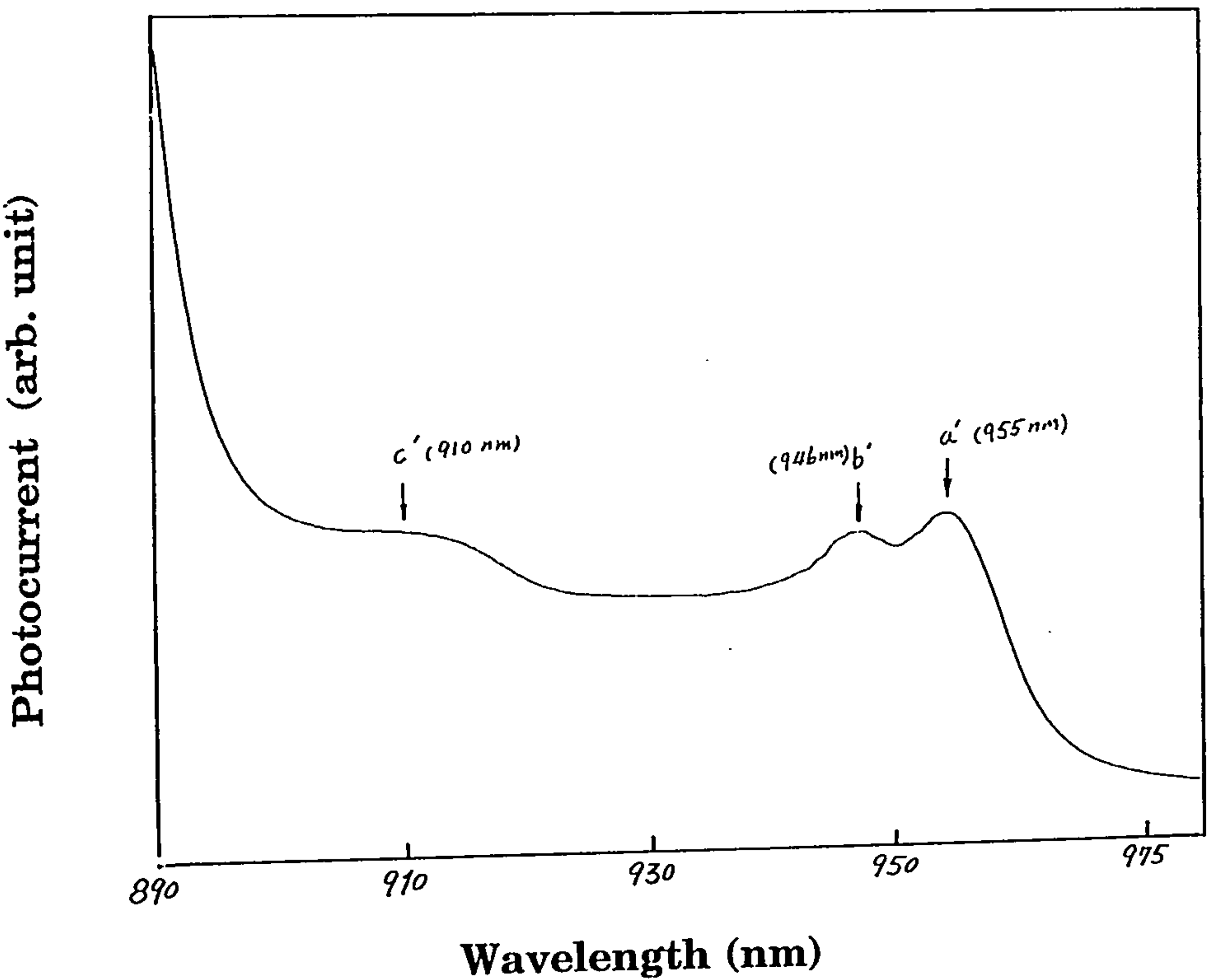

Fig. 3.18 PC spectrum for sample MO98 at T=300K in a dark environment.

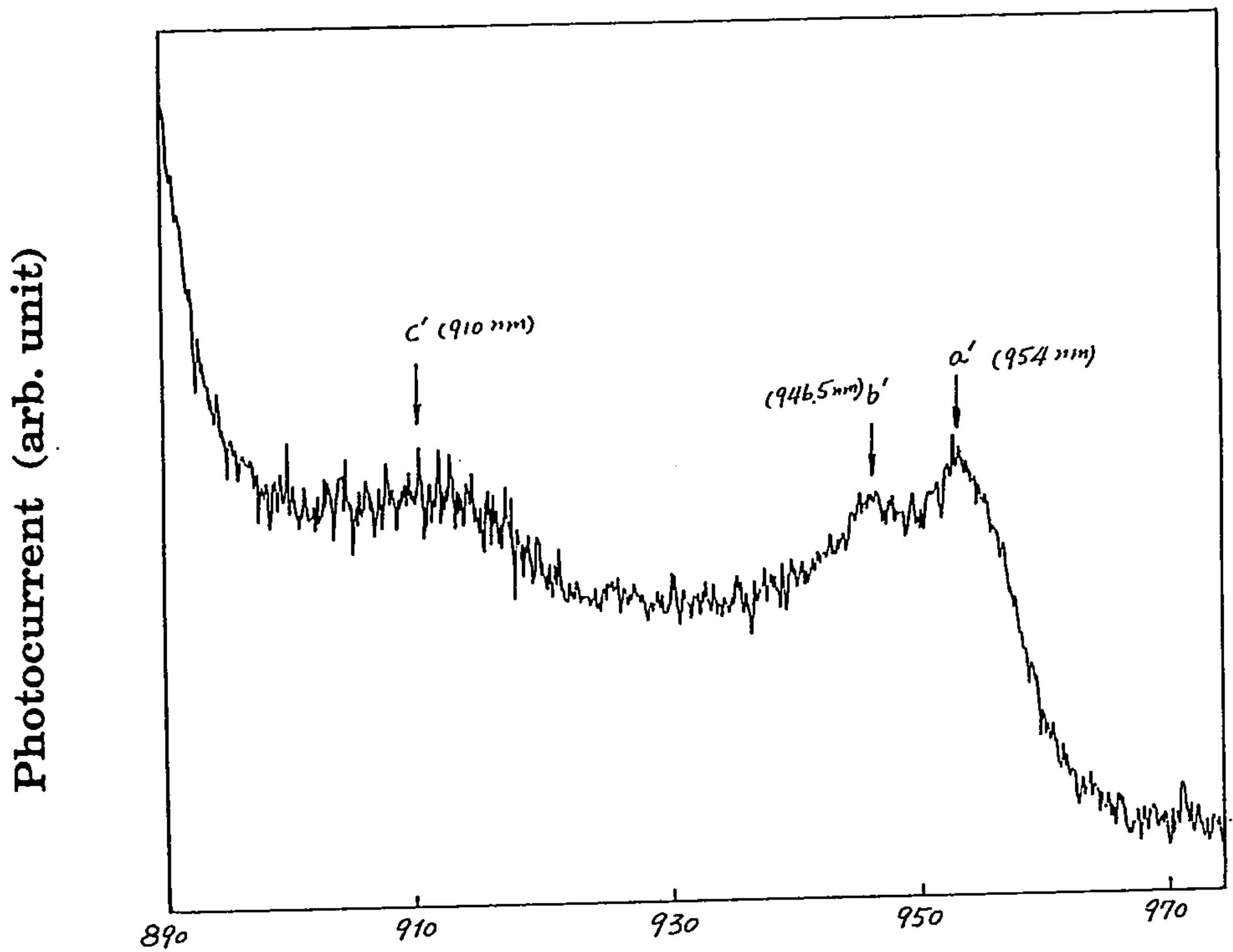

Fig. 3.19 PC spectrum for sample MO98 at T=300K with DC white light on.

to the GaAs intrinsic energy gap. Structure "f " in Fig. 3.15, which vanished in Fig. 3.17, may also be considered as the effect of the Cr--doped substrate. Table 3.7 shows the fitted positions of the transition, from both the theoretical calculations and experimental measurements.

Temperatures	Transitions	Theoretical energies (eV)	Experimental energies(eV)	Wavelength (exp.) (nm)
T=77K	a 11H	1.386	1.379	899
	b 11L	1.390	1.390	892
	c 21H	1.447	1.445	858
	d effect from substrate			
	e E_g(GaAs)		1.506	823.5
T=300K	a' 11H	1.298	1.298	955
	b' 11L	1.316	1.311	946
	c' 21H	1.365	1.363	910

Table 3.7 Identification of PC spectral structures for sample MO98

In MQW's, because of the coupling between the wells, the energy levels of the SQW's change into energy "minibands" with having a certain band width. This causes the transition difference between the Γ point (centre of

the reduced Brillouin zone) and Π point (edge of the zone). If the barriers' width is large, the band width will be very narrow so that it is hard to distinguish the transition difference between the Γ point and Π point, or the transitions at Γ and Π will be unresolved. From Fig. 3.15--3.19, peak a(a') is not assigned as 11H(Γ) nor is b(b') assigned as 11H(Π). This is because: (1) the energy difference between a(a') and b(b') is 11meV which is much larger than the energy difference between 11H(Γ) and 11H(Π) (about 2meV); (2) the photoluminescence (PL) measurements done in Italy by A. Serpi and E. Fortin on the same sample display two peaks A and B in the 11H region (Fig. 3.20). This phenomenon has been observed and explained by C. Weisbuch.[3.14] Peak A is the PL signal due to the emission light by recombination of electrons with heavy--holes. Peak B is the PL signal due to the recombination of electrons with light--holes.

Fig. 3.18 and Fig. 3.19 show the room temperature spectra for MO98. Fig. 3.18 was obtained by using one light source (AC light) method, while Fig. 3.19 was obtianed by using two light sources (AC and DC light) method. One can see that there is not much difference between the two spectra. This is due to trapping at room temperature being less than that at liquid nitrogen temperature so that the substrate's influence at room temperature is much smaller than at liquid nitrogen temperature.

(4) Sample MO33

MO33 is different from all previously studied samples: it is a SQW on an undoped substrate. The growth parameters are $x=0.241\pm0.005$,

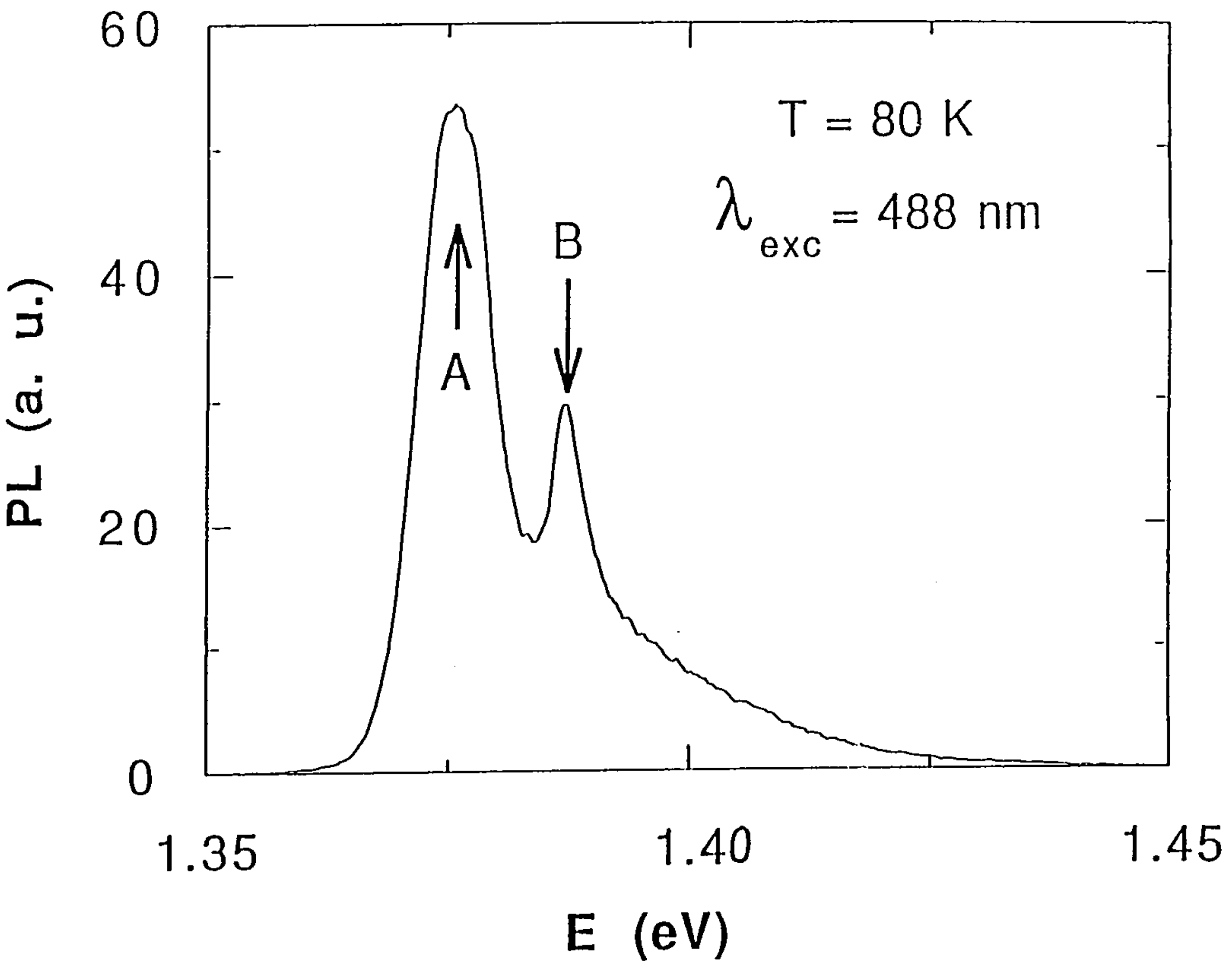

Fig. 3.20 PL spectrum for sample MO98 at T=80K.

L_W=60±3Å. The valence band offset was Q=0.36. Table 3.8 exhibits the calculated energy structure of this sample.

Energy (eV)	T=77K	T=300K
E_g(InGaAs)	1.175	1.092
ΔE_C	0.147	0.141
ΔE_{HH}	0.083	0.091
ΔE_{LH}	-0.028	-0.016
E_{gh}	1.610	1.191
E_{gL}	1.278	1.298

Table 3.8 Calculated band structure parameters for sample MO33.

Fig. 3.21 presents the PC spectrum of MO33 at T=77K. Fig. 3.22 is the same spectrum for an undoped GaAs substrate at T=77K . This substrate is the same as the one on which sample MO33 was grown. As shown in Fig. 3.21, peak "1" is assigned to be the 11H transition and peak "2" is associated with transition of either e1--E_v(GaAs) or e1--cH because these two structures cannot be resolved. Feature "5" is the GaAs gap. Besides the 11H peak "1", there is a weak broader "1' ". As for sample MO97, this small broader "1'" can also be assumed to be the excited state of 11H because the energy difference between "1" and "1' " is about 8meV which is the approximate value for the excitonic binding energy.[3.12] [3.13] Comparing

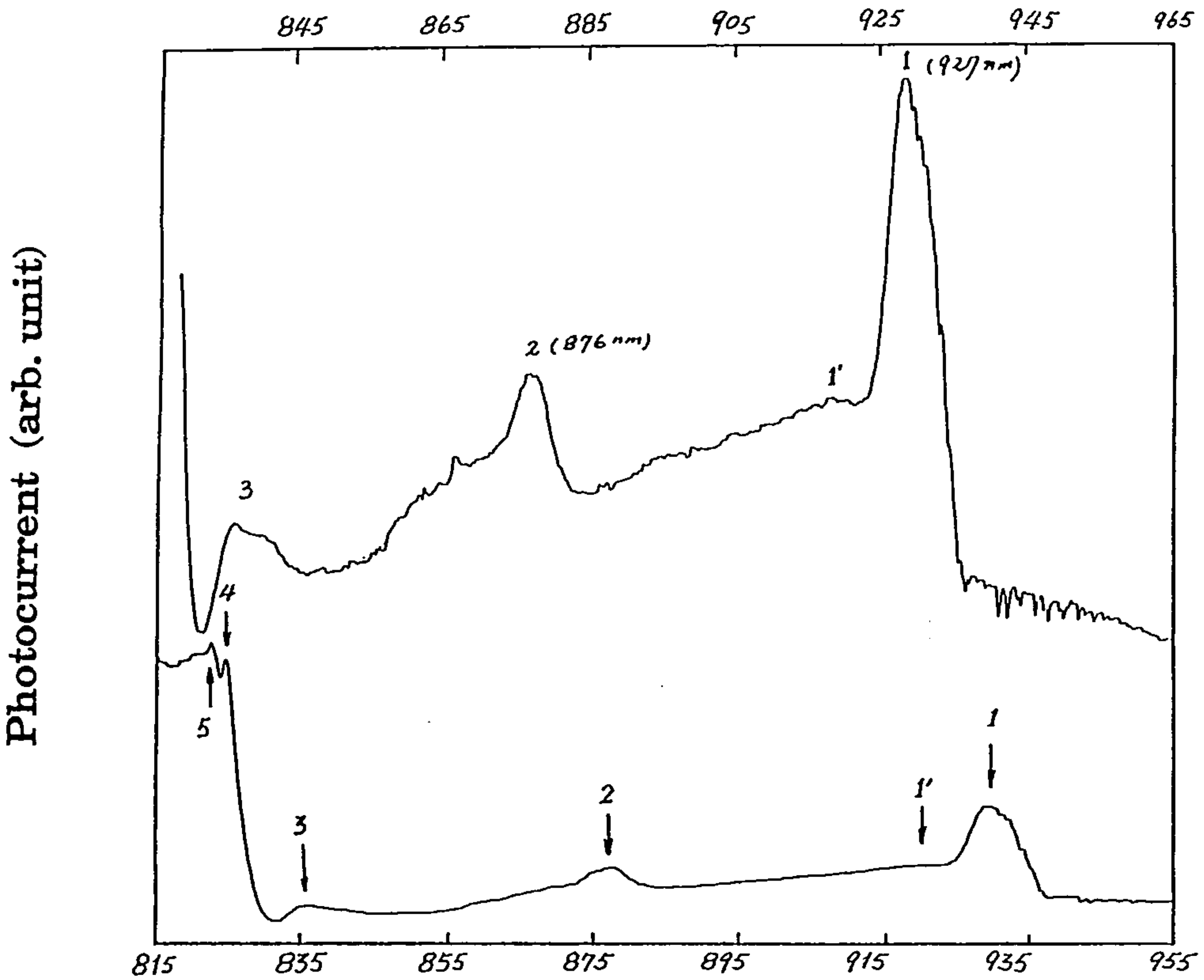

Fig. 3.21 PC spectra for sample MO33 at T=77K.

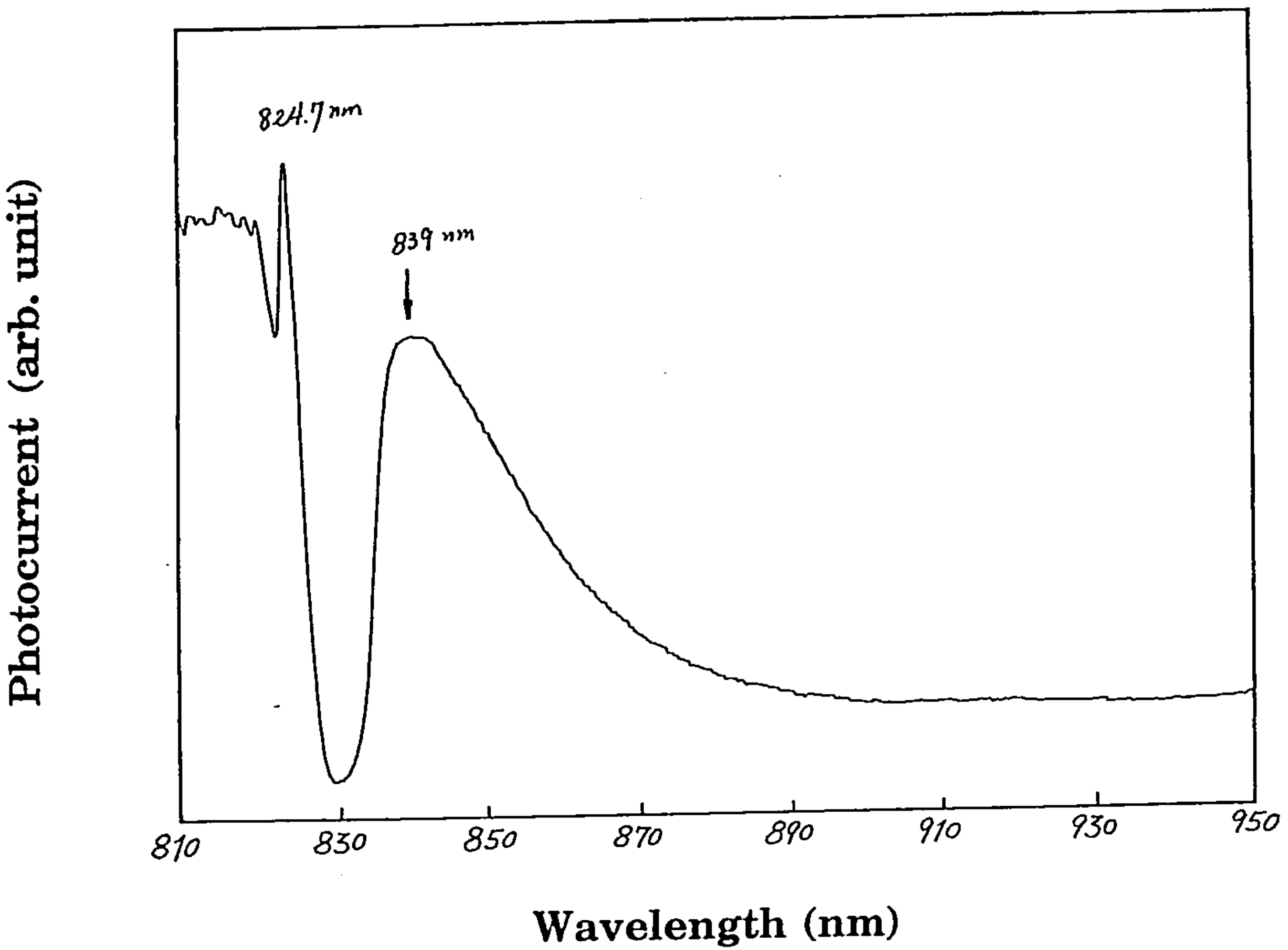

Fig. 3.22 PC spectrum for undoped GaAs substrate at T=77K.

with the spectrum of the substrate(fig. 3.22), one can easily see that feature "3" and "4" are not QW related structures but are effects of the substrate.

The transition energies for this sample from calculation and measurements are given in Table 3.9.

Temperatures	Transitions	Calculated Energies (eV)	Experimental Energies (eV)	Wavelength (exp.) (nm)
	1 11H	1.346	1.338	927
	1' excited state of 11H exciton		1.346	921
T=77K	2 e1--E_v(GaAs)	1.414	1.414	877
	or: e1--cH	1.414		
	3 substrate effect			
	4 substrate effect			
	5 E_g(GaAs)		1.508	822.3

Table 3.9 Identification of PC spectral structures for sample MO33.

There is a very interesting phenomenon appearing during the measurements for this sample. At energies below the 11H transition (E_{11H}=1.338eV) or at wavelengths longer than λ=927nm, there is a spectral oscillation in this infrared region. It starts from the top of 11H peak and vanishes at λ>960nm. This oscillation is very regular and reproducible. Its

energy period is about 1meV. Figs. 3.23, 3.24, 3.25 together with Fig. 3.21 and 3.22 show this feature. In the measurements on the QW samples grown on the Cr--doped substrate, we did not observe this phenomenon. It appears only in the measurements on this QW sample grown on the undoped substrate. These oscillations do not come from the effect of the substrate (Fig.3.26), or from the effect of water vapor (Fig. 3.27), nor from the effect of the epitaxial layer (Fig. 3.28), since all those PC spectra are very quiet in that region. The optical quenching technique can not "kill" this oscillation either. This oscillation thus appears to be related to the QW, the interference of reflected light from different heterojunctions' surfaces, or defects inside the sample, or other unknown causes. It may be an important phenomenon or it may be of no value at all. So far it cannot be explained clearly.

3.3.2 PV Spectroscopy

Photovoltaic (PV) spectroscopy is a well known technique which has been used in the past to study the electronic properties of bulk semiconductors[3.15] [3.16] Althrough it is a simple technique, it still can provide valuable information concerning the intrinsic optical transitions in QW's.

Samples studied in this measurement were MO96 with a barrier contact as mentioned in §3.2.1 and MO98, MO33 with omhic contacts which are also explained in §3.2.1.

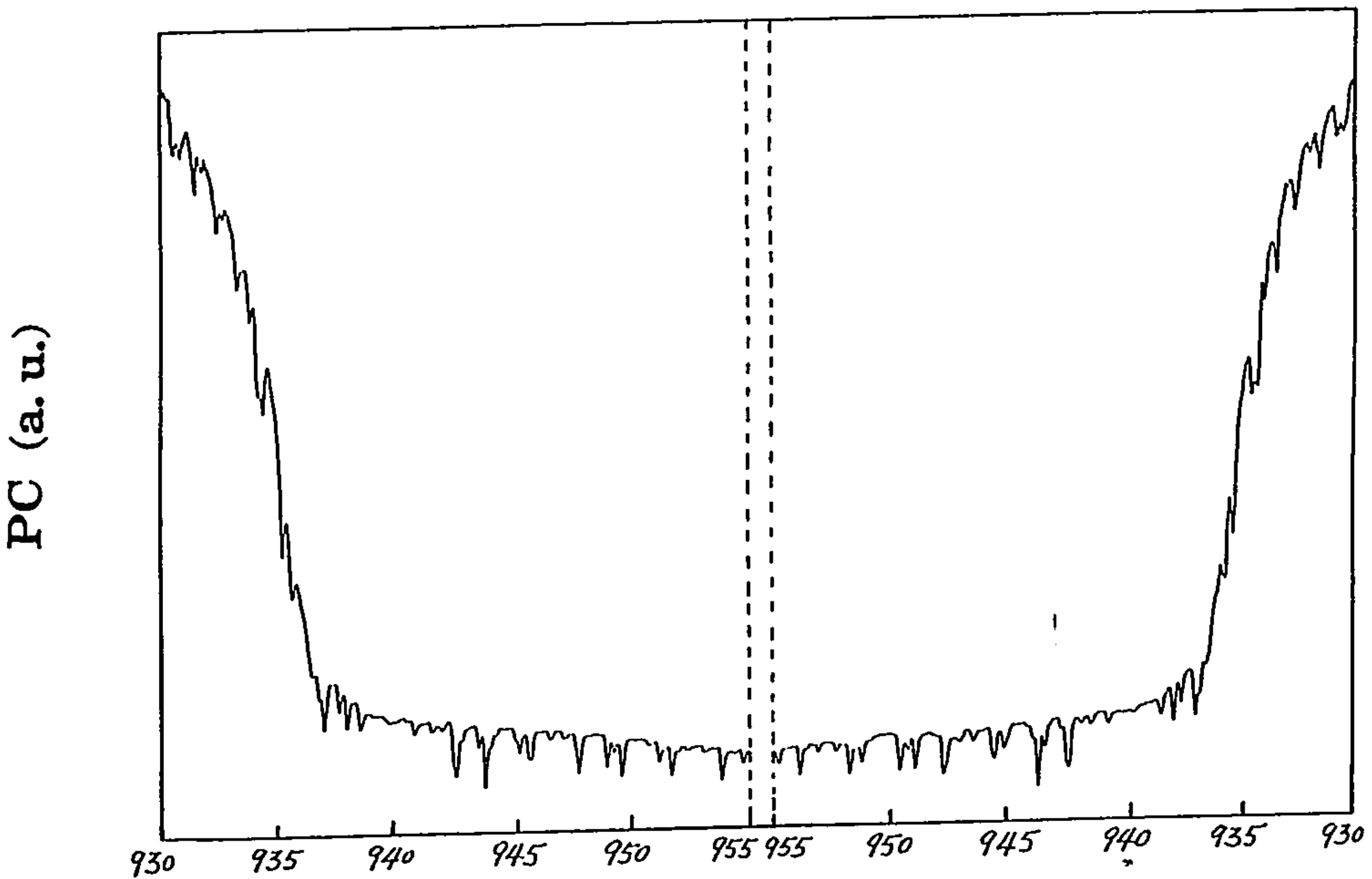

Fig. 3.23 PC oscillatory spectra for sample MO33 at T=77K.

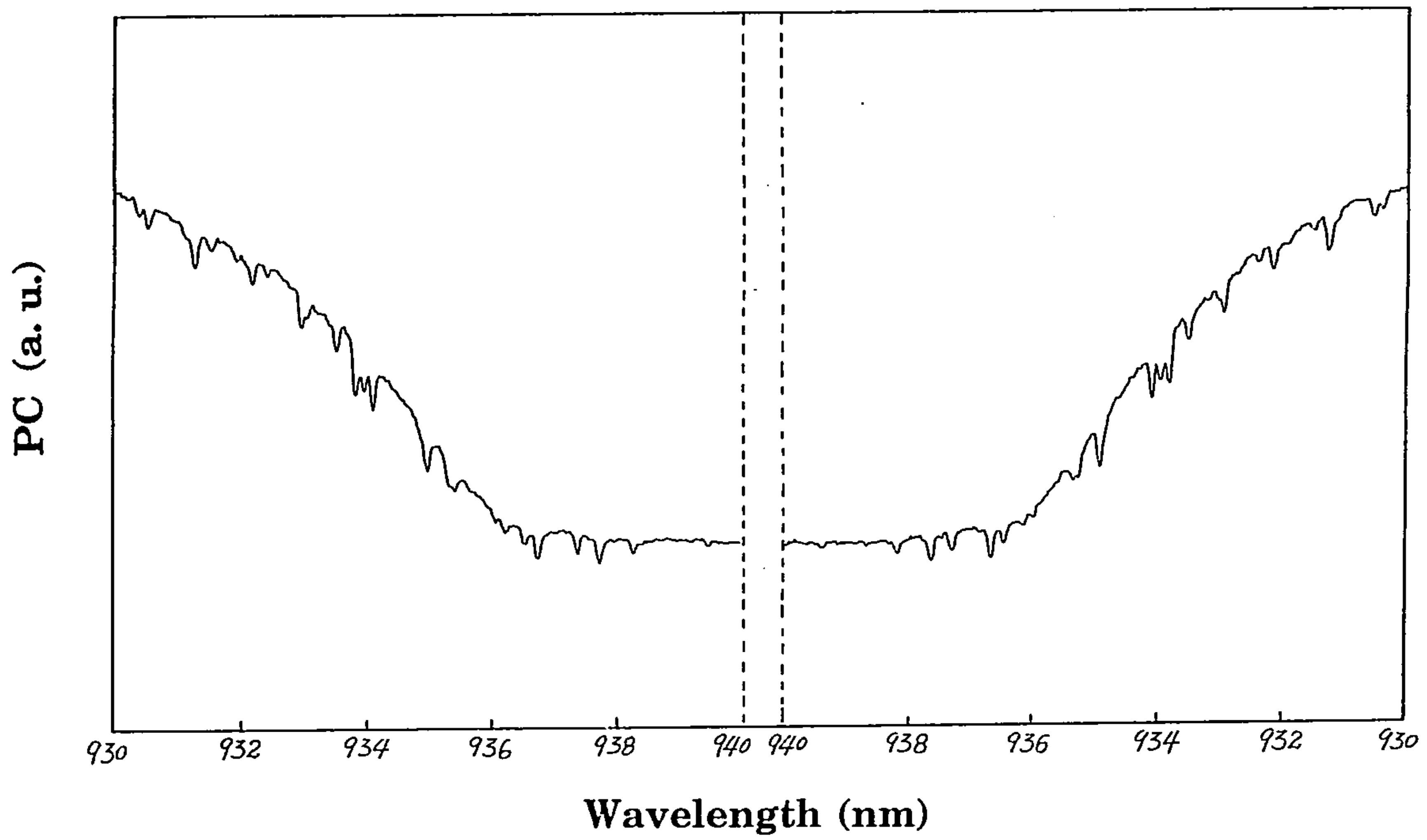

Fig. 3.24 PC oscillatory spectra for sample MO33 at T=77K

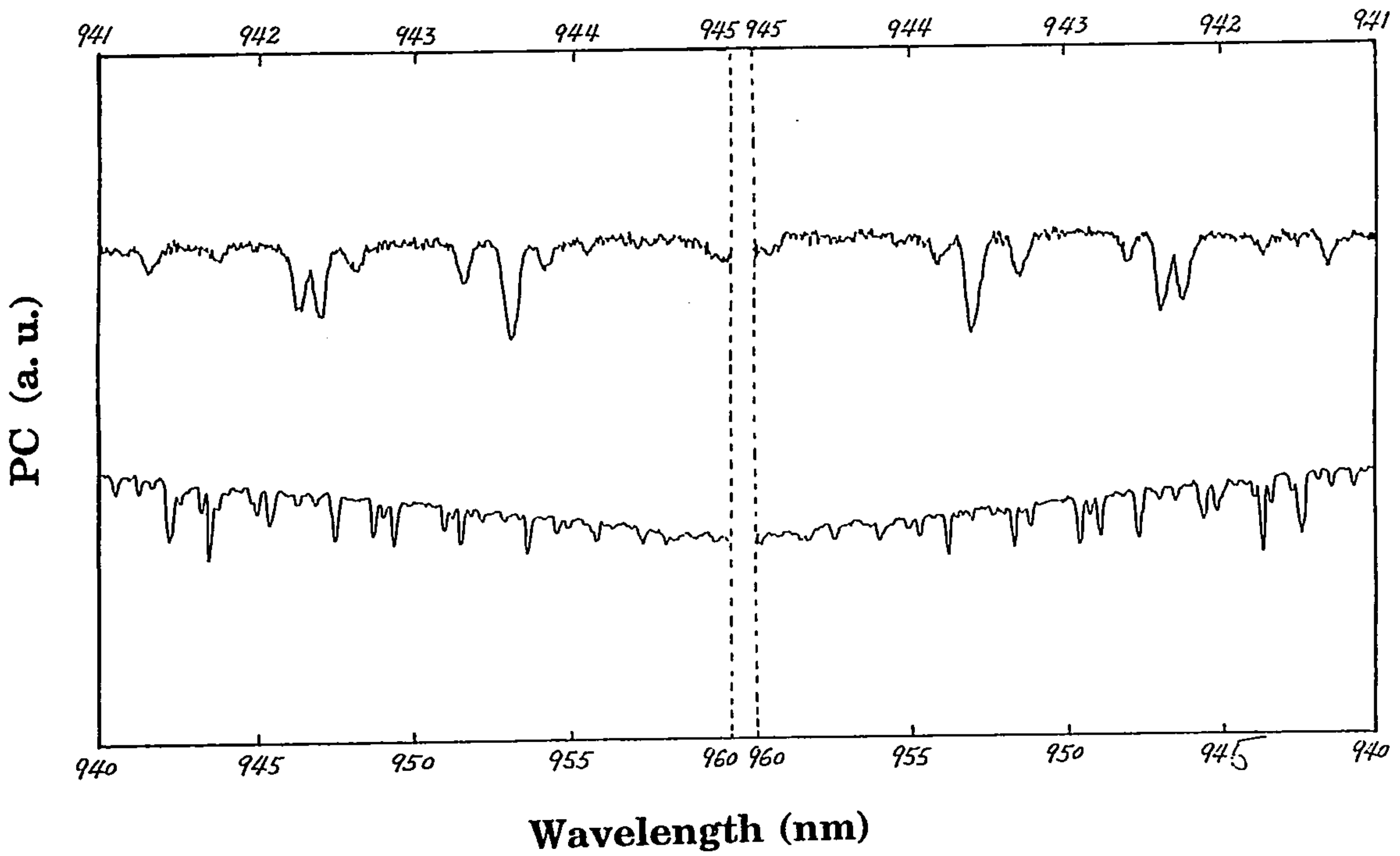

Fig. 3.25 PC oscillatory spectra for sample MO33 at T=77K.

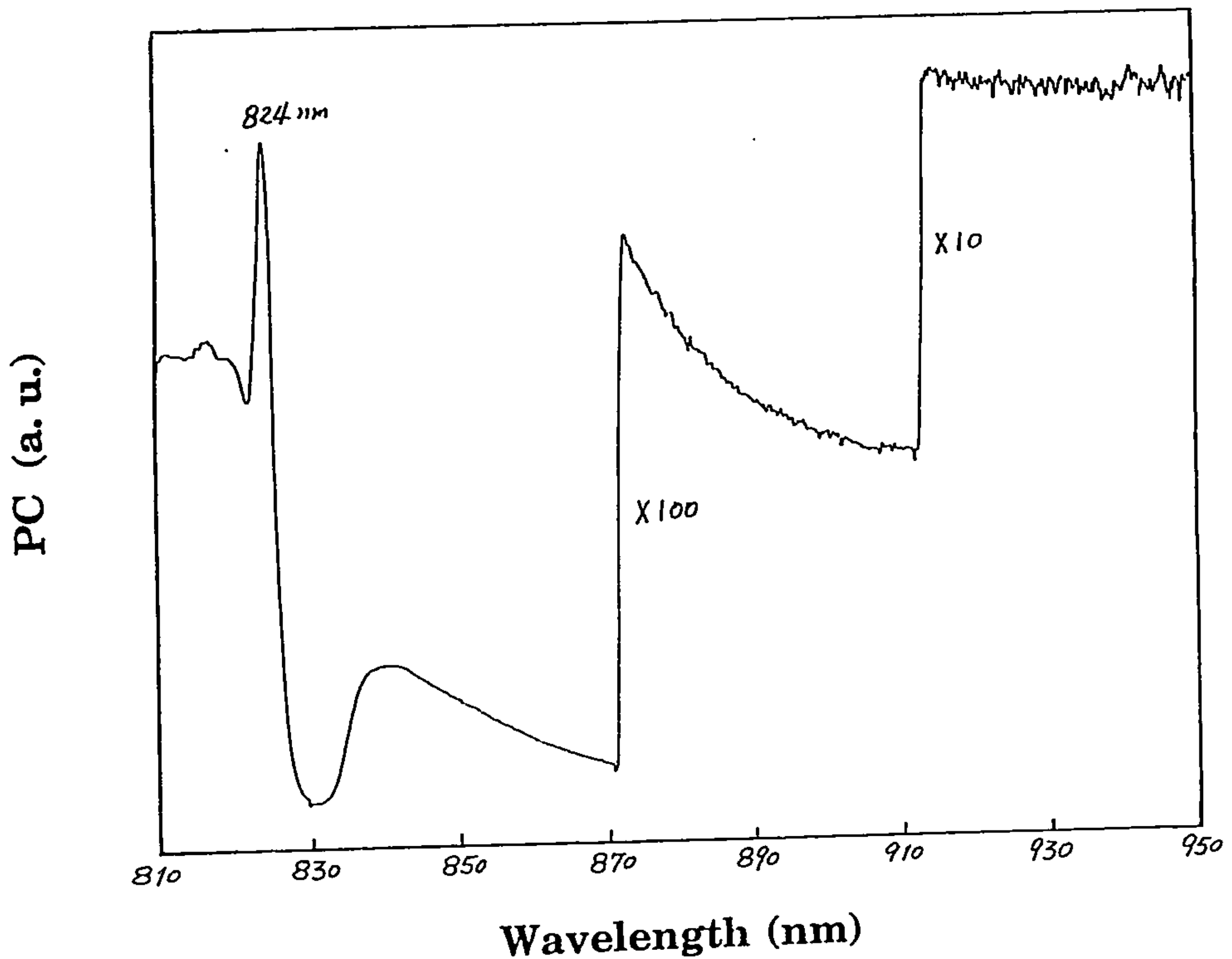

Fig. 3.26 PC spectrum for undoped GaAs substrate at T=77K.

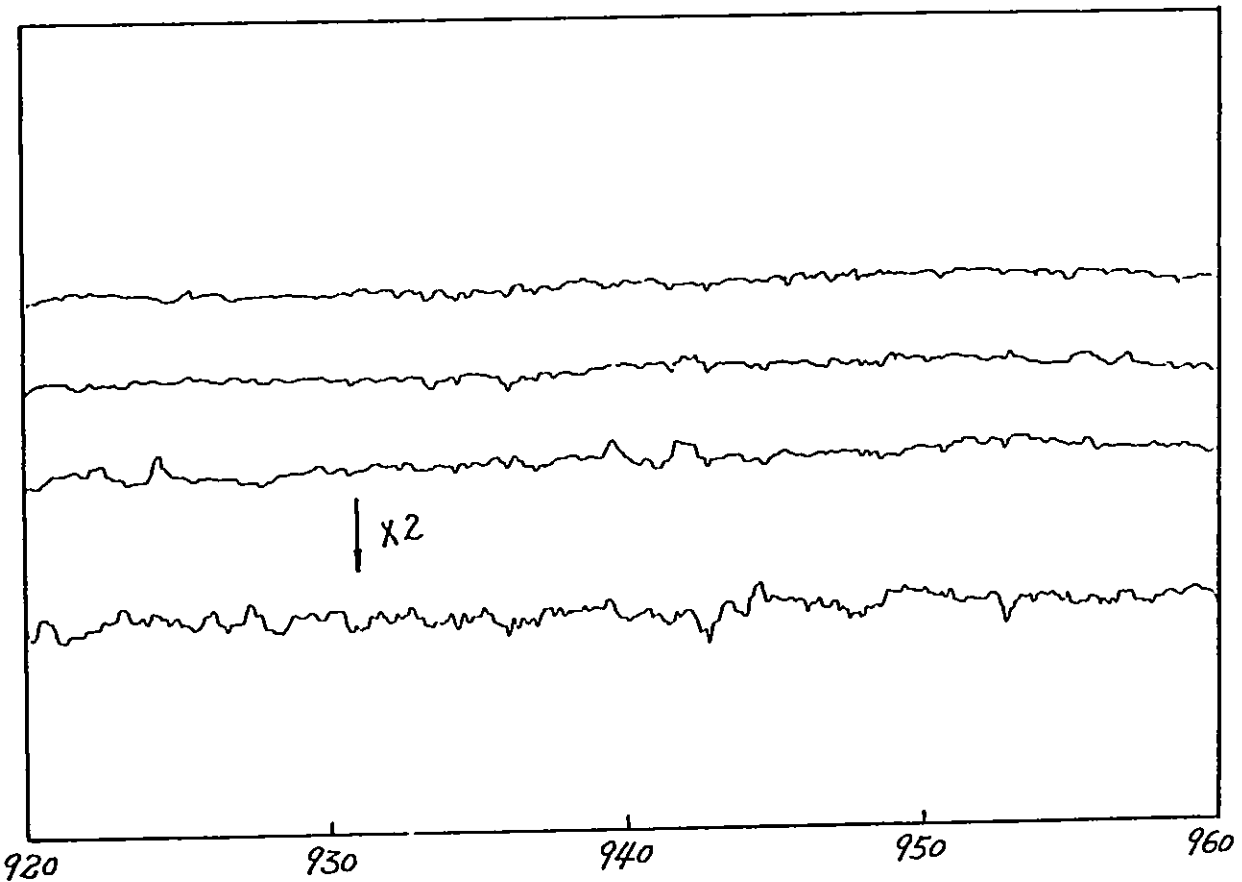

Fig. 3.27 Blank spectrum from flat Si--detector.

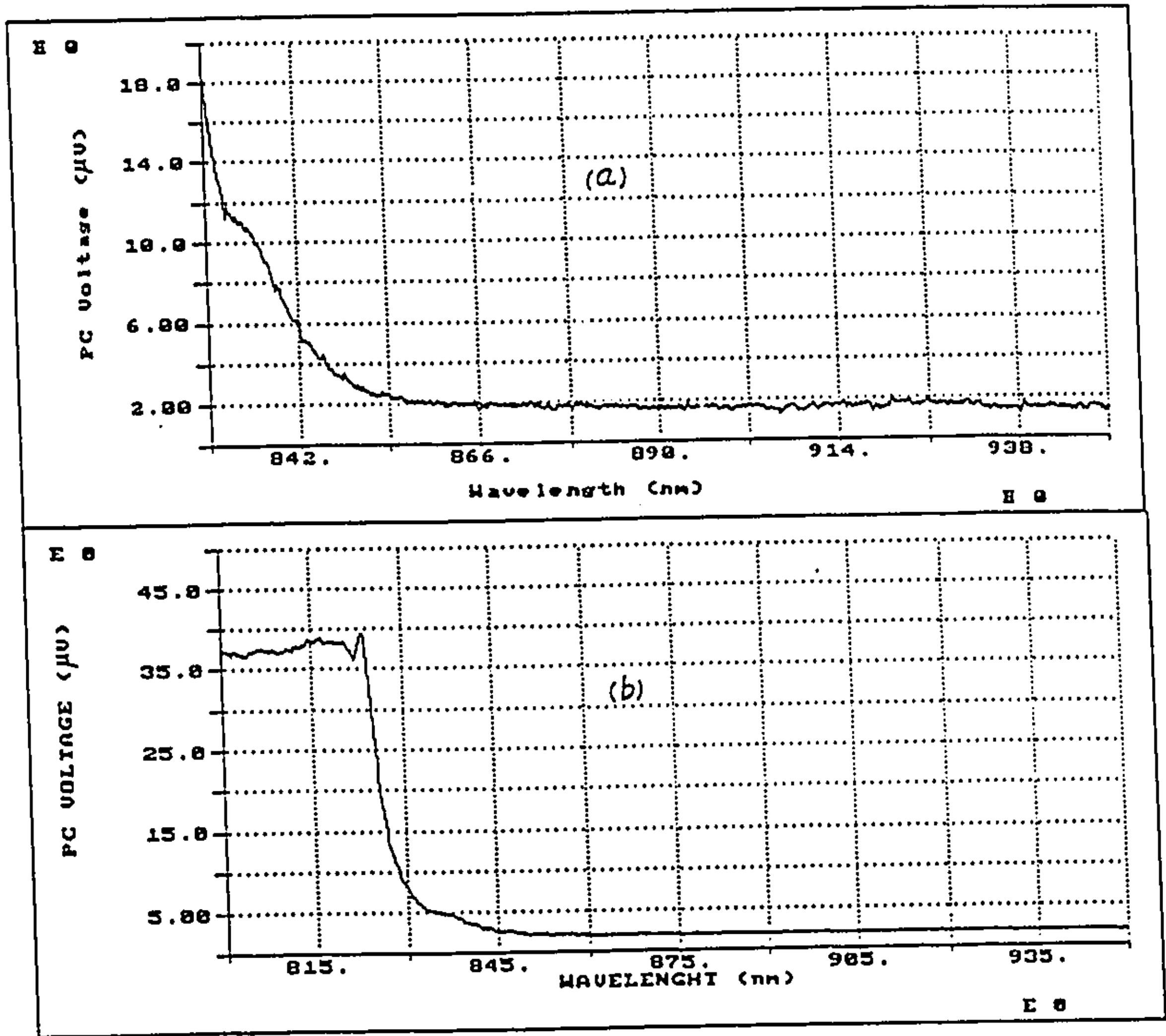

Fig. 3.28 PC spectrum for GaAs epilayer at T=77K. (a) is the amplified spectrum of (b).

Fig. 3.29--3.31 are the PV spectra of sample MO96 at T=77K in a dark environment (Fig.3.29), in a bright DC white light environment (Fig. 3.30) and back to dark environment (Fig. 3.31). Peak A is the 11H transition and peak B is the e1--E_v(GaAs) or ec--1H transition, while peak C is the GaAs gap and the feature D which is in Fig.3.29 and 3.31 but disappears in Fig. 3.30 may be explained as the effect from the substrate since it can be erased by white light.

Fig. 3.32 shows the PV spectrum of sample MO98 at T=77K. Feature "a" is 11H, "b" is 11L, "c" is 21H, "d" is the effect from substrate, and "e" is the GaAs gap.

Fig. 3.33 illustrates the PV spectrum of sample MO33 at T=77K. Feature α is 11H, β is 12H, γ is a convolution feature of e1--E_v(GaAs) and e1--cH, θ may be the 21H or ec--1H (i.e. the transition between first heavy--hole level and electron continuum state), and τ is the effect of the substrate.

All identifications and explanations are the same as those mentioned for PC measurements.

3.4 Summary

In this chapter, four $In_xGa_{1-x}As/GaAs$ samples have been investigated: three of them are SQW and one of them is a MQW. The PC and PV spectroscopy, the well known and relatively simple techniques used to detect photocurrent and photovoltage through the samples, can clearly show the carriers' transport properties and transitions in QW's. The

results obtained from experiments fit the theoretical calculations very well with valence band offsets taken between 0.3--0.4. In PC measurements, the effect from the substrate can be erased by using two light source (AC and DC light) technique. Also, an interesting investigation has been made, which shows how the influence from the Cr--doped substrate depends on the applied voltage and from these we have seen that a decrease in the applied volatge has the same function as using two light sources to eliminate the effect from the substrate. There is another interesting observation made in this measurement, i.e. regular and reproducible spectral oscillations in the infrared region were observed during PC measurements for sample MO33 which is a SQW on an undoped substrate. But so far this phenomenon cannot be clearly interpreted.

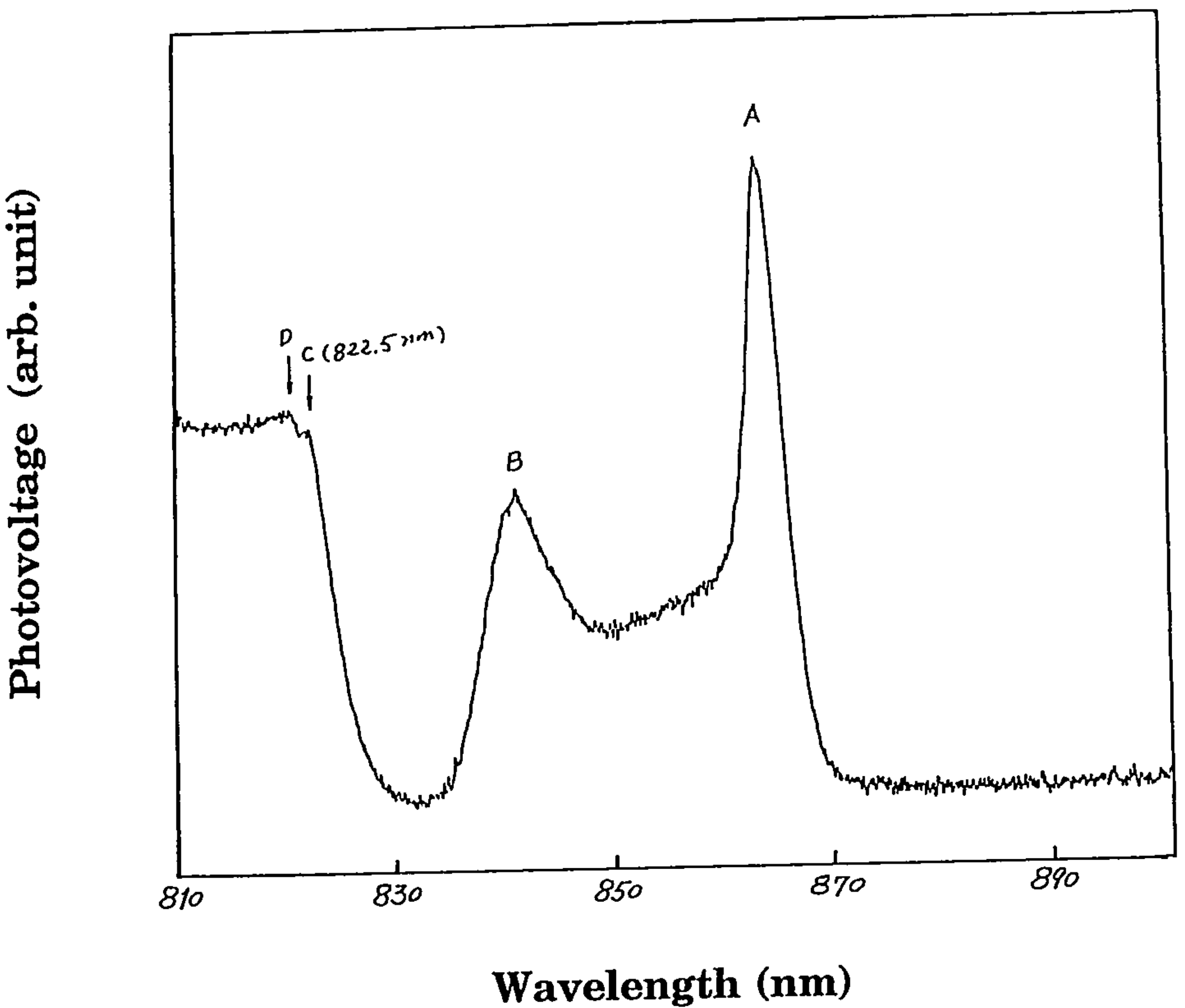

Fig. 3.29 PV spectrum for sample MO96 at T=77K in a dark environment.

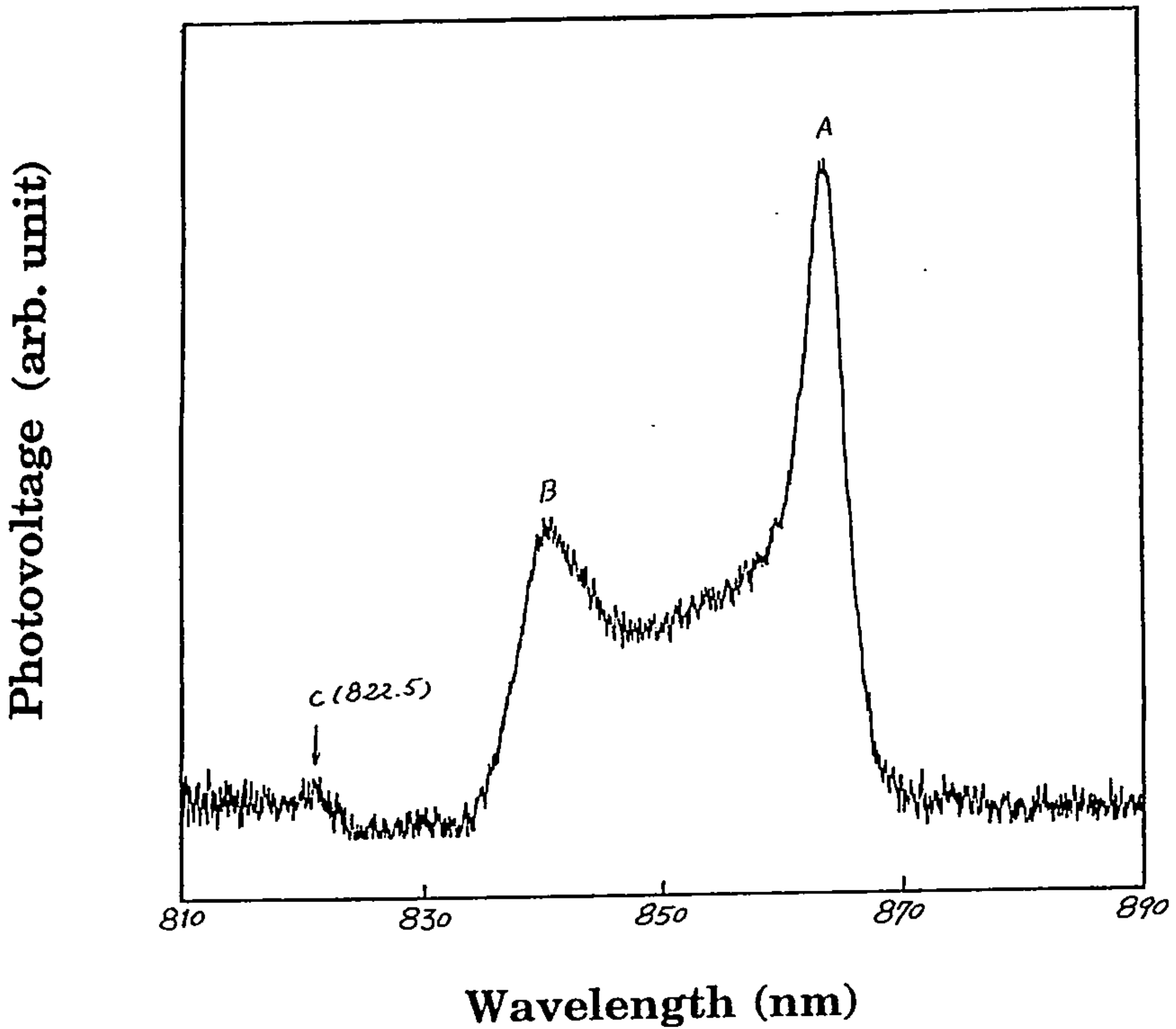

Fig. 3.30 PV spectrum for sample MO96 at T=77K with DC white light on.

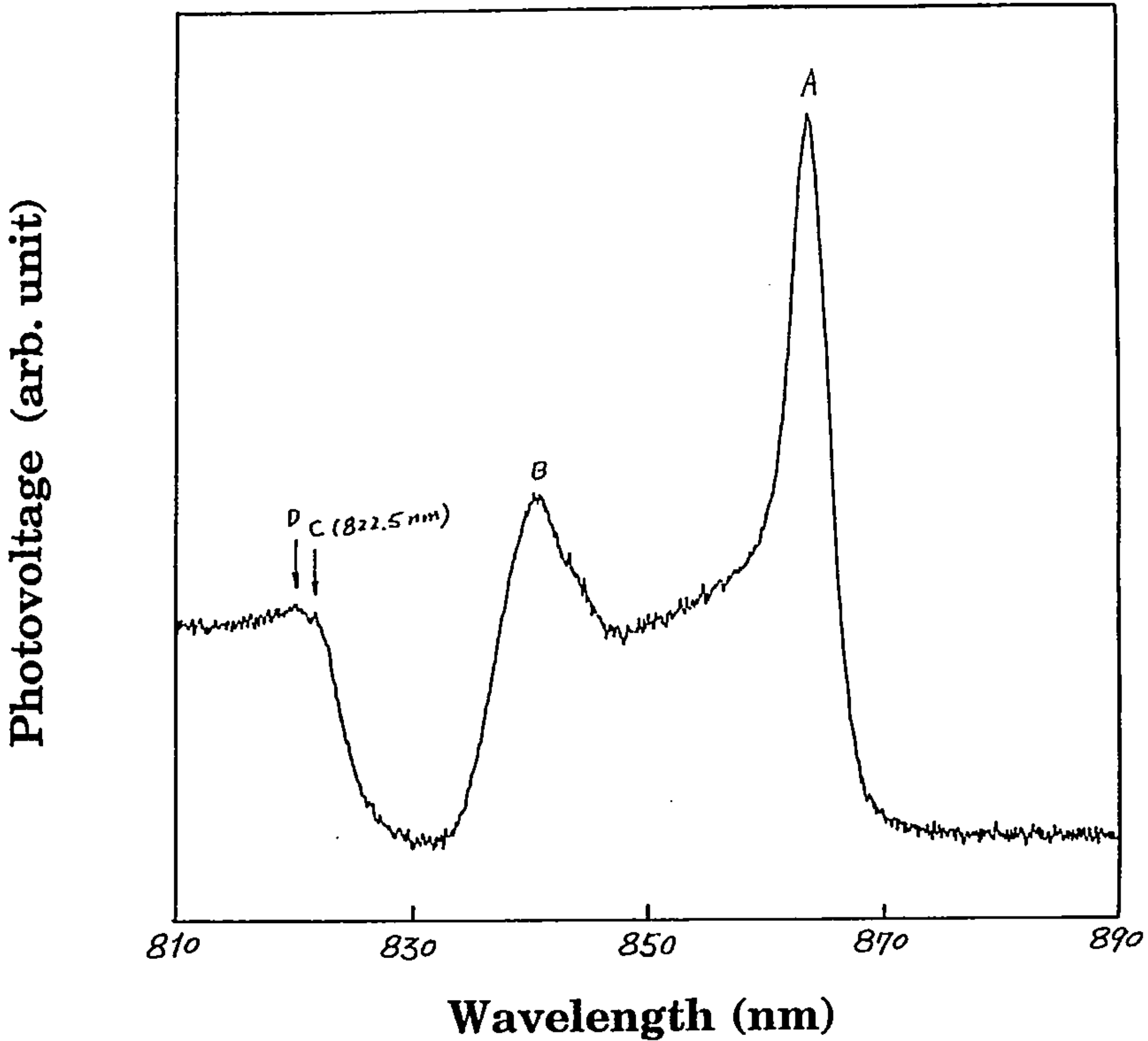

Fig. 3.31 PV spectrum for sample MO96 at T=77K in a dark environment after DC white light on.

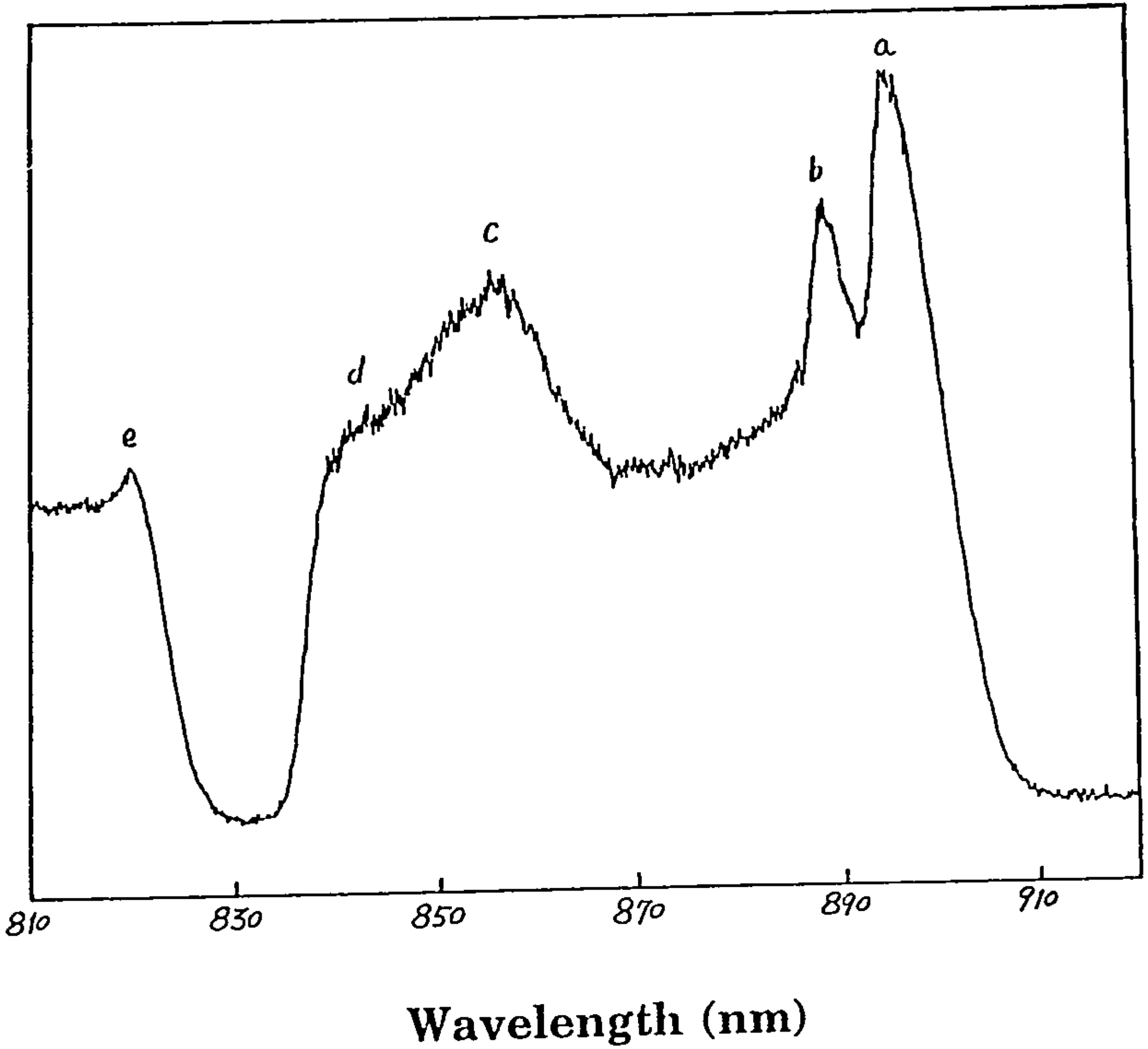

Fig. 3.32 PV spectrum for sample MO98 at T=77K.

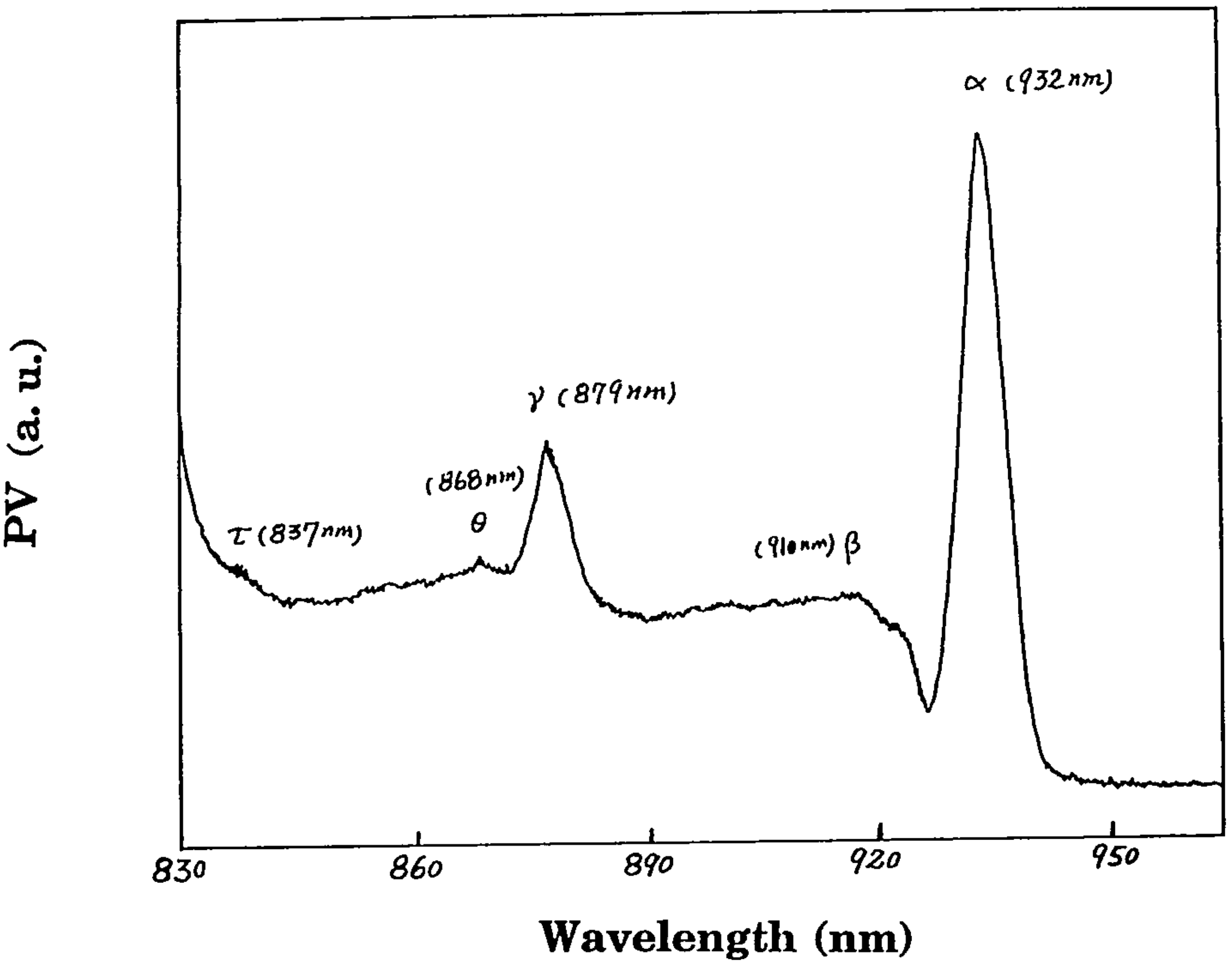

Fig. 3.33 PV spectrum for sample MO33 at T=77K.

REFERENCES

3.1 G. Bastard and J. A. Brum, IEEE J. Quant. Electron QE-22, 1625, (1986).

3.2 G. Bastard, Phys. Rev. B25, 7584 (1982.

3.3 G. Bartard, ibid, B24, 5693 (1981); B25, 7594 (1982).

3.4 E. O. Kane, J. Phys. Chem. Solids, 249 (1957).

3.5 Willardson and Beer, 1987, Semiconductor and Semimetal, Vol 24, P. 9.United Kingdom Edition, Academic Press Inc. (London)

3.6 J. Y. Marzin, M. N. Charasse and B. Sermage, Phys. Rev. B31, 8298 (1985).

3.7 T. G. Anderson, Z. G. Chen, Phys. Rev., B37, 4032 (1988).

3.8 S. H. Pan, H. Shen, et, al, ibid, B38, 3375 (1988).

3.9 R. People, S. K. Sputz, ibid, B41, 8431 (1990).

3.10 E. Fortin, S. Charbonneau and S. Meikle, J. Appl. Phys. 56 (4), 1141 (1984).

3.11 F. Prat, E. Fortin, Canadian Journal of Physics, 50, 2551--4 (1972).

3.12 X. M. Fang, X. C. Shen, et al, Surface Sciece, 228, 351 (1990).

3.13 B. Hua, E. Fortin, A. Roth, Phys. Rev., B39 (15) 10887--91 (1989).

3.14 Willardson and Beer, 1987, Semiconductor and Semimetal, Vol. 24, P. 51, United Kingdom Edition, Academic Press Inc. (London).

3.15 P. Rochon and E. Fortin, Phys. Rev. B15, 2025 (1977).

3.16 A. P. Roth and E. Fortin, Can. J. Phys., 56, 1468 (1978).

CHAPTER 4
CONCLUSION

A detailed study on photocarriers transport properties in GaAs substrates and GaAs epitaxial layers has been undertaken by using PEM effect measurements. It was shown that these measurements can reflect the carriers' transport properties and determine some parameters of the carriers very well, although it is a relatively simple and relatively unknown method.

In the substrate measurements, the samples studied were undoped semi-insulating GaAs substrates (100). The relationship between V_{PEM} and B at T=77K indicates that the surface recombination velocity of the carriers is high in those samples. The carriers mobility μ with a value of 40,000 $cm^2V^{-1}s^{-1}$ at T=77K for the samples can be determined directly from the PEM effect results. The relationship between V_{PEM} and I at both T=300K and T=77K shows that high excitation levels are reached at moderate illumination intensities I in these samples, resulting in a saturation of the PEM voltage with the intensity of radiation in the high intensity region. From the value of the saturated V_{PEM}, the diffusion length of carriers was calculated, with a value of L_D=0.27μm at T=300K and L_D=0.44 μm at T=77K. The values of diffusion length obtained in the present experiment are in good agreement with those reported by using other measurement techniques.

Using the PEM effect to measure the diffusion length in GaAs epitaxial

layer materials has not been reported by others. The samples studied here were 3.4 μm thick GaAs epitaxial layer, grown on the same substrate as above by MOCVD. The PEM spectra showed excellent behaviour in those epilayer samples at T=300K, T=77K and T=5K. The excitation level in those samples stayed low at both T=300K and T=77K. Due to this low excitation level, the value of diffusion length is related to the quantum yield coefficient β. Considering the good quality of the layer, the value of β was taken as unity. In this way the diffusion length was found to be $L_D \geq 2.6$ μm at T=300K and $L_D \geq 3.1$ μm at T=77K. At T=5K, the high excitation state results in the saturation of V_{PEM} on I as well as on B, and the value of diffusion length at this temperature is about 3.5 μm. These L_D values are close to the value of the thickness of the epi-layer, which means that perpendicular carrier transport approaches the ballistic regime, where the PEM theory may not be entirely applicable. The PEM effect was also tried in quantum wells. However, it was not successful because the diffusion length is much longer than the well width of the single quantum well or total thickness of the multiple quantum wells. (10--1,000 times depending on the temperature).

An extensive investigation on the PC effect in $In_xGa_{1-x}As/GaAs$ quantum well samples has been made. The photocurrent spectra clearly display the inter-subband transitions inside the wells. The experimental positions of the transitions were compared to those obtained from the theoretical calculations with valence band offset between 0.3-0.4. An

excellent agreement is obtained between the experimental measurements and the theoretical calculations. Therefore PC measurements can be applied to reveal the quantum transitions in quantum wells. However, care should be taken when this method is used since the substrate may affect the PC spectra results: deep Cr-donor and acceptor levels in Cr-doped substrates and some impurity levels in undoped GaAs substrates affect the PC measurement on those quantum wells. Optical quenching techniques (using AC plus DC light) can remove those effects. This is because the strong DC white light excites all trapped donors and acceptors into the conduction and valence bands. When only the signal due to AC light was detected, the influence from the substrate disappeared from the spectra.

An interesting phenomenon was observed during the PC measurement. Reproducible oscillations in the longer wavelength spectral region was always detected for and only for quantum well samples grown on the undoped substrate. The oscillations are difficult to erase by optical quenching. We are unable to explain them presently.

PV spectroscopy was also performed on some of the quantum wells. This relatively simple technique also can clearly display the quantum transitions inside quantum wells and it gives good spectra as well.

In the future, $Al_xGa_{1-x}As$/GaAs QW, or other lattice matched system, are the possible materials to be used to measure the carriers' diffusion length because they do not have lattice mismatch and thus it can be very thick without any strain. If the thickness of such materials is $\geq L_D$, the measurements of carriers' diffusion length in these materials will be meaningful.